Report Documentation Page Information

Title and subtitle:

AISI/DOE Advanced Process Control Program
Vol. 1 of 6: Optical Sensors and Controls for Improved Basic Oxygen Furnace Operation

Authors:

Sarah Allendorf – Combustion Chemistry Department, David Ottesen – Analytical Materials Science, and Donald Hardesty – Combustion & Industrial Technology

Performing Organization Names, Addresses:

Sandia National Laboratory
PO Box 969
Livermore, CA 94551-0969

Abstract:

The development of an optical sensor for basic oxygen furnace (BOF) off-gas composition and temperature in this Advanced Process Control project has seen a laboratory spectroscopic method evolve into a pre-commercialization prototype sensor system. The sensor simultaneously detects an infrared tunable diode laser (TDL) beam transmitted through the process off-gas directly above the furnace mouth, and the infrared greybody emission from the particulate-laden off-gas stream. Following developmental laboratory and field-testing, the sensor prototype was successfully tested in four long-term field trials at Bethlehem Steel's Sparrows Point plant in Baltimore, MD. The resulting optical data were analyzed and reveal correlations with four important process variables: (1) bath turndown temperature; (2) carbon monoxide post-combustion control; (3) bath carbon concentration; and (4) furnace slopping behavior. The optical sensor measurement of the off-gas temperature is modestly correlated with bath turndown temperature ($R^2 = 0.30$). A detailed regression analysis of over 200 heats suggests that a dynamic control level of ± 25 °F can be attained with a stand-alone laser-based optical sensor. The ability to track off-gas temperatures to control post-combustion lance practice is also demonstrated, and may be of great use in optimizing post-combustion efficiency in electric furnace steelmaking operations. In addition to the laser-based absorption spectroscopy data collected by this sensor, a concurrent signal generated by greybody emission from the particle-laden off-gas was collected and analyzed. A detailed regression analysis shows an excellent correlation ($R^2 = 0.81$) of a single variable with final bath turndown carbon concentration. Extended field trials in 1998 and early 1999 show a response range from below 0.03% to at least 0.15% carbon concentration with a precision of ± 0.007%. Finally, a strong correlation was also observed between prolonged drops in the off-gas emission signal and furnace slopping events. A simple computer algorithm was written that successfully predicts furnace slopping for 90% of the heats observed; over 80% are predicted with at least a 30-second warning prior to the initial slopping events.

(RDP Standard Form, Form 298)

Sponsor TBD Report No.:

AISI/DOE Advanced Process Control Program

Vol. 1 of 6: OPTICAL SENSORS AND CONTROLS FOR IMPROVED BASIC OXYGEN FURNACE OPERATIONS

FINAL REPORT
June 1, 1993 – February 28, 1999

Edited By

Joe Vehec

April, 2002

Work performed under Cooperative Agreement No. DE-FC07-93ID13205

Prepared by
American Iron and Steel Institute
For
U.S. Department of Energy

DISCLAIMER

Contents

Figures

Page

Figures

Page

Figures

Page

Tables

Page

Executive Summary

The development of an optical sensor for basic oxygen furnace (BOF) off-gas composition and temperature in this Advanced Process Control project has seen a laboratory spectroscopic method evolve into a pre-commercialization prototype sensor system. The sensor simultaneously detects an infrared tunable diode laser (TDL) beam transmitted through the process off-gas directly above the furnace mouth, and the infrared greybody emission from the particulate-laden off-gas stream. The sensor prototype was successfully tested in four long-term field trials at Bethlehem Steel's Sparrows Point plant in Baltimore, MD.

This extensive research and development project involved close cooperation among personnel from several organizations: Sandia National Laboratories, Bethlehem Steel Corporation (Homer Research Laboratories and Sparrows Point Division), Insitec Inc., and Hubbard Associates. Financial support and program management was supplied by the US Department of Energy (Office of Industrial Technology) and member companies of the American Iron and Steel Institute through the Advanced Process Control Program.

The original intended application of the laser-based off-gas sensor was dynamic control of bath turndown carbon concentration for BOF operations. During the course of the five-year development project, the range of potential applications was expended to include dynamic control of: (1) bath turndown temperature; (2) furnace slopping behavior; and (3) carbon monoxide post-combustion. The possibility of detecting significant changes in the water vapor content of the off-gas as a function of hydrogen concentration was also considered, and may be particularly useful for some electric furnace operations.

A combination of laboratory research at Sandia's Combustion Research Facility (CRF) and pilot-scale testing at Bethlehem Steel's Homer Research Laboratories (HRL) provided two major advances in the 1993 – 1994 phase of the project. First, it was demonstrated that a method based on absorption spectroscopy using a very high-resolution tunable diode laser (TDL) was the best choice for an off-gas sensor. Testing at HRL showed that a single-ended emission-based spectroscopic sensor was not feasible for characterizing both off-gas composition and temperature due to the optical thickness of the off-gas stream. A second major advance during this initial stage of the project was the hardening of the optical sensor system for rapid deployment and long-term stable operation in an industrial operating environment.

Following a brief full-scale feasibility trial at Bethlehem Steel's Bethlehem BOF plant in early 1995, full-scale testing with a laser-absorption-based optical sensor was conducted through February 1999. During this period, the feasibility of off-gas composition and temperature measurements in real time was demonstrated. A hardened pre-commercial prototype instrument was constructed and performed reliably during two one-month field trials. The optical data were analyzed and reveal correlations with four important process variables: (1) bath turndown temperature; (2) carbon monoxide post-combustion control; (3) bath carbon concentration; and (4) furnace slopping behavior.

The correlation of bath turndown temperature relies most strongly on the optical sensor measurement of the off-gas temperature. A detailed regression analysis of over 200 heats shows a dynamic predictive capability of approximately ± 25 °F with a modest correlation coefficient of

$R^2 = 0.30$, and is based on a long-term average range of ± 30 °F for bath turndown temperature at Sparrows Point. The consensus of Sandia, Bethlehem Steel, and Insitec personnel is that a control level of ± 20 °F or better is necessary for such a stand-alone optical sensor method to be commercially successful. This goal may be attainable by combining the laser-based sensor with other independent sensor systems, or with additional static and real-time input from the plant computer control system in a separately funded development program.

During late 1996, post-combustion oxygen lance technology was installed at Sparrows Point and was marked by a distinct increase in both off-gas CO_2 concentration and temperature as revealed in the laser-based sensor data. While these data were useful in an assessment of BOF hood design by Bethlehem Steel, the steady-state nature of the post-combustion process at Sparrows Point does not benefit greatly from a real-time control system. It was concluded that a much more fruitful implementation of the laser-based sensor is for real-time post-combustion control in the electric arc furnace steelmaking process. The rapidly changing off-gas in that process is very amenable to a dynamic control system for optimizing energy efficiency and reducing CO emissions. As a result of this work in the Advanced Process Control program, a new AISI Technology Roadmap project has been approved (TRP 9851) and is now underway to develop this technology for the electric furnace process.

In addition to the laser-based absorption spectroscopy data collected by this sensor, a concurrent signal generated by greybody emission from the particle-laden off-gas was collected and analyzed. A detailed regression analysis of these data shows an excellent correlation ($R^2 = 0.81$) of a single variable with bath turndown carbon concentration. This sensor configuration is single-ended and resembles the recently developed and patented Bethlehem Steel "carbon light meter." However, an operation in the mid-infrared region, as dictated by this tunable diode laser, yields valid dynamic control data over a much wider range of bath carbon concentrations. Extended field trials in 1998 and early 1999 show a response range from below 0.03% to at least 0.15% carbon concentration with a precision of ± 0.007%. A new AISI Technology Roadmap project has been approved to develop and optimize this method for improved dynamic bath carbon control.

Finally, during the course of the project, significant changes in the real-time off-gas emission sensor signal during furnace slopping events were also observed. During the final series of field trials time-stamped videotapes were made of 100 heats, and computer-aided analyses of furnace slopping were compared with simultaneous off-gas emission signals. A strong correlation is observed with prolonged drops in the emission signal and furnace slopping. A simple computer algorithm was written that successfully predicts furnace slopping for 90% of the heats observed. Over 80% are predicted with at least a 30-second warning prior to the initial slopping events. Perhaps as many as 50% of the BOF shops in North America suffer product loss and increased maintenance costs as a result of slopping due to smaller capacity furnaces. As a result, it was also recommend that an off-gas emission sensor be developed for dynamic control of furnace slopping in a follow-on program. This work was also approved by the AISI Technology Roadmap program, and will be combined with the development of an extended range carbon control sensor as mentioned above.

Acknowledgments

The Sandia team specifically wishes to acknowledge the critical support of the industrial partner, Bethlehem Steel Corporation (BSC). The strong support from management at BSC, both in Research and at Sparrows Point, was essential to the success of this program. In addition, the strong program management of the American Iron and Steel Institute's Advance Process Control Program helped keep the team on schedule and focused on industry needs. Finally, it has been a pleasure to work with many talented individuals over the course of this long-running project. The Sandia team lists here the major participants (in pseudo-chronological order) and thanks them for their important contributions:

AISI: Larry Kavanagh, Joe Vehec, and Ed Schoenauer
BSC, Homer Research Laboratories: Bob Bouman, Phil Stelts, Dale Brinker, Kathy Chen, Dan Goldstein, Alok Sharon, and Tim Miller
BSC, Sparrows Point Division: Colvin Smith, Tom Russo, and Gary Garadetsky
Cornell University Coop students: Daniel Jung, Jason Wang, and David Rosenberg
Hubbard Associates: Gary Hubbard
Insitec Measurement Systems: Michel Bonin, Andrew Malcolmson, Soren Jensen, and Don Holve
Sandia National Laboratories: Peter Ludowise, Ben Chorpening, Howard Johnsen, Bill Kent, James Ross, Alan Salmi, and Lee Bertram

1. Introduction

This final report summarizes research and development efforts on optical sensors for gas-phase composition and temperature in basic oxygen steelmaking operations by Sandia National Laboratories, Bethlehem Steel Corporation and Insitec Inc. over the 1993 – 1999 time period. The results are organized into three sections (R&D, pilot-scale testing, and full-scale testing), and are presented in a chronological fashion in order to preserve a reasonable level of detail. Throughout the report, achievements of major importance are highlighted by italics and a notation of "Major Milestone Achieved."

A major impediment to improved process control in basic oxygen steelmaking is the lack of rapid, accurate sensor systems for measurements in the incredibly hostile environment of the BOF. Many of these environmental problems can be minimized by the use of remote-sensing optical systems, and one of the primary opportunities for monitoring BOF operations is the off-gas exiting the furnace mouth.

Although off-gas composition analysis by infrared or mass spectrometric technologies is commonly employed in the steelmaking industry, these measurements are only feasible for clean, room temperature samples extracted from the off-gas flow far downstream from the furnace. The resulting time delay and changes in chemical composition due to continued reaction and air infiltration make it very difficult to use these data for dynamic process control.

Previous work between Sandia and Bethlehem Steel's Homer Research Laboratories [Ottesen, 1993] revealed the feasibility of quantitatively probing the composition and temperature of furnace off-gases near the furnace mouth with infrared optical systems. At the completion of this early work in 1992, it was concluded that techniques involving either the transmission of an infrared laser beam through the off-gas, or the spectral resolution of infrared emission from the off-gas, appeared promising as methods for dynamically measuring the concentrations and temperature of CO and CO_2 in the gas stream exiting the furnace.

Bethlehem Steel's capability for pilot-scale testing with a 2-ton capacity furnace at their Homer Research Laboratories (HRL) was an essential factor in demonstrating the feasibility of the concept during the early stages of this project. Experiments at HRL allowed us to select the laser-based absorption spectroscopy method for further development. The emission-spectroscopy method was rejected as technically unfeasible for the characterization of gas-phase temperature due to limitations in spectral resolution.

A dramatic change in the optical sensor data near the end of the oxygen blow was expected due to rapidly changing concentrations of CO and CO_2 in the off-gas stream. The reduction of CO concentration from a steady state value of 80–90% is due to decarburization of the melt and a more complete oxidation of the gas within the furnace. As a result, it was anticipated that the infrared optical sensor signal would be strongly correlated with the bath carbon concentration and could be used to control that variable.

Furthermore, spectrally resolved measurements of CO and CO_2 absorption or emission line intensities can be used to derive an average gas-phase temperature in the off-gas. It was believed

that this measurement might reflect, to some degree, the temperature of the melt within the furnace, and could possibly be used to control the final turndown melt temperature, as well as carbon monoxide post-combustion processes.

Finally, as with any exploratory research effort, novel measurements on poorly characterized systems often reveal unexpected information that can be related to specific events occurring within the process under observation. This turned out to be the case in this development of an optical off-gas sensor and has led to a method for predicting and controlling the slopping behavior of foaming slag within the basic oxygen furnace.

2. Off-Gas Sensor Research and Development

The development of a real-time optical sensor for BOF off-gas measurements was greatly facilitated by cooperative work between Sandia and Bethlehem Steel prior to the inception of the current project. Two series of experiments at the HRL pilot-scale BOF demonstrated conclusively that sensors based on light transmission through the furnace off-gas would not be successful for wavelengths shorter than about 2 μm [Ottesen, 1993]. Laser beam transmission losses are due largely to absorption and scattering of the beam by particles in the off-gas, and depend inversely on the first power, at least, of the wavelength of the light. The particulate is predominantly FeO with a size distribution 99% < 1 μm diameter [Stelts, 1994].

This loss mechanism greatly favors the use of infrared light as a probe medium for the hot, particle-laden off-gas, and the project was formulated around measurements in the 4.5 to 5.5 μm wavelength range in the mid-infrared spectral region. In addition to the greater penetrating capability of infrared light relative to near-infrared and visible wavelengths, molecules of CO, CO_2 and H_2O all possess characteristic absorption (and emission) features in this wavelength range. These absorptions arise from transitions between molecular vibration-rotation energy levels, and can be quantitatively analyzed to infer both molecular concentrations and temperatures averaged along the optical line-of-sight through the furnace off-gas.

It was also chosen to evaluate two competitive infrared sensor designs: (1) a laser-based absorption method; and (2) a spectrometer-based emission method. Both approaches have distinct advantages and disadvantages. The project was approved by the AISI/DOE and was initiated in 1993. A series of three field trials was planned for the first two years with the more favorable approach being selected for further testing and development at a full-scale BOF. Each field trial involved a substantial preparative research and development effort at Sandia, and these supporting laboratory activities are described below.

2.1 Initial Laser-Absorption Measurements

This laser-absorption off-gas sensor uses a mid-infrared tunable diode laser (TDL) as the source of the infrared optical probe beam. A sensor based on the laser-absorption method is attractive for several reasons: (1) absorption spectra are directly quantifiable in terms of molecular concentrations and temperature; (2) modulation of the laser source permits sensitive detection and discrimination against signal loss by particle scattering; and (3) the tunable laser source allows a simple, inexpensive detector to be used.

Drawbacks to the laser-absorption method include the following: (1) the sensor is double-ended, consisting of transmitter and receiver components that must be maintained in optical alignment; (2) currently available TDLs in the 4.5 - 5.5 μm range possess low output powers thus yielding very low signal levels after beam attenuation by dust entrained in the furnace off-gas and beam-steering by the turbulent reacting flow of the furnace effluent; and (3) currently available mid-infrared TDLs require cooling to cryogenic temperatures (near 77° K) for operation.

A commercially available TDL system was obtained from Laser Photonics, Andover, MA. The lasers are "lead-salt" alloy semiconductor devices installed in a vacuum insulated cryostat that emit coherent radiation when cooled to temperatures between 80° and 120° K, and injected with currents up to 500 mA. Primarily the device temperature controls the wavelength of the output laser light, and a Laser Photonics controller was used to maintain the device temperature within ± 0.001° K. Output wavelengths are rapidly tuned over a small wavelength interval by modulating the input current in a variety of waveforms. Programmable function generators were used in conjunction with the Laser Photonics controller to repeatably and precisely tune the laser output over the desired wavelength range.

Light from the TDL exiting the cryostat is highly diverging, and optical elements (positive lenses or off-axis paraboloids) are used to collimate the beam with a diameter of approximately 12 mm. These optical devices are mounted on a 30 x 36" breadboard assembly as shown in Figure 1. This breadboard also contains a sealed gas cell filled with low-pressure carbon monoxide. Approximately 5% of the infrared laser energy is extracted from the collimated beam using a pellicle beam splitter and transmitted through the gas cell. Characteristic absorption features of the carbon monoxide gas are measured with a liquid-nitrogen cooled InSb infrared detector and associated focusing lens (CaF_2), and this reference spectrum serves as a monitor for stable laser output power and tuning range.

A second breadboard assembly contains an identical InSb infrared detector and associated focusing lens. A narrow bandpass optical filter is placed between the focusing lens and detector to reject thermal emission from the off-gas outside the TDL tuning range. Variable diameter irises are also used to limit the amount of off-axis light falling on the detector.

Reference and receiver detector signals, and timing signals from the TDL controller unit are transmitted to a computerized data acquisition system. The data are digitized, time-averaged and stored on hard disk using custom software written by Hubbard Associates. The operating software also provides a real-time display of either the reference or receiver detector signal, as well as trends in selectable variables such as laser transmittance and intensity ratios of gas-phase absorption lines.

Computer codes were also written to calculate high-temperature absorption spectra of carbon monoxide in order to accurately predict and model the experimentally measured spectral data. Since all calculations in this report are performed using wavenumbers (as opposed to wavelength) in units of cm^{-1}, all spectral data are also presented in wavenumbers as well. Wavenumbers are related to wavelength by the following equation:

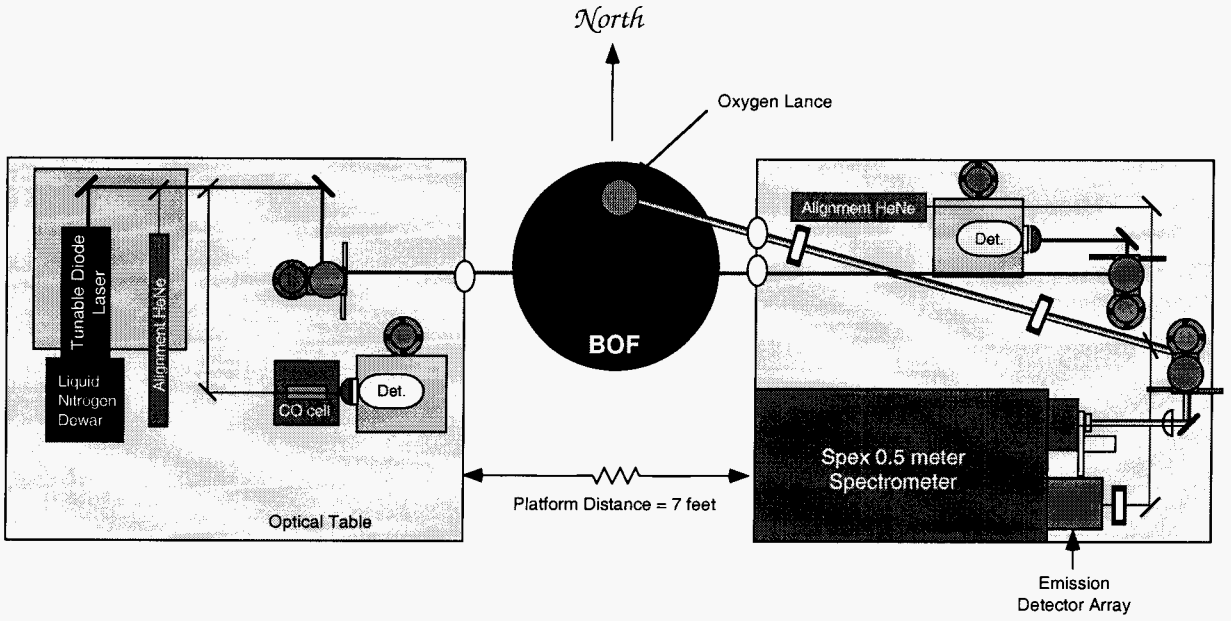

Figure 1. Experimental layout for infrared absorption and emission sensors at Bethlehem Steel pilot-scale field trials.

$$\text{Wavenumber } (cm^{-1}) = 10000\ (\mu m\ cm^{-1}) / \text{Wavelength } (\mu m) \quad (1)$$

Therefore, a wavelength of 5 μm is equivalent to a wavenumber of 2000 cm^{-1}. Although wavenumbers will be used here to describe detailed spectral measurements, wavelengths will also be provided when discussing general spectral regions of measurement.

Literature values of Dunham coefficients for CO [Farrenq, 1991] are used as input to calculate the wavenumber and energy levels for each CO vibration-rotation transition for all ^{12}C, ^{13}C, ^{17}O, ^{18}O isotopes, vibrational quantum numbers up to V=10, and rotational quantum numbers up to J=100. These data are then used to calculate off-gas absorption spectra using Voigt profiles [Pierluissi, 1977] for the CO absorption line shapes. The Voigt profile takes into account absorption line broadening due to both Doppler and collisional broadening effects as a function of gas pressure and temperature. The resulting calculation can then be directly compared with experimental measurements of off-gas transmission.

The TDL sensor was built and tested at Sandia's Combustion Research Facility (CRF) using a pilot-scale combustor facility. These experiments were useful in aligning the sensor optics and interfacing the sensor components with the data acquisition. However, it was found that the hot gas produced by the pilot-scale combustor was not a good simulation for either the CO/CO_2 concentration ratio, gas temperature, or particle loading expected to be measured at the HRL pilot-scale BOF. As a result, an additional simulator was constructed comprising a blackbody infrared source (to simulate the hot off-gas) and a variable beam attenuator (to simulate the varying off-gas particle loading density).

2.2 Initial Off-Gas Emission Measurements

During the first year of the project, a high-resolution infrared-emission spectroscopic technique for off-gas concentration and temperature measurements was also evaluated. The emission approach has several advantages: (1) the technique is single-ended (requiring only a receiver module), and is very easy to align; and (2) only light emitted from the process is measured, eliminating the need for a laser source and its associated hardware.

Conversely, emission methods suffer from several disadvantages: (1) emission measurements are inherently more difficult to quantify than absorption measurements; (2) emission from molecules in the center of the off-gas stream may be reabsorbed by other molecules before it can escape the hot region and be measured by the sensor; and (3) the optical hardware available for a practical sensor has a much poorer spectral resolving power than the laser-absorption sensor.

Although the disadvantages of an off-gas emission sensor appeared substantial, it was believed that it should be thoroughly evaluated due to the far greater simplicity of the final installation and resulting ease of operation. Accordingly, a 256-element, PbSe linear-array detector from Litton Instruments, Phoenix, AZ was acquired. The detector was mounted on a 0.5-m focal length spectrometer with a mid-infrared grating. Light from the source to be measured was modulated with a rotating mechanical chopper and focused onto the spectrometer entrance slit with a CaF_2 spherical lens.

A prototype controller from Litton was used to interface the detector output with the data acquisition system. The emission sensor was tested in the laboratory and demonstrated a resolution of 0.25 cm^{-1} in the spectral range of interest. Although this is a respectable degree of resolution for such a compact system, it is approximately five times greater than the anticipated CO emission line widths of 0.05 cm^{-1} for hot gas at a temperature of 2000° K (3140 °F). It is also much greater than the demonstrated resolution of less than 0.01 cm^{-1} for the TDL absorption sensor, discussed above.

For the sake of compactness in the pilot-scale field trials, the emission sensor was mounted on the same optical breadboard as the laser-absorption detector hardware. This also allowed the team to conduct experiments for both the off-gas emission and laser-absorption sensors simultaneously, and to directly compare experimental data for both approaches. The resulting layout of the hardware is shown in Figure 1.

3. Pilot-Scale Testing

A series of three field trials were conducted at Bethlehem Steel's HRL during December 1993, June 1994, and December 1994. The purpose of the tests was to evaluate the two sensor concepts using an off-gas stream that was a reasonably accurate one-tenth (linear scale) representation of a full-scale commercial BOF off-gas stream. At the conclusion of pilot-scale testing, the more successful sensor method was incorporated into a hardened prototype instrument for extensive full-scale testing.

The laser transmitter and detector receiver modules were installed in two equipment bays located on either side of the BOF at the HRL (Figure 1). The infrared laser beam passed midway between the vessel mouth and the off-gas exhaust hood at a point located 18 cm to the side of the oxygen lance.

The off-gas emission sensor line-of-sight was nearly parallel to that of the TDL, and intersected it in the middle of the off-gas stream.

3.1 December 1993 Field Trial

The goal of the first field trial was to determine the feasibility of both laser-absorption and emission sensor methods at the pilot-scale. The sensor components were shipped to the HRL, reassembled and aligned. A series of four one-ton heats were made during December 13-16, 1993. Metal and slag samples were obtained periodically during and after oxygen blowing using a sampling lance (which interrupted the optical path of the TDL beam during sampling).

Off-Gas Laser-Absorption Measurements. Laser-absorption spectra were acquired over the 2100 - 2150 cm^{-1} region. The approach was to make a comprehensive series of measurements using two wavelength regions during each of three heats. Measurements during a fourth heat were limited by a vessel breakout. The results of the tests demonstrated: (1) real-time detection of infrared-active gas molecules (CO, CO_2 and H_2O); (2) calculation of real-time line-of-sight gas temperatures using relative CO line intensities; (3) calculation of real-time CO concentrations; and (4) determination of overall laser beam transmittance to evaluate the effects of particle scattering and beamsteering.

An example of the off-gas laser-absorption data is shown in Figure 2. These spectra were collected by averaging 100 scans over a 0.1-second measurement time. The detection of all three molecular species using the infrared absorption method was successfully demonstrated. Figure 2 shows the infrared absorption spectra from a BOF preheat (upper curve) and 9.3 minutes into the oxygen blow in the heat on December 16 (lower curve). The intense absorption line near 2111.6 cm^{-1} is due to CO and is present in both curves. The other strong line observed during the preheat near 2114.5 cm^{-1} is due to H_2O formed during the combustion of anthracite; this line is not observed during oxygen blowing. Other strong lines observed during the oxygen blow are due to hot CO, while some of the less intense features are due to CO_2.

In Figure 3, the previous infrared absorption spectrum during oxygen blowing (solid) is compared with a calculated curve (dashed) for 10% CO at a temperature of 2125 °F (1435° K). Two important conclusions may be drawn from this figure. First, the excellent agreement of relative intensities for the three high energy ("hot band") transitions (at 2112.3, 2112.6 and 2113.0 cm^{-1}) demonstrates the ability of the sensor to extract line-of-sight temperatures in the BOF off-gas environment. The relatively low value of the measured temperature is due to the large amount of ambient air entrained into the exhaust stream in the open exhaust-hood configuration. Second, CO absorption lines dominate this wavelength region. Comparison of the experimental curve with the calculation for CO shows that only the weaker absorption features can be attributed to CO_2. CO_2 lines are expected to be relatively weak in this wavenumber range due to both spectroscopic considerations and the fact that the CO_2 concentration is low until the end of the oxygen blow. The spectroscopic parameters needed to accurately calculate CO_2 absorption spectra, as a function of temperature and concentration are not available.

Off-gas Emission Measurements. A 0.5-m focal length spectrometer was equipped with the 256-element, lead selenide multiplexed detector array (MDA) described above. CO emission lines were clearly observed during the heat on December 14, and an average of 600 scans acquired in three 0.2-second measurements is shown in Figure 4 (solid- curve). For comparison, an FTIR transmittance spectrum (dashed- curve) of an acetylene-oxygen flame acquired in the laboratory at Sandia was

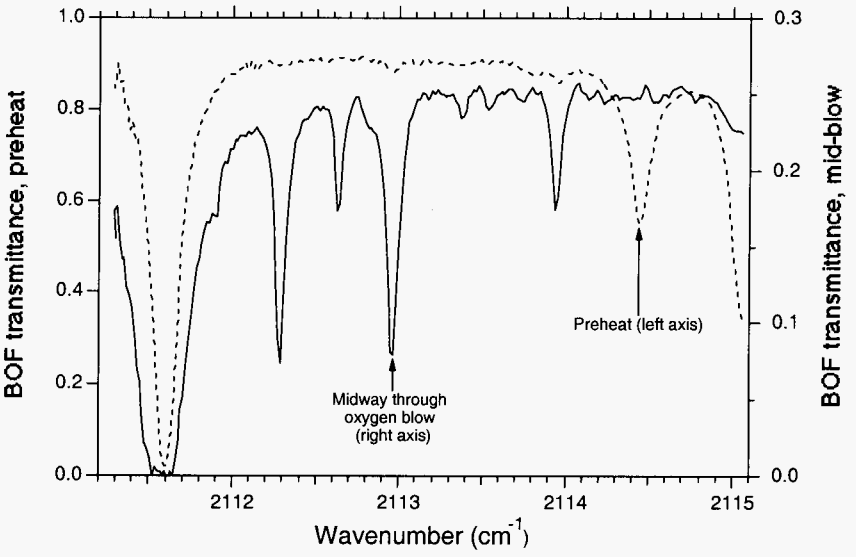

Figure 2. Gas-phase absorption spectra during BOF pre-heat (dashed curve) and oxygen blowing (solid curve). Absorption features due to CO, CO_2 and H_2O are observed in this wavenumber region.

also shown.

Upward-going CO emission lines are clearly visible in the lower curve and are spectrally aligned with their downward-going FTIR transmittance counterparts. The evenly spaced intense lines in both spectra are due to ground state CO vibrations. Although the noise level is high in the emission spectrum, additional weaker features are also observed due to CO hot-band transitions. The relative intensity of these lines was used to calculate temperatures and concentrations in a fashion analogous to the results for the TDL absorption sensor described above.

The gas-phase emission lines are offset from the horizontal axis in Figure 4. This offset is due to broadband emission from particulates in the sensor field of view at the same wavenumber as the gas-phase lines. Since it is greybody in nature, the emission from these solid particles has no spectral structure over the sensor bandwidth, and thus appears as a constant offset in this detector output. Pilot-scale field tests show that this particulate emission component does not interfere with the measurement of gas-phase emission lines at the pilot-scale.

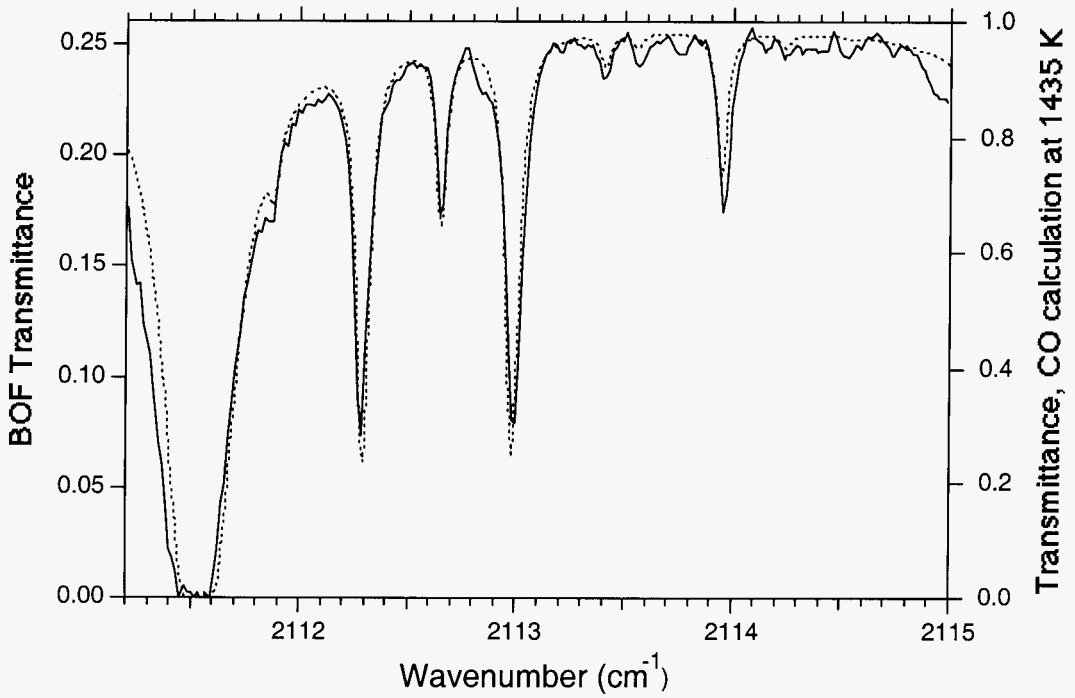

Figure 3. Gas-phase absorption spectrum during BOF oxygen blow (solid) and calculated CO absorption spectrum (dashed). Very good agreement is obtained for a calculated temperature of 2125 °F (1435° K) and CO concentration of 10%.

To summarize, the results of the first pilot-scale field trial were extremely encouraging for both optical sensor methods. The results of the tests suggested numerous improvements in sensor design, and these were incorporated prior to the second pilot-scale field trial described below.

3.2 June 1994 Field Trial

A second series of pilot-scale field trials of both infrared absorption and emission sensors at Bethlehem Steel's HRL was conducted during June 1994. Laboratory equipment was tested at Sandia and shipped to Bethlehem in early June, and an advance team from Sandia set up and tested the equipment in the HRL during June 16-19. The sensor placement was identical to that of the December 1993 field trial.

A series of three one-ton heats was made during June 20-22. Metal and slag samples were obtained periodically during and after oxygen blowing using a sampling lance. The primary goal during this series of trials was to optimize the emission sensor and to confirm the absorption sensor data

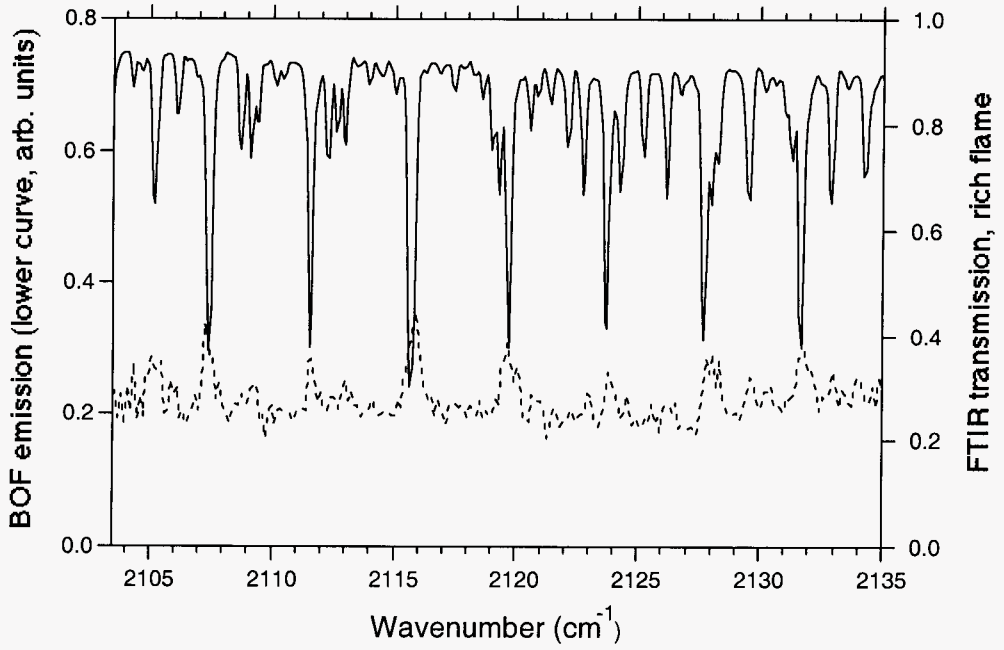

Figure 4. Emission sensor signal during BOF oxygen blowing (lower curve) showing CO emission lines superimposed on a constant particulate emission offset. FTIR transmission spectrum for laboratory burner flame (upper curve) is shown for comparison

obtained during experiments conducted at Bethlehem Steel during December 1993. A major simplification in the design of the emission sensor optical components was tested successfully. Emission data were collected along a different line of sight during each of the three heats to determine the optimum field of view for this method. Improvements in the absorption sensor, primarily in the data acquisition software, were also tested during these trials.

Off-Gas Laser-Absorption Measurements. Laser-absorption spectra were acquired with the TDL-based sensor from 2111 - 2115 cm^{-1}. The first pilot-scale field trial identified this wavenumber region to be optimal for pilot-scale testing. Several important process variables were also measured and recorded: the O_2 flow rate, the O_2 lance height, and thermocouple readings of the melt temperature.

The objectives for the laser-absorption measurements and data analysis were: (1) simultaneous detection of infrared-active gas molecules (CO, CO_2 and H_2O); (2) calculation of real-time line-of-sight gas temperatures using relative CO line intensities; (3) calculation of real-time CO concentrations; (4) identification of melt decarburization using trends in the CO and CO_2 concentrations; and (5) determination of overall laser beam transmittance to evaluate the effects of particle scattering and beamsteering.

TDL data were collected by averaging 200 scans over a 0.2-sec measurement time for each absorption spectrum. Included in the data acquisition software are routines to reduce the spectra in real-time to plots of overall transmittance, CO concentration, CO temperature, and the ratio of CO

to CO_2. As in the first pilot-scale field trial, CO, CO_2, and H_2O were detected using the infrared absorption method. H_2O was observed only during the furnace preheat due to the combustion of carbon. Regions in the spectra where no gas-phase absorption is observed are used to monitor the maximum transmittance of the laser radiation through the off-gas.

Figure 5 presents the CO temperature (upper curve) and laser transmittance (lower curve, left axis, no symbols) as a function of computer time, for the third heat of the trial. ("Computer time" refers to the beginning of a data acquisition run). In general, data were started to be taken shortly before the oxygen blow commenced in order to record hot metal temperature. For instance, in Figure 5 the oxygen blow began at 365 seconds on this time basis. The data shown in Figure 5 are for the period after stable ignition was achieved. Blank regions are times when samples were taken and the sample lance interrupted the laser beam. No smoothing has been applied to these data. Each point reflects a 0.2-second measurement time.

These results suggest that the average gas temperature along the line-of-sight is reasonably stable. Some of the scatter is due to uncertainties in reading the detector signal caused by overall instrument noise and corresponds to a variation in calculated temperature of ±20° K (±35 °F). Most of the observed scatter, ±70° K (±125 °F), is therefore due to real fluctuations in the instantaneous volume-averaged gas temperature along the line-of-sight. Both the transmittance and the calculated CO temperature are much more stable than was observed in the first field trial due to improvements

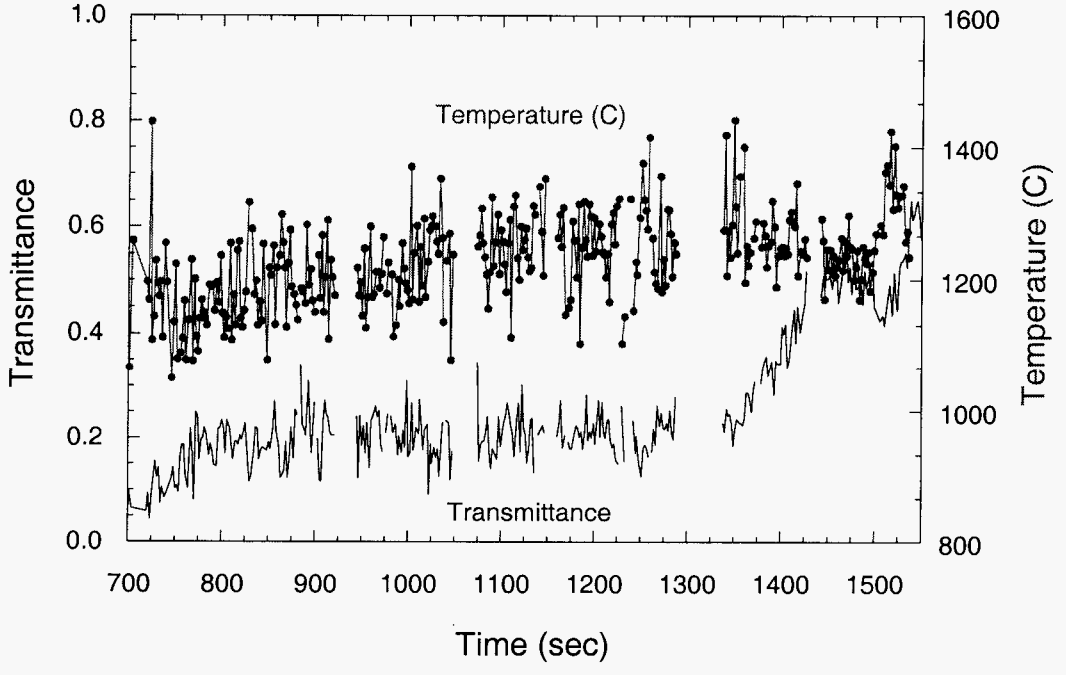

Figure 5. Off-gas temperature (upper curve) and TDL transmittance (lower curve) during the oxygen blow for heat 3 of the second pilot-scale field trial.

in optical alignment. The relatively low average value of the measured gas temperature for these

pilot-scale experiments is due to the large amount of ambient air entrained into the two-ton vessel in the open-exhaust-hood configuration.

Once a temperature has been calculated for CO in the off-gas, one can immediately extract a CO concentration along the sensor line-of-sight as a function of time during the oxygen blow. Figure 6 shows the concentration of CO and laser transmittance as a function of computer time, as in Figure 5. A higher and more constant rate of CO production was observed during these tests than during our first pilot-scale experiments. The average is around 40%, slowly increasing as the oxygen blow proceeds. There is a sudden drop in the CO concentration at 1500 seconds in Figure 6 indicating melt decarburization.

To further illustrate melt decarburization, the ratio of absorbance values for two individual carbon monoxide and carbon dioxide absorption lines is plotted in Figure 7 in the form: $Abs_{CO} / (Abs_{CO} + 10*Abs_{CO2})$. Since an accurate calibration for CO_2 concentration as a function of absorption line intensity is not available, this ratio does not represent an actual concentration ratio, but it still serves to illustrate trends in concentrations. The pronounced drop in this absorbance ratio at 1500 seconds is striking, however, and indicates a rapid drop in CO gas-phase production due to depletion of carbon in the melt phase and a concurrent increase in the relative CO_2 concentration.

An initial assessment of the likelihood for successful application of the infrared absorption method to a commercial-scale BOF by examining the maximum transmittance of the tunable diode laser beam during oxygen blowing was made. To estimate the effects of scale-up, a logarithmic attenuation of laser beam power with distance along the line of sight due to particulate scattering is assumed. This is a conservative assessment since the effects of beamsteering, which are most severe at the hot-cold gas-phase boundary, will be overemphasized in this approach. Laser-absorption measurements in the pilot-scale BOF were made over an optical path of at least 1.5 feet (the furnace opening). For a full-scale BOF opening of 12 feet, the linear increase in scale is a factor of eight. If the particle number density in the two-ton BOF off-gas is the same as that of a full-scale BOF, then one can make the following predictions:

Total transmittance in the range of 1.0 to 0.7 for pilot-scale results would lead directly to an infrared absorption sensor at the commercial scale with little additional development. Since these pilot-scale tests yielded an average maximum transmittance of the TDL beam near 0.2 following ignition (left-axis, Figures 3 and 6), it was anticipated that scale-up to a commercial BOF would be difficult using a direct absorption method. Modifications were made following the second pilot-scale field trials to enhance the laser-absorption sensor by incorporating high-frequency modulation and phase-sensitive detection methods. These tools improve discrimination against background thermal emission from the off-gas.

Off-gas Emission Measurements. Emission spectra for the second pilot-scale field trial were acquired with the MDA-based sensor system incorporating the following changes: (1) incorporation of high-speed data acquisition capabilities; (2) improvement in data acquisition software, including pixel-to-pixel response normalization; (3) integration of larger collection optics; (4) addition of a larger grating, improving the collection efficiency of the spectrometer; and (5) incorporation of a high-temperature emission source into the experimental setup for alignment and line-width calibration.

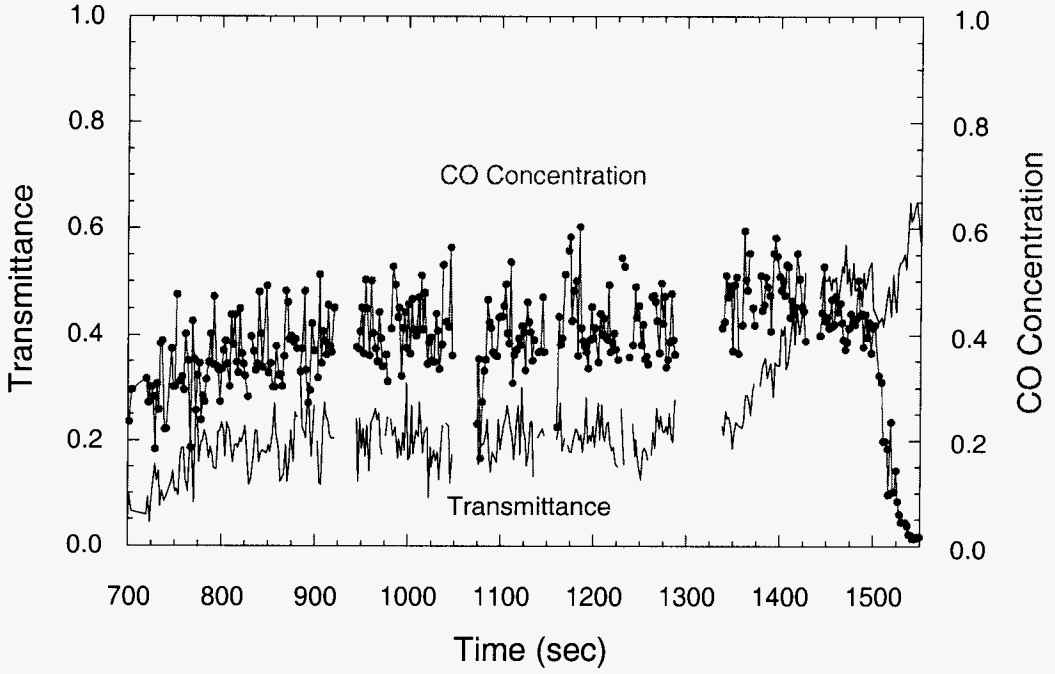

Figure 6. CO concentration (upper curve) and TDL transmittance (lower curve) during oxygen blowing for heat 3 of the second pilot-scale field trial.

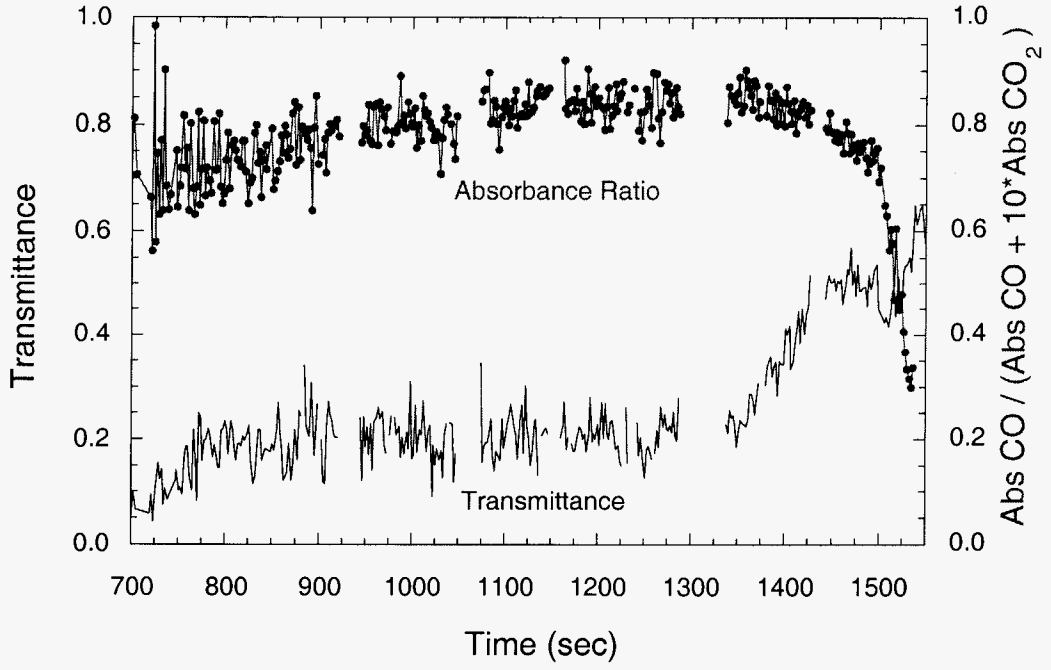

Figure 7. Absorbance ratio Abs_{CO} / (Abs_{CO} + 10*Abs_{CO2}) (upper curve) and TDL transmittance (lower curve) during the oxygen blow for heat 3 of the second pilot-scale field trial.

An example of data collected with the emission sensor is shown in Figure 8. The off-gas emission signal is presented for two "computer times" during the first heat of the trial (oxygen blowing began at 103 seconds for this heat). The observed emission signal consists of two distinct components: (1) a series of discrete emission lines; and (2) a constant offset from the horizontal axis. The distinct features are due to CO and CO_2 molecular emission for various vibration-rotation transitions. The offset of the baseline is due to broadband emission from both particulates and closely spaced CO_2 molecular vibrations. This broadband emission component does not interfere with the measurement of gas-phase CO emission lines in these pilot-scale field tests.

The stronger series of evenly spaced emission lines in Figure 8 are due to v=1 $\rightarrow$ v=0 transitions in CO vibrational energy levels (so-called $v_{1\text{-}0}$ transitions). Additional weaker features due to CO hot-band transitions that are $v_{2\text{-}1}$ transitions are also observed. The relative intensity of these lines can potentially be used to calculate temperatures and concentrations in a manner analogous to the results for the TDL absorption sensor described above.

During different heats, the emission sensor optics was aligned on: (1) the fiberfrax heat-shield insulation on the far side of the BOF; (2) a hole in the far-side heat shield with a room-temperature background; and (3) the water-cooled oxygen lance. During the first two heats, when the operators lowered the sample lance into the BOF, the sample lance intercepted the line-of-sight and became the background target. The effect of this cold object on the signal is demonstrated very clearly in

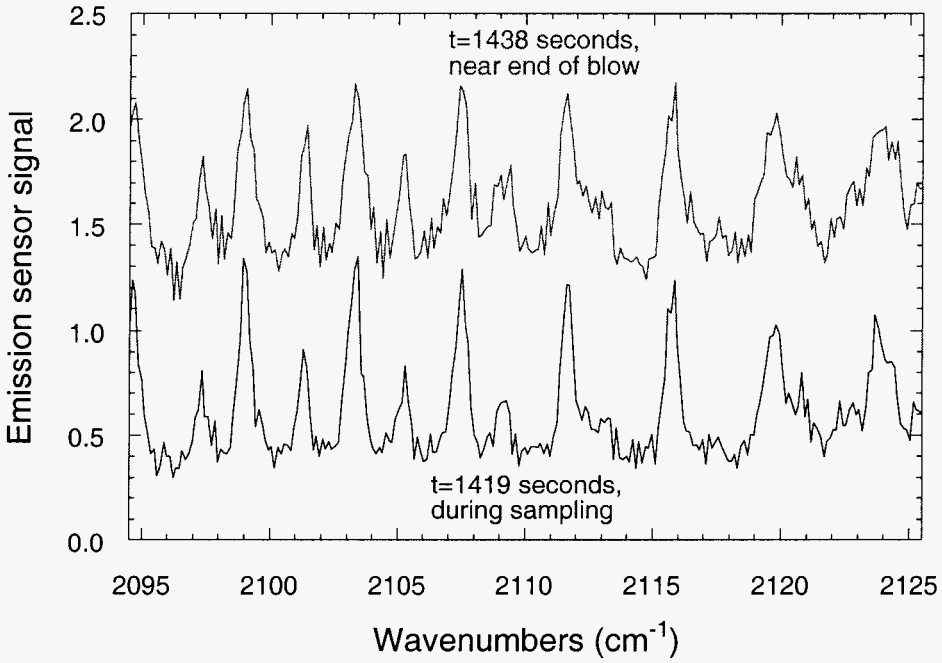

Figure 8. Emission sensor signal during the oxygen blow for heat 1 of the second pilot-scale field trial: through entire off-gas flow (top curve), and with the sample lance shortening the line of sight (bottom curve).

Figure 8. During most of the oxygen blow, particulate greybody emission contributed significantly to the background emission, as seen in the upper curve. However, when the sample lance was lowered into the line of sight, much less broadband radiation was observed.

The data analysis algorithms for the off-gas emission sensor were not mature at the time of the second pilot-scale field trial. A simple analysis of the results for three different wavelengths (a v_{1-0} emission feature, a v_{2-1} emission feature, and a wavelength where no molecular emission is observed) is presented in Figure 9. In order to clarify changes in the gas-phase emission features, the difference between the v_{1-0} and v_{2-1} emission features and the greybody emission as a function of time are shown in Figure 10. While both the discrete CO emission and the broadband emission drop sharply at the end of the heat, the v_{1-0} emission first *increases*, then decreases. In contrast, the v_{2-1} emission signal and the greybody background signals are reasonably flat with a sudden decrease at the end of the heat.

Emission signals for all three heats during the field trial were recorded. While the overall signal levels and emission levels varied from heat to heat, the contrast between discrete CO emission and greybody particulate emission followed the same pattern for each heat over similar time scales. Once ignition occurs, a brief increase in the gas-phase emission, a plateau for approximately 500 seconds, and then a sharp increase, followed by a rapid fall to zero emission are observed.

Three factors influence the contrast between gas-phase emission features and greybody particle emission: (1) the *molecular emission*, which changes with the concentration and temperature of CO molecules emitting in the detector's field-of-view; (2) the *greybody emission*, which changes with particle size, number density and temperature; and (3) the sensor's *field-of-view*. The term, *field-of-view,* refers to the volume from which the emission is generated and ultimately arrives at the detector. A similar term, *line-of-sight*, denotes the geometric optical axis available to the detector. Another important phenomenon that affects the detected gas-phase emission signal is *self-absorption.* Emission radiated by CO molecules along the sensor's line-of-sight that does not reach the detector due to reabsorption by intervening CO molecules is said to be self- absorbed.

Evidence of self-absorption in the pilot-scale BOF is seen in Figure 8, recorded during the first heat of the trial when the line-of-sight ended at the fiberfrax on the far-side heat shield. The relative contrast between v_{1-0} and v_{2-1} line emission intensities increases considerably when the sample lance is lowered. At t = 1438 seconds (upper curve), the detector's field-of-view for v_{1-0} emission extends only part way across the furnace off-gas stream. This means that v_{1-0} emission from CO molecules on the far side of the off-gas column does not reach the detector, due to reabsorption by intervening CO molecules. Therefore, when the sample lance is lowered, the intensities of the v_{1-0} emission lines do not change substantially. Conversely, the relative intensities of the CO v_{2-1} lines decrease when the sample lance is lowered. Evidently, the field-of-view for the v_{2-1} emission lines extends past the center of the off-gas flow, and the sample lance has blocked a significant number of CO v_{2-1} emitters.

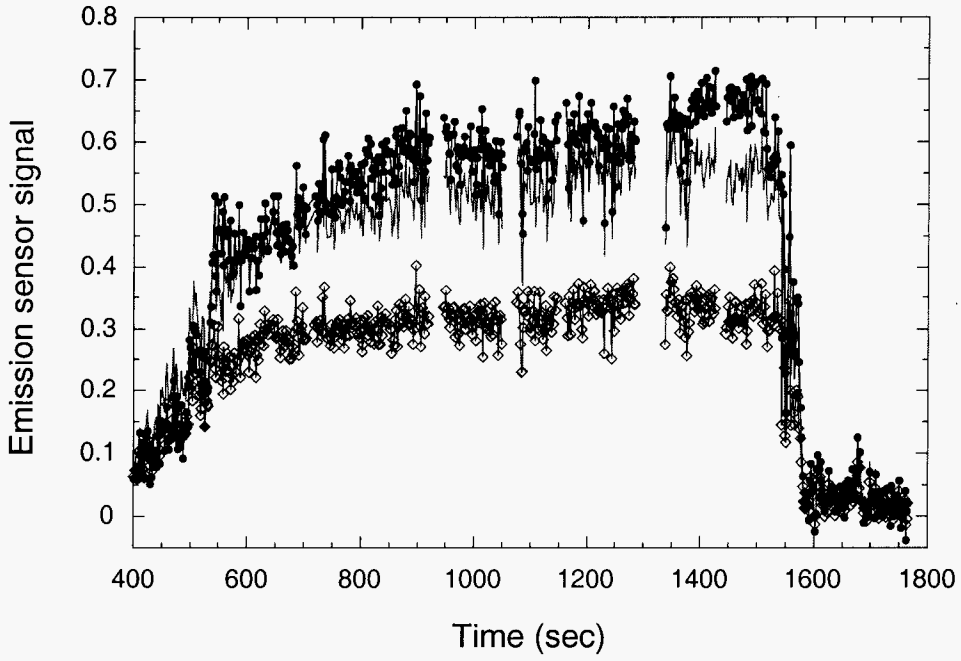

Figure 9. Trends in the v_{1-0} emission (top, filled circles), v_{2-1} emission (middle), and background greybody emission (bottom, open diamonds) during heat 3 of the second pilot-scale field trial.

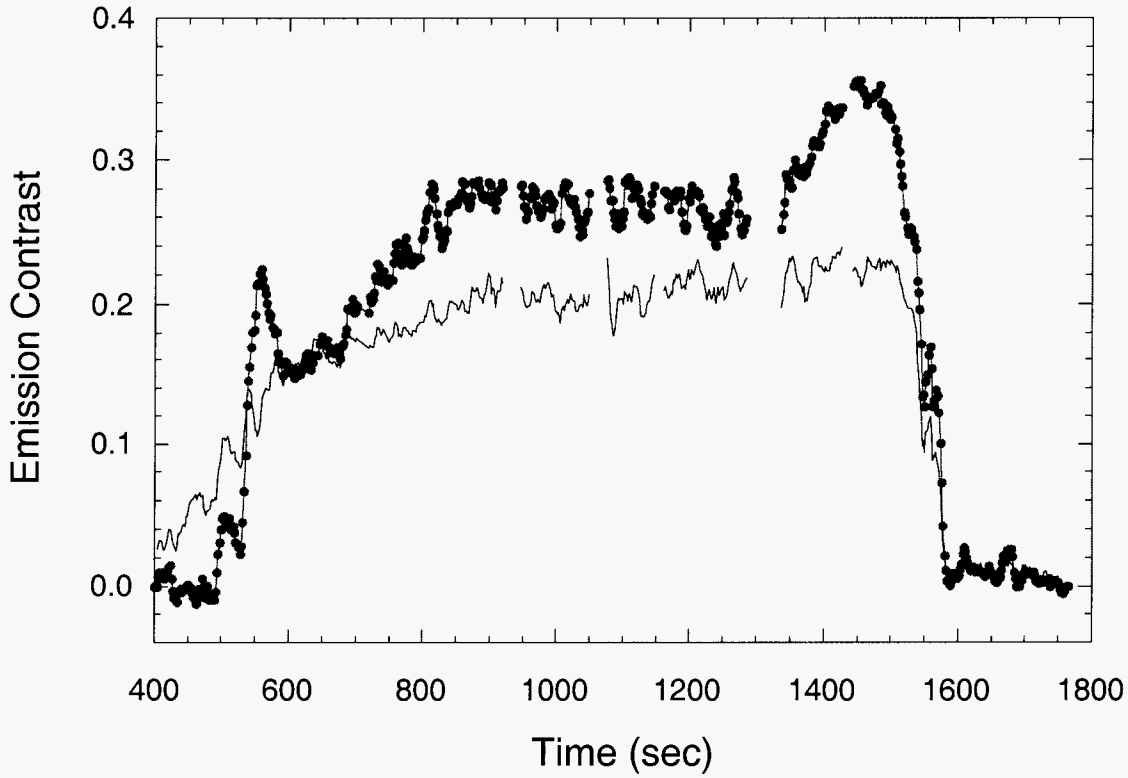

Figure 10. Change in the v_{1-0} emission contrast (upper curve) and the v_{2-1} emission contrast (lower curve) during heat 3 of the second pilot-scale field trial.

The ultimate success of a high-resolution off-gas emission sensor depends upon the contrast between discrete gas-phase emission lines and the featureless particulate greybody emission. The amount of contrast is determined largely by the sensor's field-of-view along its line of sight. The results of the June 1994 field trial suggest that a sensor field-of-view extending several feet to the oxygen lance in a full-scale BOF will result in an emission signal dominated by greybody particle emission during the initial period of the oxygen blow.

A simpler emission-sensor design with either low spectral resolution or a fixed wavelength response will be evaluated during later stages of the project. Although such a sensor system will not be capable of measuring either off-gas temperature or concentration, its time-dependent response during the final stages of melt decarburization may offer a simple means of real-time carbon control.

3.3 December 1994 Field Trial

A third series of pilot-scale field trials is conducted during December 5-7, 1994. Goals for this final series of experiments were to fabricate and test modular sensor packages, demonstrate increased sensitivity for both laser-absorption and off-gas emission sensors, perform intensive metal sampling during oxygen blowing, and determine dust loadings in the pilot-scale BOF off-gas by extractive sampling in the exhaust duct.

Modular packages for the optical hardware in both absorption and emission sensors were designed and fabricated. These new designs made it possible to ship equipment from California to Pennsylvania with a minimum of assembly and alignment. The time required to set up the equipment prior to the trials was reduced by 50% in comparison to previous pilot-scale tests.

Off-Gas Laser-Absorption Measurements. Major improvements were made in the sensitivity of the laser-absorption sensor. While the previous sensor configuration yielded excellent results for CO and CO_2 in the pilot-scale BOF off-gas, severe attenuation of the tunable diode laser (TDL) beam was anticipated at a full-scale BOF due to particle scattering over an optical path length of a few meters. Accordingly, a method was developed incorporating high-frequency modulation of the TDL beam with phase-sensitive "lock-in" detection to overcome this problem. A rotatable filter wheel in the laser transmitter module allowed the team to simulate increased particle scattering by attenuating the laser power by factors of 10, 100, 1000, and 10,000 prior to transmission through the particle-laden off-gas.

After stable ignition in the BOF was achieved, the lock-in signal for each attenuation factor was evaluated. Results for individual spectra are shown in Figure 11. Each spectrum in the figure consists of two components. The upper curve is the raw detector output showing a combination of sharp gas-phase absorption line features due to CO and CO_2, a sloping baseline due to variations in laser power output with wavenumber, and a large offset from zero due to greybody emission from particles in the off-gas. The lower curve is the lock-in amplifier output at the second harmonic of the laser modulation frequency. This is similar to a mathematical second-derivative of the raw signal, and as a result, linear slopes and constant offsets are eliminated leaving derivative line shapes of the gas-phase absorptions with a zero baseline.

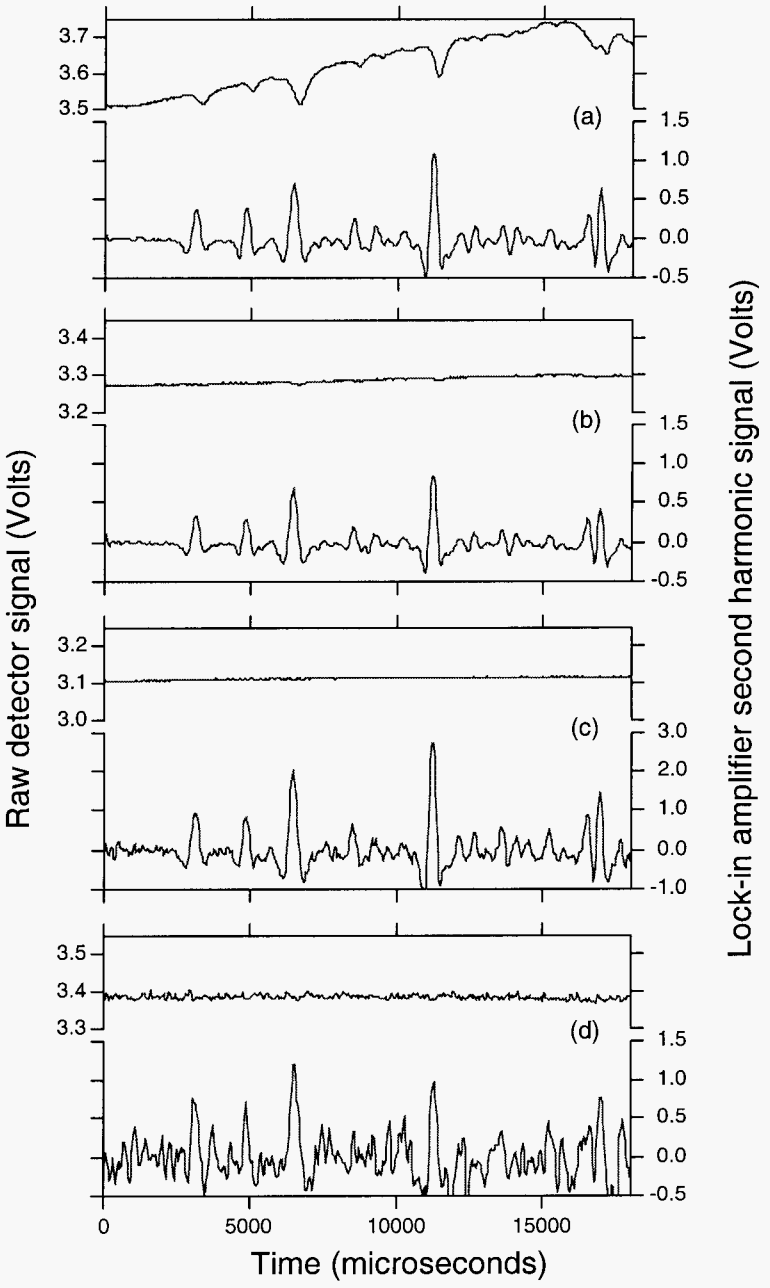

Figure 11. Attenuation of tunable diode laser during oxygen blow at pilot-scale BOF. Top curves - detector output in direct absorption mode; Bottom curves - lock-in amplifier second-harmonic signal: (a) no attenuation; (b) attenuation factor = 10; (c) attenuation factor = 100; (d) attenuation factor = 1000.

Comparing the upper curves for each laser attenuation factor, the detector signal is seen to rapidly diminish, and it is unlikely that accurate gas-phase temperature and concentrations could be extracted from attenuation factors of 10 or greater. On the other hand, characteristic gas-phase lines are seen at an attenuation of 1000, and these results are used below in evaluating predicted sensor performance at full-scale. This approach was crucial to the success of the laser-absorption sensor, and was incorporated into the equipment prior to full-scale testing.

Determinations of the off-gas temperature and concentration were comparable with laser-absorption sensor results in the two previous pilot-scale field trials. A concerted effort was made to obtain several metal samples toward the end of oxygen blowing in order to correlate carbon content with our sensor signals. Sampling is accomplished using an installed sample lance on the pilot-scale BOF. It is technically very challenging due to the very thin layer of metal present at the bottom of the furnace during these one-ton heats. An excellent series of samples was obtained for the heat on December 7, and the results are presented in Figure 12.

Percent carbon content is plotted along with maximum laser transmittance and a ratio of CO and CO_2 absorption line intensities. Sampling times are clearly indicated in the laser transmittance record as drop-outs in the data due to blocking of the laser beam by the sample lance. Clearly discernible differences in both transmittance and absorption ratio trends occur near the sampling point at 1300 seconds. Carbon content at this time in the oxygen blow was 0.67% and suggested that the absorption sensor may provide valuable endpoint information for steel with a wide range of desired carbon content.

Large fluctuations in both laser transmittance and absorption intensity ratios are observed near 1350 seconds for this heat. A large increase in carbon monoxide temperature also occurs at this time, rising from an average value of 1450° K (2150 °F) to 1600° K (2420 °F). This unusual upset condition may possibly be due to either large slag deposits falling from the exhaust hood into the furnace, or due to reactions of highly oxygenated slag during the later stages of oxygen blowing. In either case, the absorption sensor measurements allow the team to follow its effects on off-gas composition and temperature quantitatively and in real-time.

An analysis of dust loading in the BOF off-gas was also performed by Bethlehem Steel personnel during these field trials in order to quantitatively determine the volumetric mass loading and accurately predict the performance of our optical sensors at full-scale. Stainless steel extraction probes were installed in the exhaust duct above the BOF, and from four to six discrete, time-averaged samples were obtained throughout oxygen blowing for each of the three heats. An example of results obtained is shown in Figure 13.

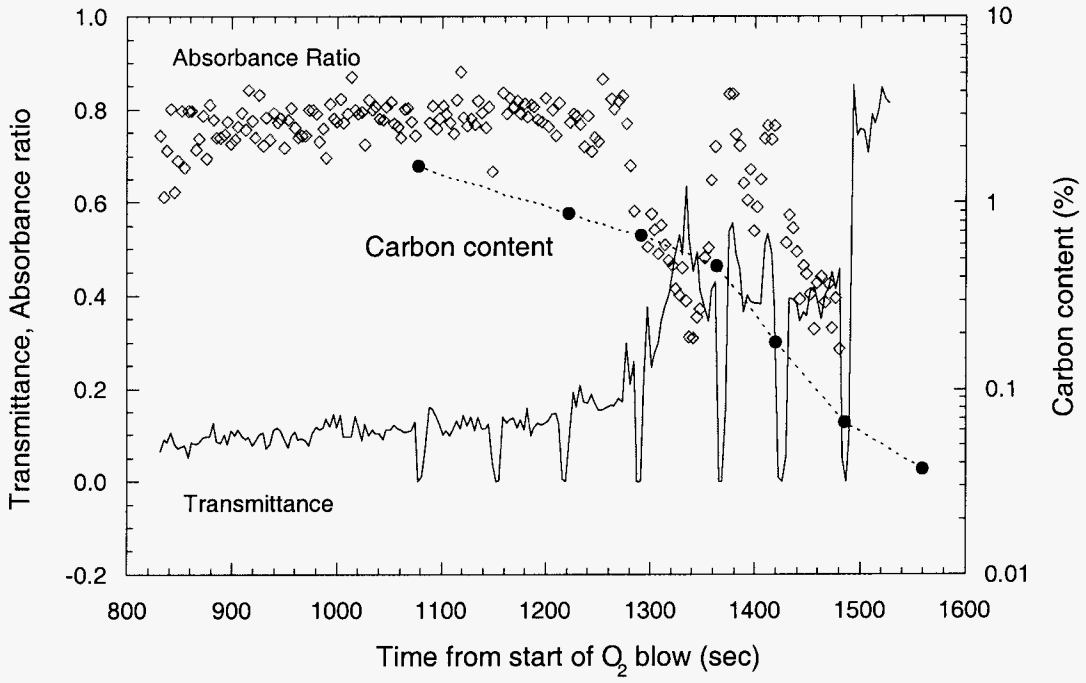

Figure 12. Comparison of metal carbon content (filled circles, right-hand axis) with laser transmittance (solid curve, left-hand axis) and a ratio of absorption line intensities, $Abs_{CO}/(Abs_{CO}+f*Abs_{CO2})$ (diamonds, left-hand axis) during oxygen blow. The sample lance causes dips in the laser transmittance.

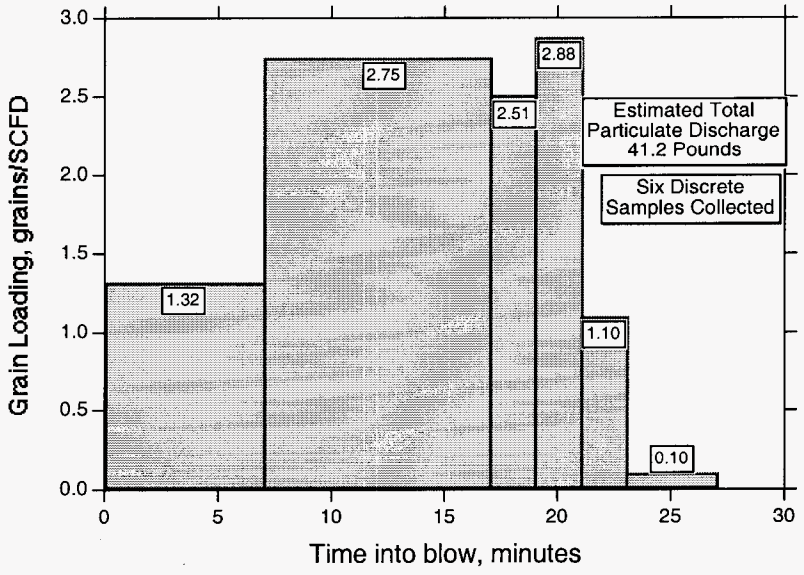

Figure 13. Volumetric mass-loading of dust in BOF off-gas as a function of blowing time for heat on December 7.

Results from the three heats indicated an average total weight of particulate discharged equal to 20.5 kg per metric ton (41 pounds per ton) of steel during a heat. This quantity is comparable to full-scale BOF performance and gives the team confidence that these pilot-scale measurements may be used to accurately simulate full-scale BOF processes. On the other hand, the average overall particulate loading was 4.2 gm/std.-m^3 (1.84 grains/SCFD), a figure that is less than one-half of the value measured for off-gas in commercial furnaces. This confirms the team's conjecture of significant air entrainment and resulting dilution of the off-gas along the optical sensor line-of-sight in previous trials at the pilot-scale furnace.

Off-Gas Emission Measurements. Significant improvements in sensitivity were demonstrated for the modular emission sensor package during this series of pilot-scale tests. Reductions in both random noise and artifacts caused by the nature of the bilinear-array detector were achieved. Sensor output with a spectrum analyzer during a portion of the oxygen blow was also measured. The results of these heats suggested a method for further significant improvements in sensor signal-to-noise ratio.

Improved emission spectra of the off-gas acquired during the final pilot-scale field trial demonstrated a serious obstacle for deployment of this sensor method at full-scale. It was found that the optical depth into the off-gas probed by the sensor during most of the oxygen blow is extremely limited. This is shown by comparing emission and absorption sensor signals measured at the same time during oxygen blowing in Figure 14.

Two emission spectra are presented in the lower half of the figure. The lower curve for a path length of 14 cm (5.5 in.) was acquired when the sample lance was lowered into the sensor's field-of-view, and well-defined emission lines principally due to CO are observed. For a path length of 35.5 cm (14 in.) as shown in the upper curve, greybody particulate radiation has almost obscured the structure of the gas-phase emission lines. This is caused not only by particulate emission, but also by gas-phase self-absorption of emitted light along the sensor's line-of-sight. The team predicts that the emission spectrum will rapidly approach a straight line with increasing path length.

Sensor Selection for Full-Scale Testing. The lack of contrast between gas-phase and particulate emission at increasing optical depths is compounded by the limited spectral resolution of the emission sensor. This is shown by a comparison with laser-absorption sensor data at the same time in the oxygen blow in the top portion of Figure 14. Although the spectral tuning range of the diode laser absorption sensor is only 10% that of the emission sensor, the information content is vastly greater. Relative intensities of several sharp, well-defined transitions are completely resolved with the absorption sensor and are used directly in calculating gas-phase concentrations and temperatures. Even if the signal-to-noise response of the emission sensor could be dramatically improved, these same spectral features are overlapped and obscured by self-absorption for the relatively short pathlength in the pilot-scale furnace off-gas.

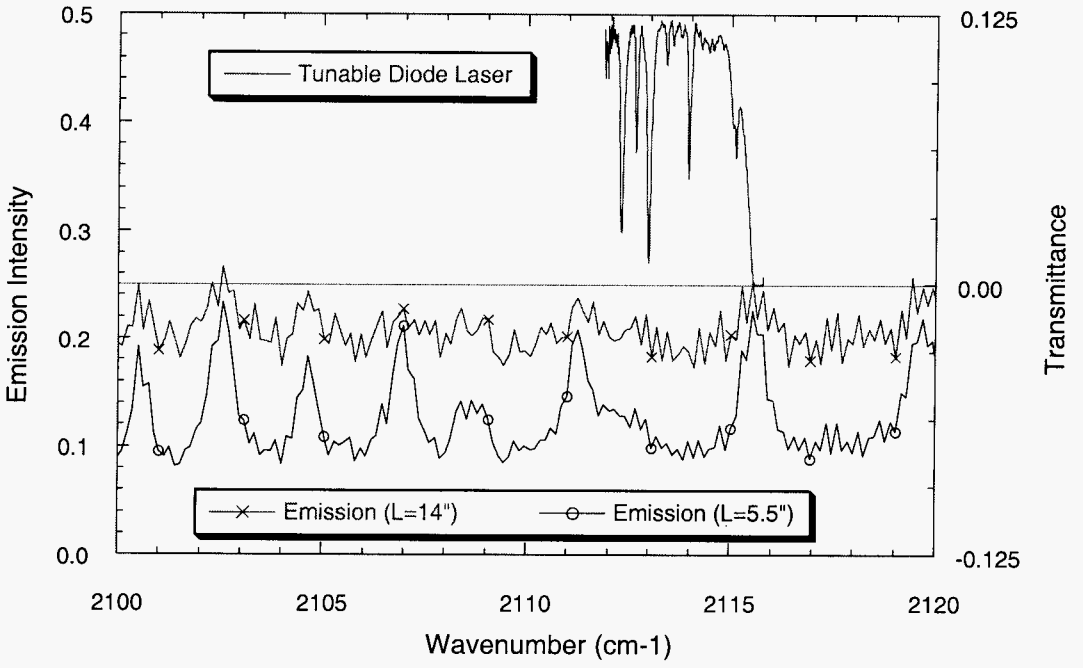

Figure 14. Comparison of emission sensor signals (lower two curves, left-hand axis) with absorption sensor signal (upper curve, right-hand axis) at the same time during oxygen blowing. Optical path lengths through off-gas indicated in parentheses.

For these reasons, work on the high-resolution emission off-gas sensor was suspended, and efforts were concentrated on further work on the development of the laser-absorption sensor for full-scale testing. Emission from the combined gases and entrained particulates in the furnace off-gas can be measured with the laser-based sensor's detector system at a fixed wavelength in the mid-infrared spectral region as defined by an associated optical bandpass filter. Possible correlation of this real-time signal with process variables (such as final turndown bath carbon and temperature) will also be examined during full-scale testing of the laser-based sensor.

4. Full-Scale Testing

Despite the increased sensitivity of the laser-absorption sensor and the high quality of the spectroscopic data obtained at the Homer Research Laboratory tests, scale-up of this sensor presented many challenges. The most significant anticipated difficulty at full-scale was laser-beam attenuation due to particle scattering. Maximum optical path lengths for the current sensor configuration were calculated based on both the dust loading measurements from the third pilot-scale field trials, and on dilution factors for CO concentrations in all three sets of field trials. These results are in good agreement and suggest that the present sensor can penetrate a distance of about 3 meters (6.5 feet) through a full-scale BOF off-gas flow. Due to the possibility of errors in these calculations (one way or the other), and the expense associated with sensor installation, it was felt prudent to carry out interim optical absorption experiments to guide the placement of the sensor package at a commercial BOF shop.

4.1 Full-Scale Feasibility Test: April 1995

A full-scale feasibility test of a laser-based off-gas sensor was carried out in April 1995 at the Bethlehem Steel BOF shop in Bethlehem, PA. The tests were extremely successful, as shown in Figure 15, demonstrating easily measurable transmittance throughout each of three heats. A CO_2 gas-laser operating at 10.6-μm wavelength was used for the tests. Attenuation due to particle scattering at this longer wavelength is reduced in comparison to our TDL pilot-scale measurements near 4.7 μm.

Analysis of the April 1995 field-trial data showed that several decreases in the observed laser transmittance were caused by variations in laser power, and did not reflect changes in the off-gas (Figure 15). Furthermore, dropouts in the data at 750-850 and 950-1100 seconds elapsed time are due to unsuccessful attempts to decrease the laser attenuation and increase the measurement sensitivity. These changes resulted in excessive laser output that saturated the detector. Missing data during these intervals are not due to any changes occurring in the steelmaking process.

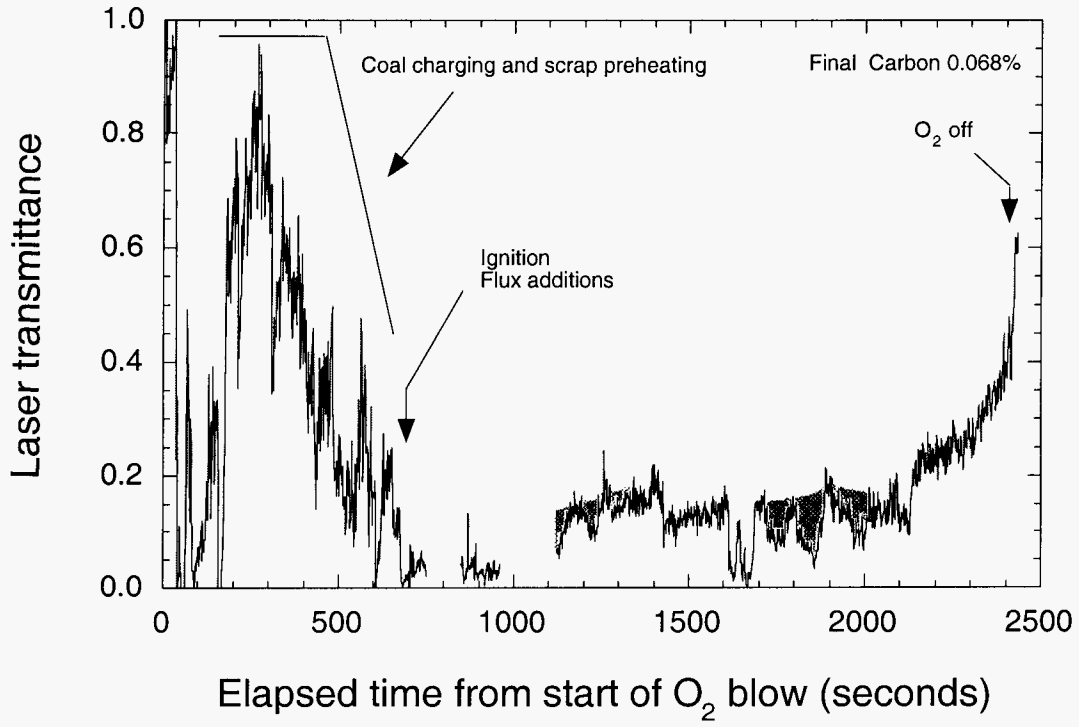

Figure 15. Record of laser transmittance during April 1995 field trial. Note that decreases in the laser transmittance, indicated by shaded regions, are due to variations in laser power.

Six periodic decreases in laser output power were detected with a reference calorimeter in the laser-transmitter module (the nature of this detector unfortunately does not permit the team to quantitatively correct for these changes in laser power). These events are indicated in the figure by shaded regions at 1100-1350 and 1700-2000 seconds elapsed blowing time. When the laser transmittance is properly normalized for changes in power output during these intervals, the sensor output is surprisingly uniform during the course of the oxygen blow following ignition.

Two major decreases in laser transmittance are observed at 1600-1700 seconds elapsed time, followed by a smaller decrease near 2100 seconds. These variations are clearly process related, but their origin is unknown. A pronounced increase in laser transmittance during the final 300 seconds of blowing time is also observed. Since the infrared laser beam is not affected by changes in CO concentration, and is only weakly absorbed by CO_2 in the off-gas, the increase in transmittance must be due primarily to a corresponding decrease in dust loading at the end of the oxygen blow. The final carbon content for this heat was determined to be 0.068%.

Extrapolating from these results to a TDL-based sensor is complicated since the CO_2 laser transmittance is affected by three principal variables: particle scattering, CO_2 gas-phase absorption, and CO_2 gas-phase temperature. Estimates for the gas-phase concentration and temperature and a value for particle scattering efficiency at this wavelength were made. Output from Mie-scattering calculations using particle diameters of 0.2 - 1.0 μm and optical constants for FeO were combined with the laser transmittance measurement to estimate the TDL sensor performance at shorter infrared wavelengths.

The results indicate a beam attenuation of six to seven orders of magnitude at 4.7 μm for the full-scale BOF off-gas conditions, and represented a significant challenge for full-scale field trials of the TDL-based sensor. The results for the full-scale measurements, however, are approximately two orders of magnitude more favorable than extrapolations from the pilot-scale tests on the two-ton BOF, and thus offered a reasonably good chance of success for this sensor.

4.2 Full-Scale Sensor Testing and Prototype Development

Based on the successful feasibility tests, the team continued with the development and testing of a TDL-based off-gas sensor at Bethlehem Steel's Sparrows Point plant in Baltimore, MD. Sandia and Insitec personnel made a two-day visit to the plant during July 1995 to determine optimal locations for sensor placement, necessary plant modifications for sensor installation and testing, and alterations in sensor design required for mill-hardening.

4.2.1 Site Visit to Bethlehem Steel's Sparrows Point Plant

A detailed examination of the area surrounding the furnaces showed that an optical line-of-sight existed between the furnace mouth and the bottom of the off-gas exhaust hood. This was determined by observing a beam from a hand-held visible diode laser through existing openings in the surrounding heat shield walls. A schematic drawing of the installation location is shown in Figure 16.

Temperatures of the ambient air at locations where the equipment could be installed ranged between 140 and 180 °F. In view these results, increased thermal insulation and active cooling were mandatory for the enclosures surrounding the infrared absorption sensor modules. Bethlehem Steel

applied additional insulation to the heat shield walls in the vicinity of the Sandia equipment to minimize radiant heat loads.

Due to these high ambient temperatures, time spent by personnel in the installation and alignment of the laser and detector modules was necessarily limited. Electronically driven mirror positioners for both laser- and detector-modules were acquired. These devices can be computer controlled, and facilitate remote laser-beam alignment as well as minimizing exposure time for personnel adjacent to the heat shield.

The equipment was exposed to occasional high levels of mechanical vibration, due primarily to process operations such as furnace deskulling, scrap charging and crane operation. To counter these effects, the team incorporated optical breadboard baseplates and rigid mounting fixtures for internal optical components.

A series of access panels was designed for the sensor modules to permit adjustment of internal optical elements without removal of the protective enclosures and resultant contamination of optical surfaces. These small openings also greatly reduced the heat load on the interior of the modules, thus decreasing alignment instability due to thermal stresses during installation and adjustment procedures. A positive pressure of a dry air purge gas was incorporated into the internal cooling system.

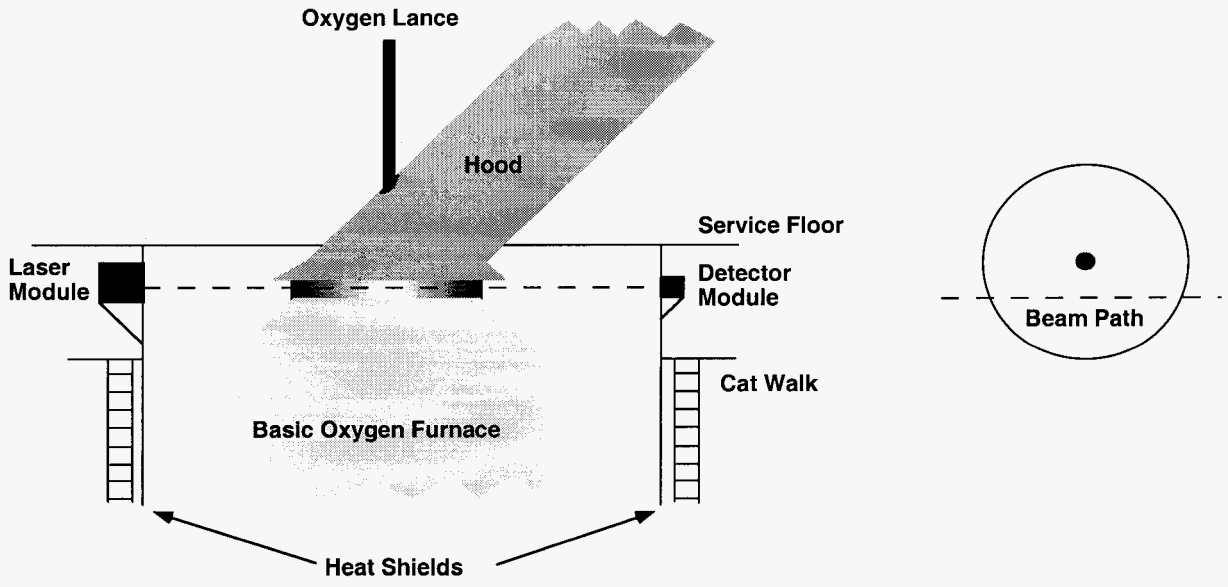

Figure 16. Schematic diagram of laser-absorption sensor installation on the heat shield walls of the BOF at Bethlehem Steel's Sparrows Point plant

The team also upgraded significantly the thermal insulation and cooling systems for both laser transmitter and receiver modules, and the sensitivity of the lock-in amplifier signal processing system. Improved narrow-band optical filters were acquired for the detector module in order to efficiently reject background thermal emission from the process off-gas. A method for combining a visible alignment laser-beam with the infrared TDL beam was incorporated into the laser transmitter.

Additional TDLs were acquired to provide access to spectral regions beyond the tuning range of the existing laser tested at the HRL. A shift to lower wavenumber (longer wavelength) was necessary to avoid extensive interference between CO_2 and CO absorption lines that lie in the same laser tuning range. The new diodes provided access to an additional 150 cm^{-1} of spectral tuning range.

Since the initial field trials were planned for only a few days duration, the data acquisition and analysis equipment was installed in a movable electronics rack and located on the charging floor near the laser transmitter module. This arrangement considerably reduced installation time and expense by minimizing cable runs from both laser and detector modules to the data acquisition system, although great care was required to minimize degradation due to air-borne particulates.

In preparation for sensor tests at Bethlehem Steel's Sparrows Point BOF shop, plant personnel installed ladders, working platforms and equipment mounting shelves on both sides of furnace #1 during the furnace reline in August 1995. These platforms are mounted to the furnace heat shields approximately 20 feet above the charging floor, and located directly above the furnace trunions.

4.2.2 January 1996 Field Trial

The first full-scale field trial of the laser-absorption off-gas sensor was performed from January 15 through January 24, 1996. Both transmitter and receiver modules were shipped fully assembled with minimal protection of individual optical components. Equipment set up was extremely rapid as a result. The use of a ruggedized electronics rack also was successful, since all electronics were shipped mounted in the rack and ready for operation. Sensor performance on the charging floor following unpacking was equivalent to laboratory values.

Following the equipment checkout and cable installation around the furnace, the team worked with plant personnel to hoist the transmitter and receiver modules into place on platforms located on each side of the BOF heat shield. The experimental arrangement is diagrammed above in Figure 16.

During the time between heats, the infrared laser-beam was aligned across the top of the furnace, into the receiver module, and onto the detector. The team was able to achieve only 25% of the maximum laser signal at the detector module, and this was reduced to 10% on following days. The reason for this reduction was due to a combination of poor alignment of transmitter and receiver modules on the heat shield mounting platforms, and degradation of mirror surfaces. These problems indicated that further improvements were needed in the design of the visible-laser alignment beam, and the protection of optical components from the harsh plant environment. The team also found that the very rapid build up of skull on the vessel mouth eventually interrupted the optical line-of-sight.

Improvements in narrow-band optical filtering for the detector module were very successful in these trials. Overlapping sets of spectral bandpass filters produced an extremely narrow bandpass near

2100 cm^{-1} (4.76 μm). This filter combination transmitted our infrared laser beam for tuning modes between 2085 and 2110 cm^{-1}, while attenuating broad-band background emission from the off-gas by a factor of two greater than the filter used in the pilot-scale experiments. As a result, the detector output was not saturated by the intense, broadband off-gas emission.

Off-Gas Sensor Measurements. Following the laser alignment and adjustments to our signal processing equipment, the team observed laser absorption patterns due to CO in the off-gas during the oxygen blow. These gas-phase absorptions were detected mid-way through two heats and were observed continuously during the remainder of oxygen blowing. *This accomplishment demonstrates the feasibility of tunable diode laser measurements of the off-gas in commercial scale steelmaking processes.* **(Major Milestone Achieved)**

The curve (a) of Figure 17 shows a reference spectrum of room temperature CO in a sealed gas-cell. The laser wavelength is scanned repeatedly in time (horizontal axis) in a triangular function at 1-Hz, first increasing, then decreasing. This scanning method was used to optimize the sensitivity of the signal processing equipment, and produces an absorption spectrum with mirror symmetry, as shown in curve (a). The laser beam was simultaneously modulated at a frequency of 20-KHz. When this reference signal is detected with a lock-in amplifier at the first harmonic of the modulation frequency, curve (b) results. This trace resembles the mathematical first-derivative of the raw detector signal, and also possesses the same mirror symmetry as curve (a).

The output from the signal detector, located in the detector module, is passed through a second lock-in amplifier tuned to the same 20-KHz frequency, and the result is shown in curve "c" for a measurement 12 minutes before the end of the oxygen blow. Although the signal-to-noise ratio of the BOF off-gas spectrum is low for these initial measurements, the mirror symmetry of the four most intense features (marked with asterisks) corresponds exactly with that of the reference spectra. This marks the first measurement of gas-phase absorption spectra in the off-gas of a commercial BOF.

Laser-Beam Alignment Stability. While laser transmission and detection during the oxygen blow were demonstrated in the first full-scale field trial, the team discovered that at the end of the blow the detected TDL signal was reduced to 1% of the level before the heat began. The team was able to restore the laser signal level by remotely adjusting the output mirror in the transmitter module. The large drop in detected laser-beam signal over the course of a heat proved to be due to a significant change in laser-beam alignment. The team did not anticipate this problem due to the excellent long-term stability of both visible and CO_2 laser beams during the tests at the Bethlehem BOF shop in April 1995.

Brief experiments following the January 1996 field trial by D. Brinker and P. Stelts of Bethlehem Steel Research showed that the furnace drive-side mounting platform for the entire transmitter module moved during the course of a heat. A very slight change in the vertical or horizontal angle of the mounting platform produced a large change in beam position over a distance of 10.7 m (35 ft), and beam displacements of up to 2 inches were observed. The magnitude of laser-beam drift easily accounted for the cyclical variations the team observed in the detected infrared laser-beam signal.

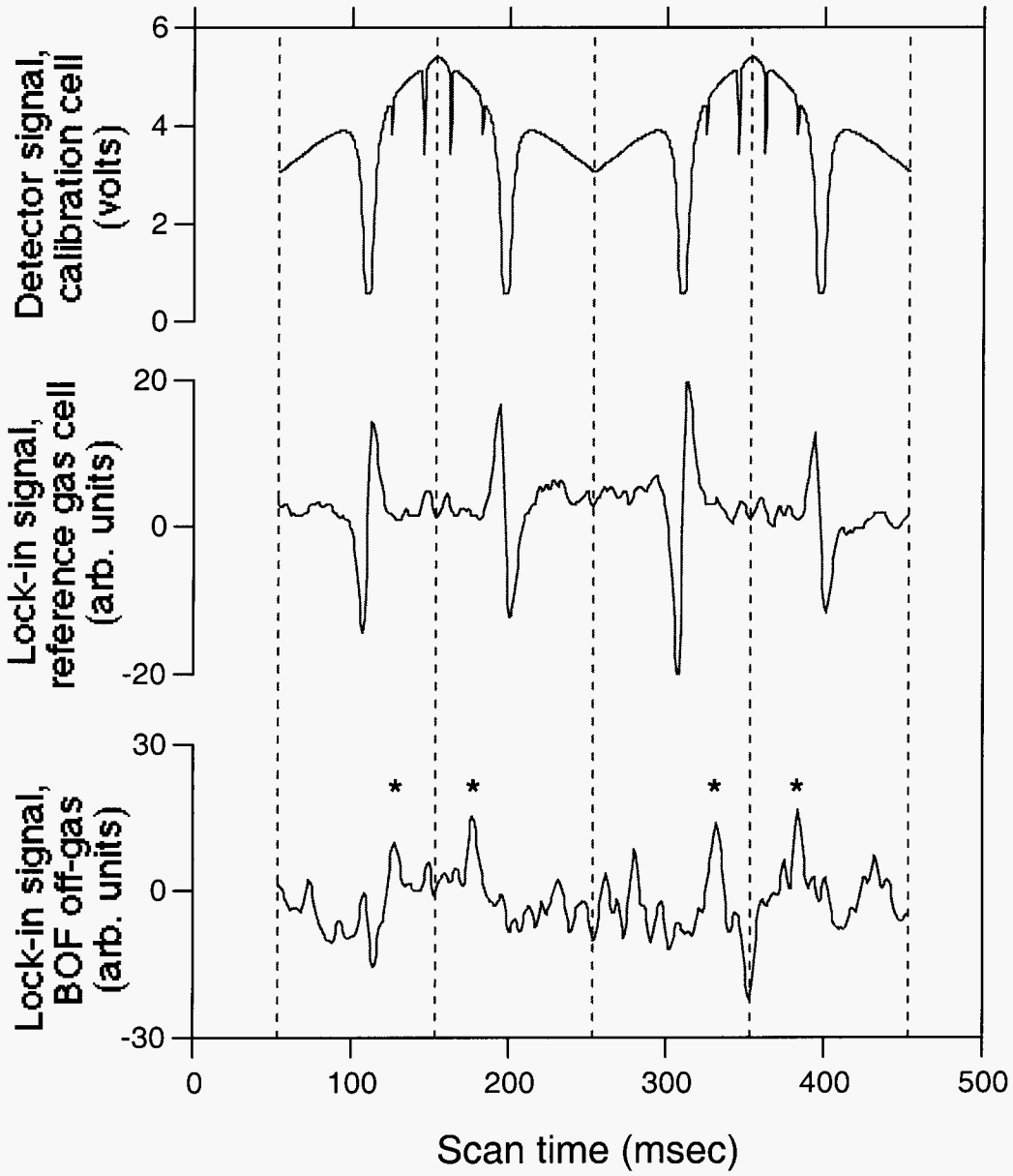

Figure 17. Tunable diode laser spectra obtained during a heat 12 minutes before end of oxygen blowing: (a) reference spectrum of room temperature CO in calibration gas cell; (b) lock-in amplifier first-harmonic ("1f") signal from reference detector; (c) lock-in amplifier 1f signal of off-gas absorption. Asterisks indicate strongest features in off-gas signal.

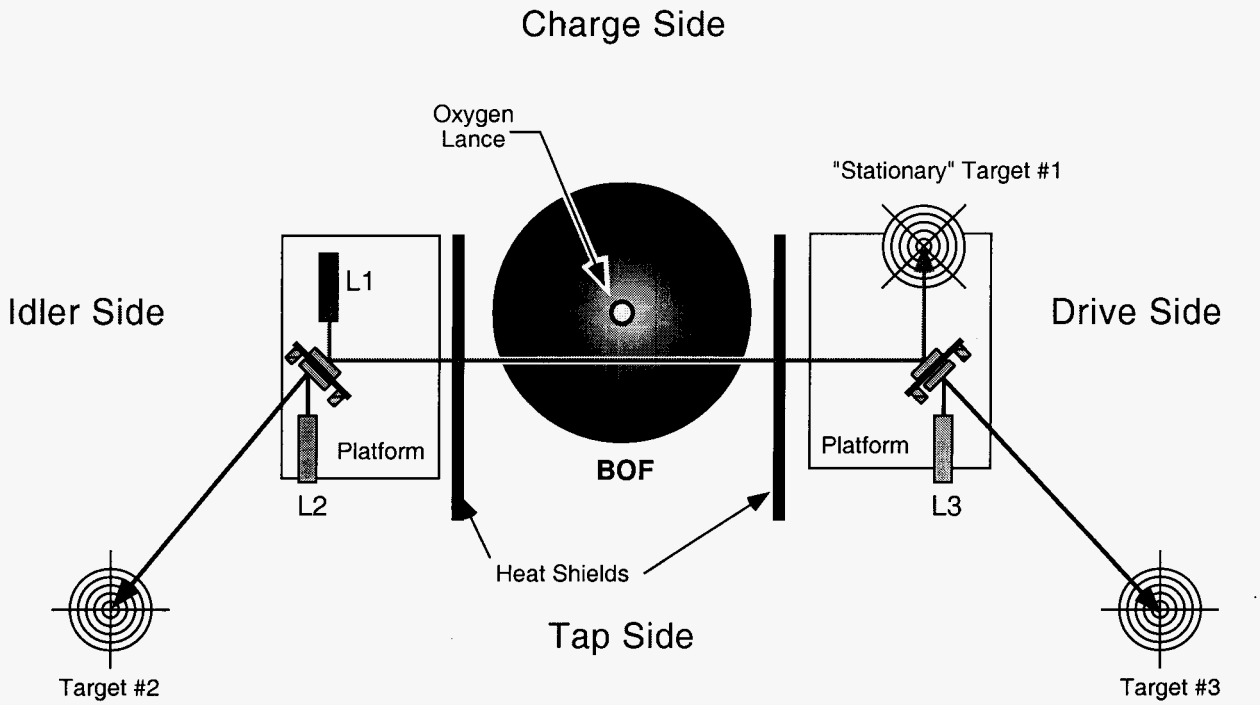

Figure 18. Experimental arrangement for assessing furnace idler-side platform stability. Laser 1 (L1) is mounted on idler-side platform (aimed through furnace off-gas at Target #1), and retro-reflected lasers (L2 and L3) are mounted on both idler and drive-side platforms (aimed at Targets #2 and #3 on charging floor).

An additional field trial was conducted in April 1996 to quantify the drift in laser-beam alignment. Three visible lasers were mounted on the equipment platforms as shown in Figure 18. Laser 1 was mounted on the furnace idler side and its beam was reflected from a remote-controlled mirror across the top of the BOF. Between heats this beam was reflected from a second remote-controlled mirror on the furnace drive side, and its position on Target #1 was monitored. The results for five heats are shown as open circles and crosses in both plots for Figure 19, and demonstrate a dramatic increase

in beam alignment stability (less than 0.25-inch displacement) simply by mounting the laser on the furnace idler side platform.

Mirrors were also attached to the backs of the two remote-controlled mirror mounts, and were used to reflect beams from the lasers 2 and 3 to targets on the charge floor (Figure 18). Since these laser beams did not pass through the furnace off-gas, they could be observed throughout a heat and were used to monitor independently the movement of both idler (Laser 2) and drive-side (Laser 3) equipment platforms. The results are shown as the filled circles and x's in Figure 19 for the idler side (upper plot) and drive side (lower plot). These measurements graphically demonstrate the far greater stability of the idler side platform. As a result, the team concluded that a straight-forward solution to the problem of laser-beam alignment stability was simply to interchange the mounting locations of the laser transmitter and detector modules.

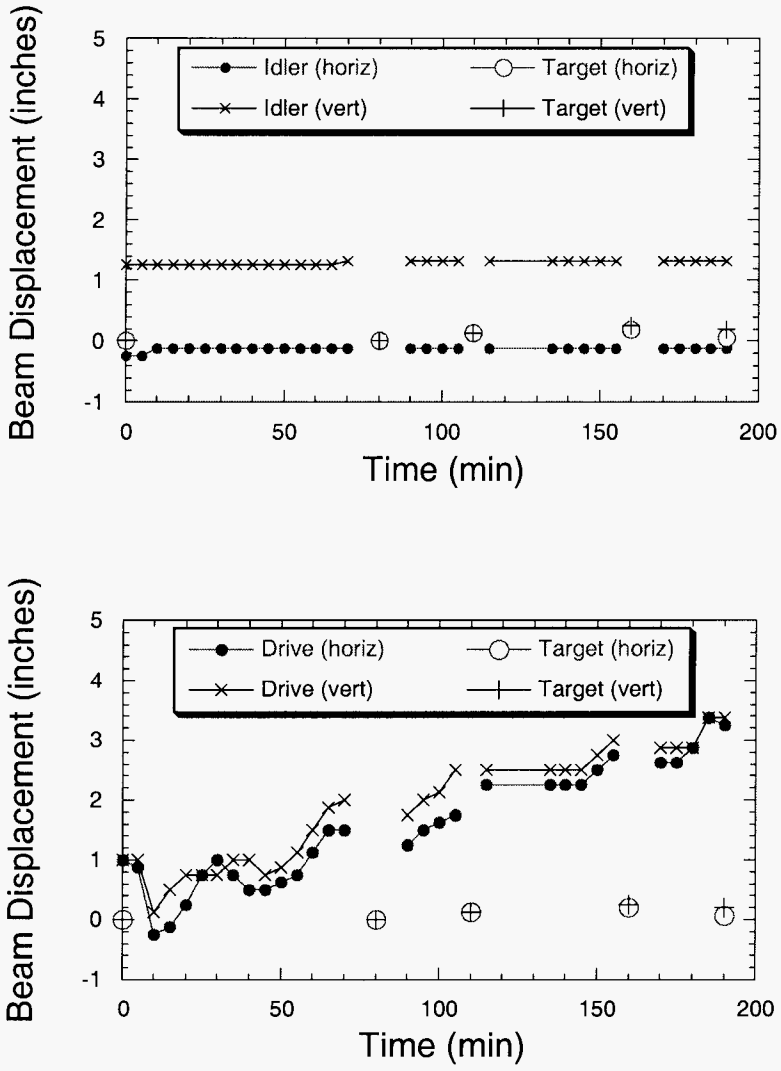

Figure 19. Vertical and horizontal stability of Laser-1 beam from idler to drive-side (open points, both plots), idler-side retro-reflected laser beam (upper plot), and drive-side retro-reflected laser beam (lower plot). Target laser mounted on furnace idler side.

Results of this field trial also showed that the motion of the target laser beam correlated quite well with a retro-reflected beam from the additional laser mounted on the furnace idler side. This feature was incorporated into a redesigned transmitter as a means for correcting the alignment of the infrared TDL beam during the oxygen blow. *The team anticipates that careful site characterization is necessary for future testing and commercial installations of the off-gas sensor, due to the unique aspects of each individual steelmaking shop. The procedure followed in this field trial will lead to a rapid definition of requirements for any necessary dynamic alignment correction to be built into the sensor package.* **(Major Milestone Achieved)**

4.2.3 June 1996 Field Trial

Off-Gas Sensor Enhancements. Several valuable lessons were learned in the January 1996 field trial of the off-gas sensor, and many improvements were incorporated into Sandia's sensor modules prior to the two subsequent field trials conducted in 1996. A hard-mounted bandpass optical filter was incorporated into the collimated TDL beam line. This component was then used to combine an overlapping visible laser-beam that remained aligned with the TDL infrared beam after shipping the module from Sandia to Sparrows Point. The stable overlapping of the laser beams allowed the team to align the infrared laser in less than 30 minutes following installation of transmitter and detector modules.

The alignment stability of the TDL beam was also greatly improved by simply interchanging the mounting locations of transmitter and receiver modules, and very little drift of the infrared laser beam was observed before and after a heat. Only small realignments of the beam were necessary to achieve full-transmitted power across the furnace mouth, and the team found it unnecessary to incorporate a dynamic beam alignment feature into the sensor transmitter module.

Severe contamination of optical surfaces in the first full-scale trials during January 1996 led to an improved design of transmitter and detector module enclosures. Gasket seals were incorporated around all ports, and sealed electrical feed-throughs were used for power and signal connectors. An air-purged window assembly was introduced for output and input optical beams in the transmitter and detector modules, respectively. These changes resulted in minimal dust intrusion into the modules during subsequent field trials.

Off-Gas Sensor Experimental Data. The primary goal of the June 1996 field trial was to enhance the sensitivity of the TDL off-gas sensor technique. Off-gas absorption spectra were measured for several different wavelength regions (2080–2120 cm^{-1}), TDL modulation conditions, and data acquisition parameters.

The improvement in laser-beam alignment stability greatly increased the strength of the sensor signal detected during oxygen blowing, and an example is shown as the solid curve in Figure 20. During these experiments, the wavelength of the TDL beam was modulated at levels comparable to the width of narrow absorption lines between 2091.3 and 2092.5 cm^{-1}. Strongly saturated absorption lines (such as the broad feature centered at 2090.7 cm^{-1} in the lower curve) are not efficiently amplified and result in the flat baseline observed in the upper curve at that wavenumber.

Comparison of the two curves in Figure 20 clearly shows an excellent correspondence between observed 2f-absorption lines in the BOF off-gas and narrow CO absorption lines in the calculated spectrum. The observed features in the off-gas spectrum are dominated by CO absorptions, although other smaller features in the 2f spectrum have been identified by high temperature laboratory spectra acquired at Sandia, and are due to CO_2 in the off-gas.

During the June 1996 field trial, it was noted that the laser beam was not uniformly transmitted through the off-gas over short time scales. Large variations in the 2f-line intensities were observed during the course of a single 1-hz scan of the wavelength range. Accordingly the data collection rate was varied in steps up to 80-hz in order to reduce the effect of these variations within a single wavelength scan. *During this field trial it was determined that a collection frequency of 40 hz was optimal for the sensor instrumentation package without resorting to faster and more costly data acquisition hardware.* **(Major Milestone Achieved)**

Formulation and Testing of a Software Algorithm. The team was not able to directly measure the gas-phase transmittance spectrum from which average line-of-sight gas temperatures and

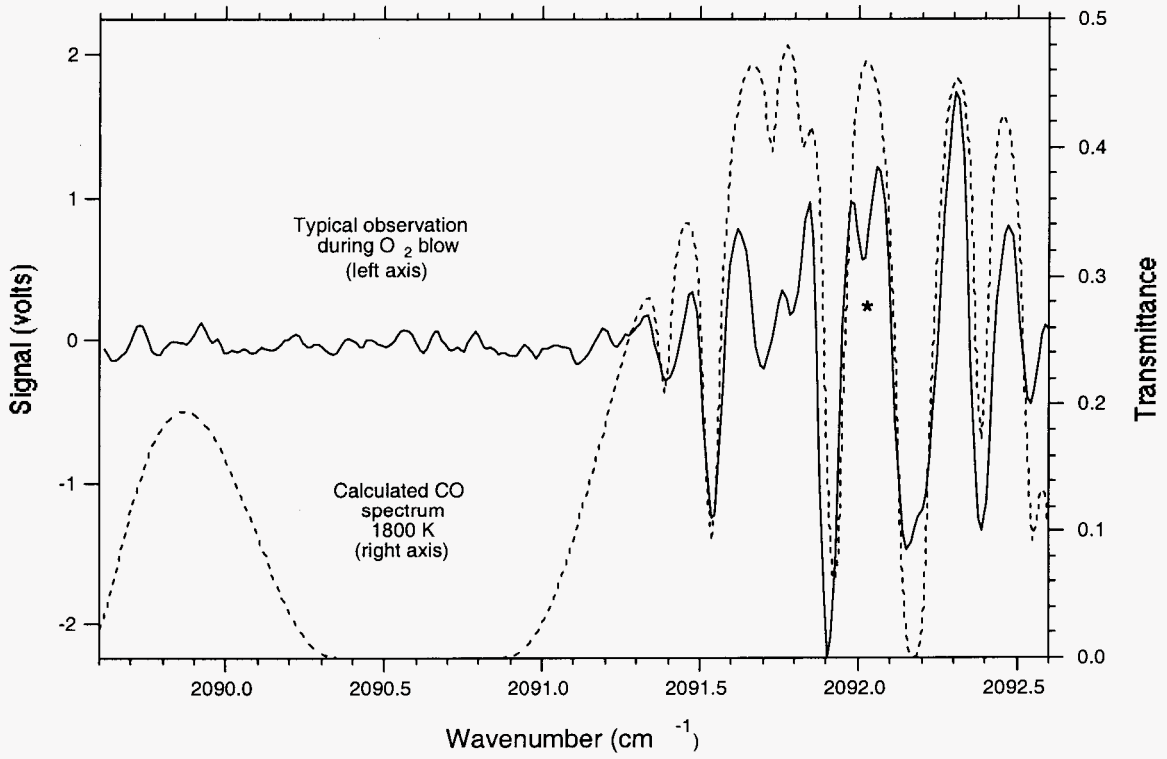

Figure 20. Correspondence of CO-absorption lines in the experimental 2f-absorption signal for BOF off-gas during oxygen blowing (upper curve) with calculated transmission spectrum of CO at 1800° K (2780° F) (lower curve). Feature marked with an asterisk is due to CO_2.

concentrations can be directly calculated. Since the laser-beam wavelength was modulated at a high frequency and a phase-sensitive lock-in amplifier was used to retrieve the second harmonic of the highly attenuated laser energy transmitted through the off-gas, well-understood absorption line profiles are converted by the lock-in amplifier into shapes resembling mathematical second derivatives.
The relationship between the transmission spectrum corresponding to the observed sensor output, however, is not a simple second derivative. Furthermore, simple analytical approximations developed elsewhere (Bomse, 1992) are not appropriate for converting these experimental 2f absorption features to simple transmission spectra due to the highly absorbing nature of the off-gas species. Accordingly, an algorithm was developed to compute the transformation of experimental or calculated transmittance spectra into lock-in-amplified, second-harmonic output signals

The algorithm accounts for several additional variables introduced during data acquisition and signal processing: (1) the amplitude of the high-frequency modulation relative to the line width of the off-gas absorption features; (2) electronic phase shifts introduced by the time response of the lock-in amplifier; and (3) changes in tunable-diode-laser output energy as the sensor is scanned through its wavelength range.

The accuracy of the algorithm can be demonstrated by application to laboratory gas-phase absorption lines for a variety of carbon monoxide line shapes and intensities, and to calculated CO absorption profiles for conditions similar to the off-gas from a BOF. Basically, the algorithm integrates the product of the original transmittance spectrum with the second harmonic of a high-frequency sine-wave component (representing the high-frequency modulation of the TDL wavelength) over the wavelength scan region. The amplitude of this sine wave is adjusted to match the amplitude of the experimental high-frequency modulation. Other terms are included in this step to incorporate the effect of the lock-in amplifier time constant. The result is then low frequency filtered to produce the output lock-in amplifier waveform, and is shown in Figure 21 for a well-characterized transmission spectrum obtained in the laboratory at Sandia.

The lower curve shows the measured transmission spectrum of a cell containing carbon monoxide in the 2089.8 to 2091.0 cm^{-1} region. The strong absorption feature at 2090.6 cm^{-1} is due to CO within in the cell (the cell pressure is adjusted so that the resulting absorption line-width is similar to that of high temperature CO in the BOF off-gas). The broader absorption feature at 2090.1 cm^{-1} is due to water vapor in the ambient atmosphere along the 10.7-m (35-ft) absorbing pathlength. The TDL drive current is then modulated at a frequency of 50-KHz with a sine-wave whose amplitude produces a wavelength modulation characteristic of the 2090.6 cm^{-1} line width, and the detector signal is amplified by the lock-in amplifier. The resulting second-harmonic (2f) lock-in amplifier output is shown in Figure 21 as the upper, solid curve.

The measured transmission spectrum (lower curve in Figure 21) is used as the input for the algorithm, and the resulting calculated 2f signal (upper, dashed curve) is in excellent agreement with the experimental 2f lock-in output signal (upper, solid curve). *This algorithm is successful at predicting experimental 2f signals for a variety of spectral features: overlapping lines, lines with different widths, lines of varying transmittance, and lines that are saturated. The example in Figure 21 shows excellent results for the two absorption features with different line widths.* **(Major Milestone Achieved)**

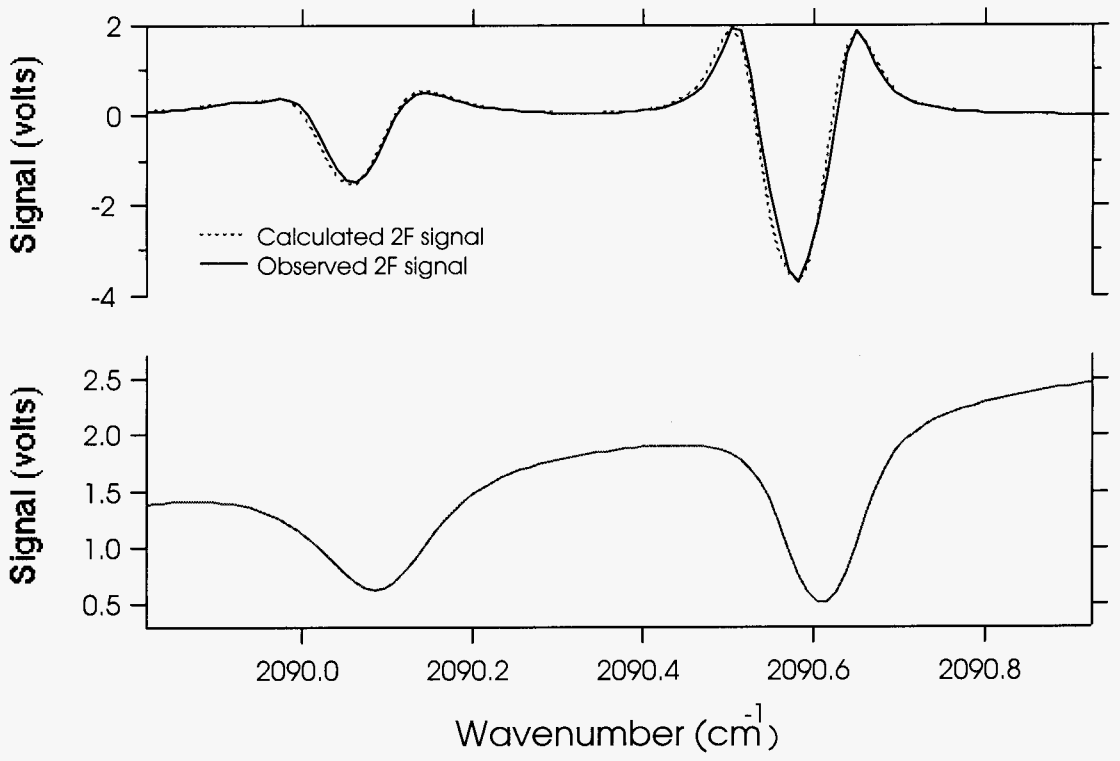

Figure 21. Experimental laboratory transmission spectrum of CO and water vapor (lower curve). Measured lock-in amplifier second-harmonic (2f) signal (upper, solid curve), and calculated 2f signal (upper, dashed curve).

Off-Gas Temperature Measurements. The algorithm was next applied to calculated transmittance spectra that simulate CO absorption spectra in the off-gas above a BOF during oxygen blowing. Since the amplitude of the high-frequency sine wave used to modulate the laser beam is known and held constant during measurements in the field, it is no longer a variable in the 2f-signal calculation. The remaining principal variables are the temperature and concentration of the absorbing gasses along the optical line-of-sight. Results for two simulations are shown in Figures 22 and 23. The lower, dashed curves in each figure are calculated transmittance spectra for carbon monoxide at a concentration of 50%, an absorbing path length of 3.7-m (12-ft), and temperatures of 1600° K (2420°F) and 1800° K (2780°F), respectively. The upper, dashed curves in both figures are calculated second harmonic signals generated from these input transmittance spectra. The calculated 2f-spectra are compared to an experimental sensor signal measured during oxygen blowing at Sparrows Point (upper, solid curves in both figures) in the June 1996 field trial.

To extract temperature information from the measured 2f signal, the relative intensity of two CO absorption lines that originate from very different energy levels is measured. A high-energy absorption transition (labeled as "a") and a low-energy transition (labeled as "b") are indicated in the two figures. The intensity of the line "a" is extremely sensitive to temperature, more than doubling in intensity for the two calculated 2f spectra. By contrast, absorption line "b has a slightly negative intensity dependence on temperature for the two calculated 2f spectra.

The ratio of 2f intensities for these two features (I_a / I_b) is 0.9 in the experimental spectrum (upper, solid curves). By contrast, the intensity ratios for the two calculated 2f spectra (upper, dashed curves) are 0.3 and 0.8 for CO temperatures of 1600 and 1800° K, respectively. These observations indicate that the best fit for an average line-of-sight temperature is slightly greater than 1800° K for this experimental measurement.

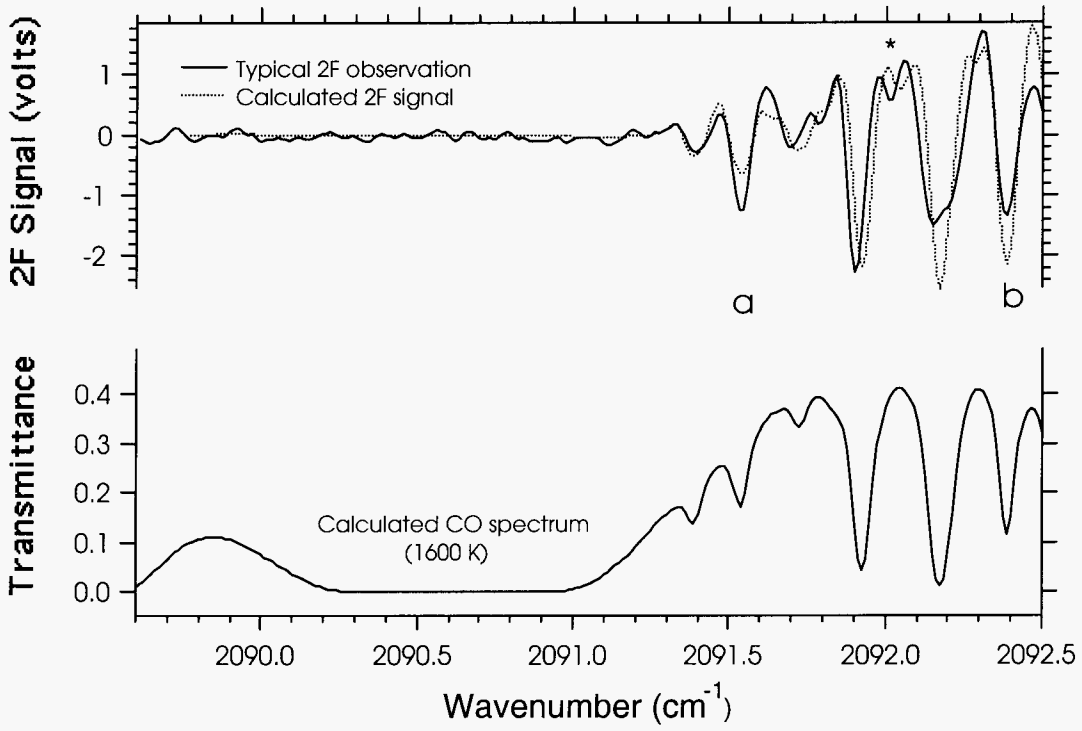

Figure 22. Calculated transmittance spectrum of CO at 1600° K (lower, dashed curve). Experimental 2f signal measured during O_2 blowing at Sparrows Point (upper, solid curve), and calculated 2f signal using °K transmittance spectrum as input (upper, dashed curve). Features identified as "a" and "b" are used to calculate CO temperature and are discussed in the text. Feature marked with asterisk was earlier attributed to CO_2.

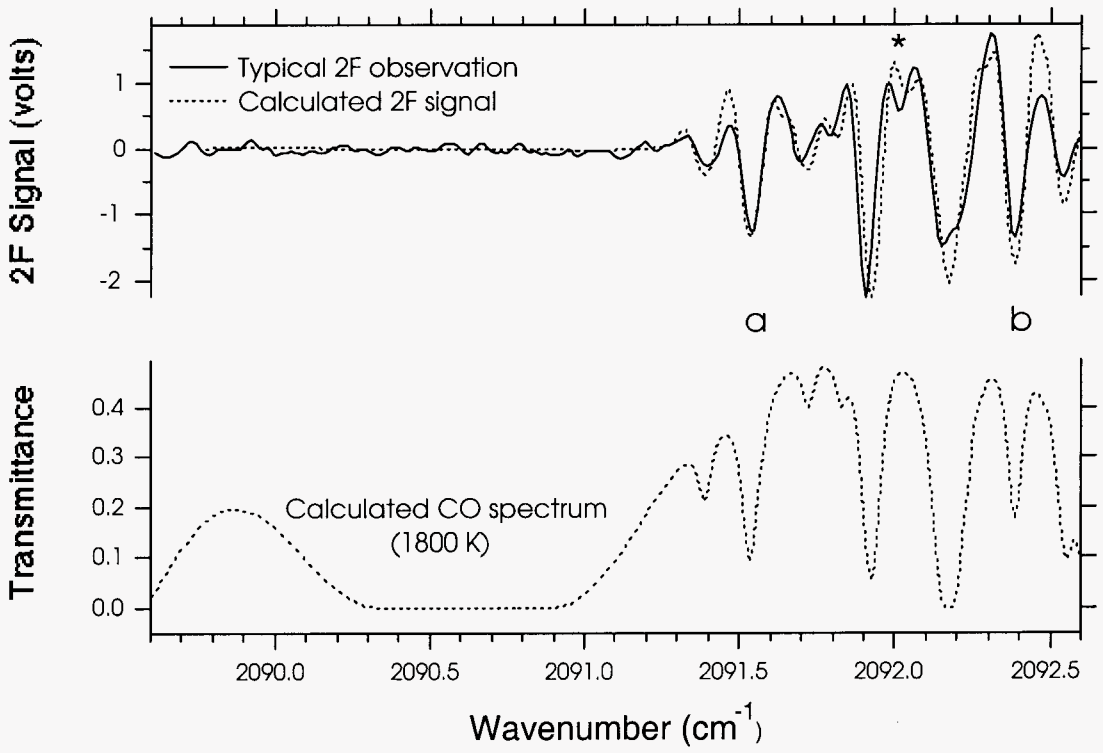

Figure 23. Calculated transmittance spectrum of CO at 1800° K (lower, dashed curve). Experimental 2f signal measured during O_2 blowing at Sparrows Point (upper, solid curve), and calculated 2f signal using 1800° K transmittance spectrum as input (upper, dashed curve). Features identified as "a" and "b" are used to calculate CO temperature and are discussed in the text. Feature marked with asterisk was earlier attributed to CO_2.

Not all of the spectral features in the experimental data are reproduced by the algorithm. This is not unexpected since the team does not have a spectral database that accurately calculates CO_2 transmission spectra at temperatures above 1000° K. Some of the "additional" spectral features, however, are not due to CO_2. Calculations performed with the transform algorithm produce small "absorption-like" features due to the interaction of the second-derivative side lobes of intense, neighboring CO absorption lines. *These results indicate the transform algorithm will be useful in conjunction with calculated CO spectra to identify possible artifacts in the sensor data arising from interference among intense 2f line shapes.* **(Major Milestone Achieved)**

4.2.4 December 1996 Field Trial

A third field trial was conducted at Sparrows Point plant during December 1996 using the optimized data acquisition and instrumentation parameters from the June 1996 field trials. The goal of these experiments was to complete testing and evaluation of the laser-absorption off-gas sensor prior to construction of a new prototype instrument. Operating conditions for BOF vessel #1 during this period differed significantly from those during our field trials in June in that a post-combustion (PC) oxygen lance was used with approximately 500-700 scfm oxygen flowing through the PC orifices during the entire blow.

Optical sensor data were collected for 36 heats over a six-day period, and usable sensor signals were obtained for approximately 75% of the heats observed. For these heats, the TDL beam was not detected during periods of furnace charging and slag ejection ("slopping") due to extinction of the beam by slag and dust particles. The sensor signal was routinely detected following slopping approximately mid-way through the oxygen blow, and was observed continuously until near the end of blowing. Build-up of slag on the furnace lip-ring, or deposits extending down from the off-gas exhaust hood, blocked the infrared laser beam in the small number of heats for which no off-gas absorption signals could be detected.

Sensor data were collected for six wavenumber ranges during the field trial in order to determine the optimal spectral region for current BOF operating parameters. The team also varied the method of sensor-signal sampling during data acquisition in order to improve the sensor's signal-to-noise ratio. In previous field trials the method for data acquisition relied on an unweighted time-average of a specified number of laser scans. During the December 1996 trials, sensor data were acquired and stored for most heats in a single-scan mode in order to develop a conditional sampling algorithm that minimizes the effect of noise on the sensor signal during data acquisition.

Off-Gas Sensor Measurements. Data were collected for three sensor signals during the course of an oxygen blow during these field trials. First, the off-gas laser-absorption signal is detected in the receiver module and demodulated at the second harmonic of the high-frequency modulation frequency, referred to below as the "2f" signal. The 2f signal was sampled at a rate of a 256-KHz with a resolution of 512 points during a single wavenumber scan of the TDL. These data were stored as single records for each scan to provide the most detailed time resolution possible in order to develop an optimized data-sampling algorithm.

Second, the undemodulated off-gas emission signal is also detected in the receiver module, and is periodically sampled at a lower rate producing a time-resolved measure of greybody emittance from the particle-laden off-gas in the 2100 cm^{-1} (4.8 μm) spectral region. Since the emission signal is dominated by the off-gas thermal emission during the oxygen blow, then it will be referred as the "emission signal" for convenience. It has a slow time-varying response that is also sensitive to process variables, and is examined in conjunction with the gas-phase 2f signals.

Finally, the emission signal from a reference detector located in the laser transmitter module is also periodically sampled. This signal is derived from a secondary beam from the TDL that is transmitted through a gas cell containing carbon monoxide, and is used to ensure stable laser operation during data acquisition.

The possibility of developing an enhanced mode of data acquisition for the sensor 2f signal became apparent during the June 1996 field trials. It was observed that the sensor signals possessed a uniform noise level, but varied greatly in the amplitude of gas-phase absorption line intensities (many single laser scans exhibiting little or no absorption line structure due to random obstruction of the laser beam by particle scattering). Traditional methods of noise reduction using unweighted time-averaging are very inefficient for samples containing such a large variation in information content. For this reason, nearly all of the sensor 2f signal data were collected during the December field trial as individual scans in order to facilitate their post-processing.

The TDL mode from 2089 to 2093 cm^{-1} was also used extensively in the December 1996 trials to provide a common basis for developing a sampling algorithm. The team also wished to compare the sensor data directly with that acquired in June 1996 prior to post-combustion lance installation. A representative four-second time average of the 2f signal in this wavenumber range is shown in Figure 24 for heats in these two field trials.

As in Figures 20, 22-23 above, almost all of the intense absorption features shown in Figure 24 are due to absorption of the laser beam by hot CO. Average off-gas temperatures of 1800° K (2780° F) and 1900° K (2960° F) for the June and December field trials, respectively, are estimated based on the intensity ratios of CO absorption peaks labeled "a" and "b". Two labeled peaks are due to CO_2, and their relative strengths mark a significant increase in absorption intensity when compared with data acquired in the previous field trial. In particular, an unresolved shoulder on a strong CO absorption in the June field trial (dashed curve) has increased in intensity in the December field trial. This transition is now visible as a distinctly resolved absorption feature at 2092.20 cm^{-1}, while the strong adjacent CO absorption feature at 2092.13 cm^{-1} has decreased in intensity. These results are in good agreement with the predicted increase in the off-gas CO_2 concentration with the addition of PC oxygen lance technology between these two field trials.

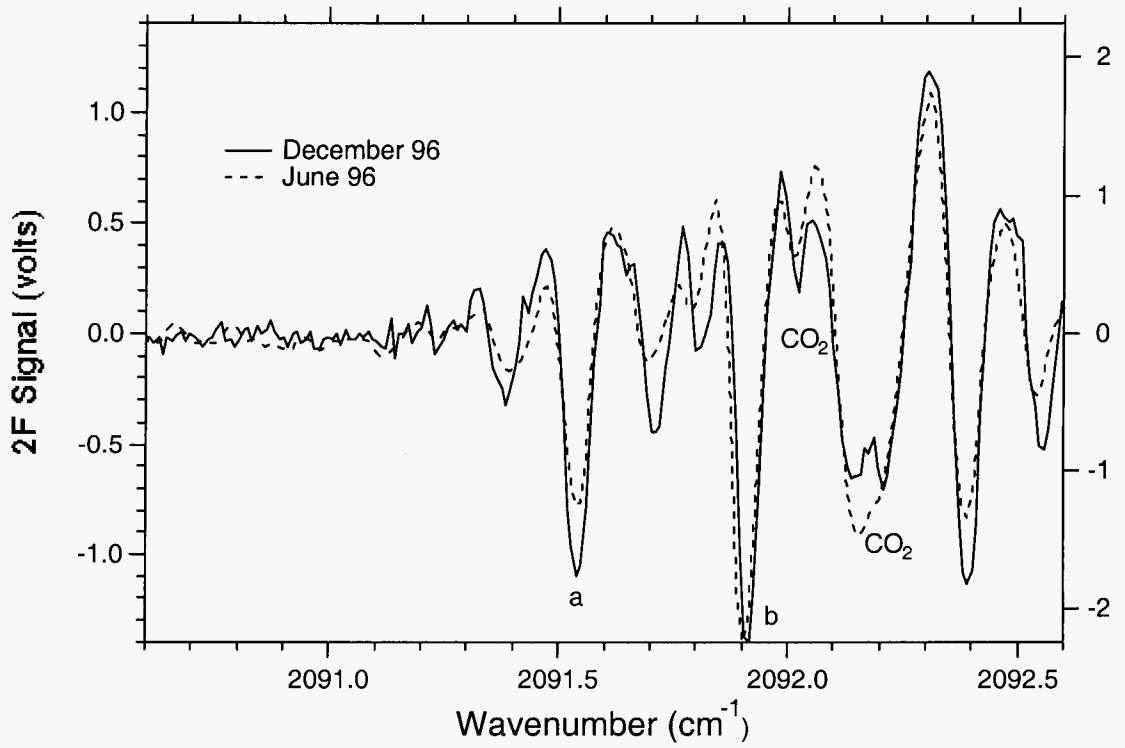

Figure 24. Comparison of off-gas sensor second harmonic (2f) signals during mid-blow for two heats: June 1996 (dashed curve) and December 1996 (solid curve). Ratio of CO absorption lines labeled "a" and "b" are used to estimate off-gas temperatures. Two features due to CO_2 are also indicated.

The significant increase in calculated off-gas temperature and relative CO_2 concentration in the December field trial is in agreement with the effects of additional secondary combustion near the top of the BOF vessel due to the addition of PC oxygen lance technology between these two field trials. **(Major Milestone Achieved)**

These optical measurements of off-gas temperature are only estimates since the effect of CO_2 absorption features are not included in the data analysis. Although the spectral absorbance of CO as a function of temperature and concentration can be calculated with great accuracy, no corresponding method exists for CO_2 under the conditions encountered in the BOF off-gas stream due to the great complexity of its absorption spectrum at elevated temperatures. Furthermore, existing spectral databases for CO_2 absorbance are in significant disagreement with Sandia's laboratory measurements.

Most of the CO_2 absorption features in the laser tuning range shown in Figure 24 are partially or completely overlapped with CO absorption features. This spectral overlap complicates the quantitative measurement of concentration ratios for these two species. For this reason, data were collected in several other laser-tuning ranges covering the spectral region 2080 - 2115 cm^{-1} during the December 1996 field trials. The 2087-2090 cm^{-1} laser tuning range was found to comprise several CO_2 absorption features that are not obscured by CO peaks, and a time-averaged 2f sensor signal of the BOF off-gas during oxygen blowing is shown is shown in Figure 25.

Seven of the intense negative-going absorption features can be assigned to CO absorptions. Of these features, four do not seem to be significantly perturbed by nearby CO_2 transitions, and preliminary calculations of 2f sensor signals for CO at temperatures of 1800° and 2000° K were in reasonable agreement with peak intensities for most of the carbon monoxide absorption lines in the experimental data.
Comparison of the three curves in Figure 25 quickly reveals several absorption features that are not accounted for in the calculated CO spectra, and are due to either CO_2 or H_2O. While this wavenumber region thus offers several discrete CO_2 transitions with significant intensity for deriving CO / CO_2 concentration ratios under current commercial BOF operating conditions, experiments at Sandia with a laboratory flow reactor showed that absorption due to hot H_2O occurs at 2087.2 and 2087.4 cm^{-1}. Interference with the CO absorption at 2087.2 cm^{-1} is especially problematic, since that feature is the most sensitive variable in off-gas temperature calculations. The 2087–2090 cm^{-1} spectral region is less useful for process control applications for this reason than the adjacent 2090-2093 cm^{-1} region discussed above.

Improvements in Data Acquisition. During the December 1996 field trials, the team also evaluated different methods for sampling and time averaging the off-gas laser absorption signal. In order to evaluate the effect of data sampling, the team formed the ratio of the maximum negative intensity of the two absorption lines, marked "a" and "b" in Figure 24. Values for this ratio were calculated in two ways: (1) a time-average of 20 laser scans; and (2) a running, selective-average of 20 laser scans whose negative intensity at three absorption lines is greater than a minimum threshold value.

The second approach provides a method of conditionally sampling the data, and computing average line-intensity ratios only for scans containing usable laser absorption signals. Scans consisting primarily of noise do not, therefore, contribute to the running average of peak intensity ratios. A plot of intensity ratios using these two methods for a single heat is shown in Figure 26. The dashed curve

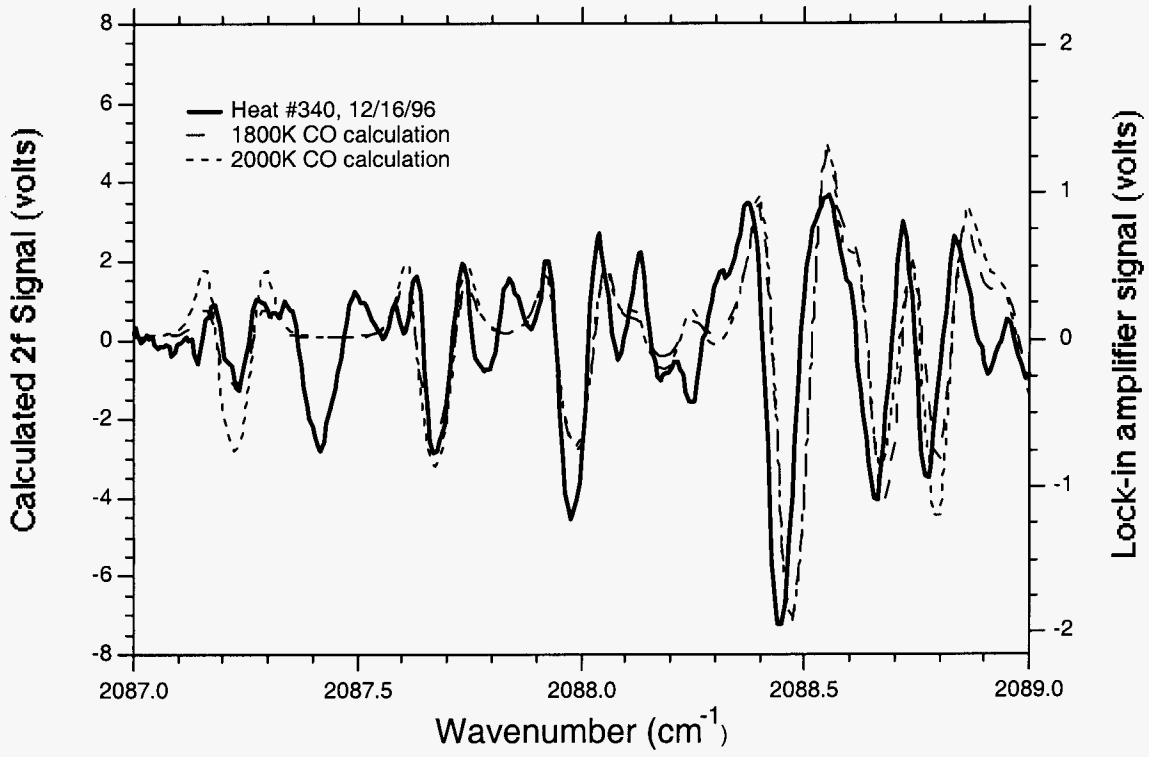

Figure 25. Comparison of time-averaged 2f signal during oxygen blowing (solid curve) with calculated 2f signals for CO at 1800° K (dashed curve) and 2000° K (dotted curve).

(open triangles) is the time average computation, which yields a rather sparse data set with very large scatter. In contrast, the running, selective-average ratio of intensity data subjected to a threshold filter is much less scattered with a mean value of the "a"/"b" intensity ratio of 0.71.

Sensor Signals as a Function of Oxygen Blowing Time. In the June and December 1996 field trials, a correspondence in the behavior of the emission signal with the degree of furnace slopping was observed, and this is shown in Figure 27 for three separate heats during December 1996.

The intensity of the emission signal is dominated by the total greybody emission by particulates and gases in the sensor detector's field-of-view. The optical response of the sensor to greybody radiation is determined not only by the characteristics of the InSb detector, but also by the associated narrow-band optical filter that is designed to pass light only in the 2080 - 2120 cm^{-1} (4.81 - 4.72 μm) range.

The observed emission signals show a rapid rise at the beginning of oxygen blowing, and a slower drop in intensity near the end of blowing. During most of the blow, a plateau region is established with periodic drops in signal intensity and duration that are quite variable from heat to heat. *The onset of fluctuations in the emission signal intensity agrees well with the start of furnace slopping, and it is believed that the ejection of large masses of slag from the furnace fills the sensor's field-of-view with relatively cool objects during these events.* **(Major Milestone Achieved)**

The extent to which the detector's field of view is filled with ejected slag also determines the degree with which TDL beam is blocked during furnace slopping. As an example, the 2f laser-absorption peak intensity ratio (from Figure 26) is plotted with the emission signal in Figure 28. Furnace slopping for this heat begins with the sharp drop in emission-signal intensity 400 seconds into the oxygen blow. Usable 2f sensor signals were first detected around 620 seconds after the oxygen blow started and continued to strengthen in intensity over the next several minutes, finally being attenuated 1150 seconds into the oxygen blow.

The 2f laser-absorption signal is blocked during the first half of the oxygen blow by the large number of particles entrained in the off-gas during furnace charging operations. Furnace slopping may further heighten this attenuation, and the team observed the onset of valid 2f sensor signals in the range of 350 - 900 seconds following the beginning of oxygen blowing for the heats observed in the June and December 1996 field trials.

The team also notes that the 2f laser-absorption signal is attenuated just before the end of oxygen blowing (as shown in Figure 28). This behavior is highly correlated with the rapid decrease in the sensor's emission-signal intensity. The attenuation in emission-signal intensity is related in a complex way to decarburization of the melt by rapid changes in CO and CO_2 concentrations, temperature, and particle loading in the off-gas. Experiments at Sandia with laboratory burners have shown that CO_2 in the 1600° to 2000° K temperature range rapidly increases in absorbance from

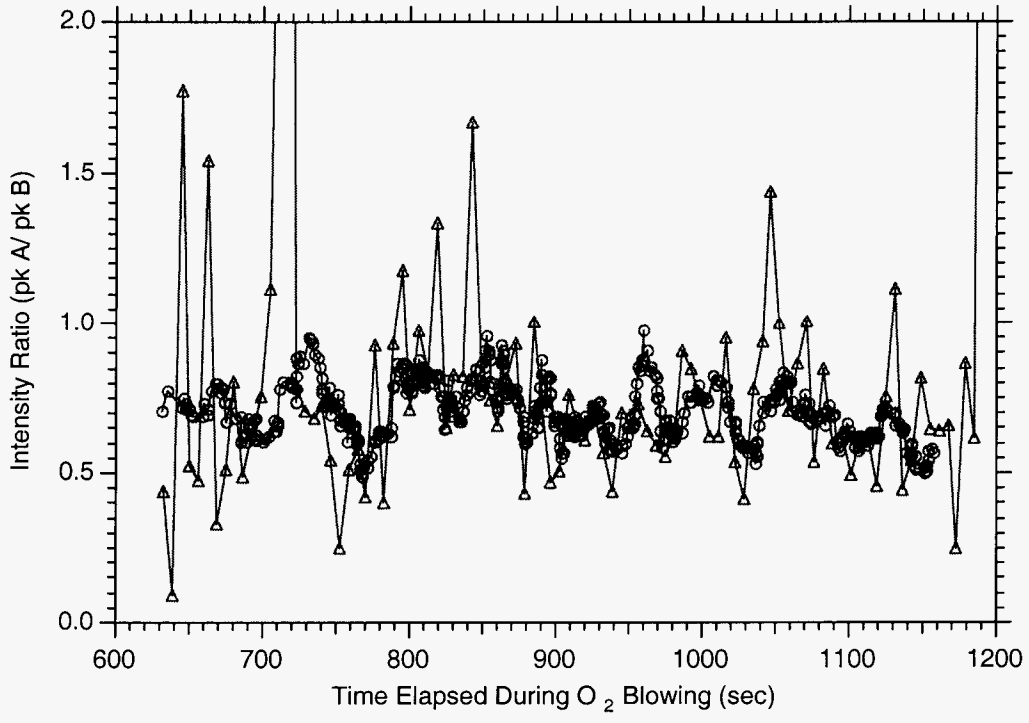

Figure 26. Comparison of intensity ratios for peaks "a" and "b" in Fig. 23 using: (1) a time-average (dashed curve, open triangles); and (2) a running-average of conditionally sampled data (solid curve, open circles).

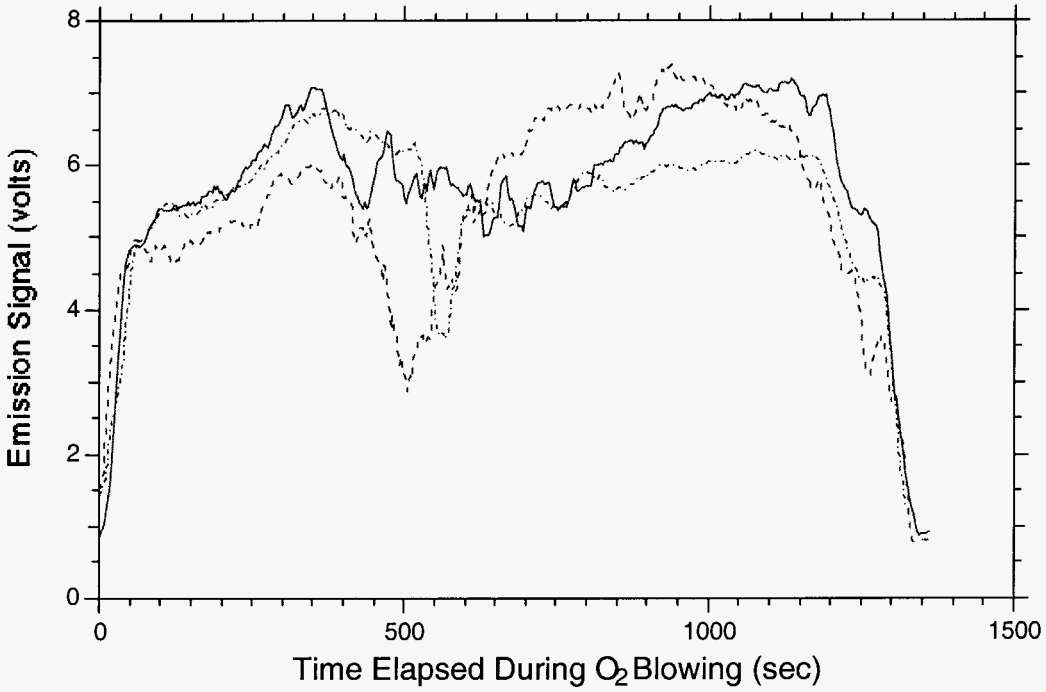

Figure 27. Comparison of emission signals for oxygen blowing in Heat #330 (solid curve), Heat #331 (dash-dot curve), and Heat #341 (dashed curve) for Sparrows Point BOF vessel #1 on 12/16/1996.

2080 to 2100 cm^{-1}. This behavior is due to an extremely large number of overlapping absorption lines that become populated at these temperatures, creating an absorption continuum. As the CO_2 concentration rises sharply in the BOF off-gas during final melt decarburization, the broadband absorption continuum increases and eventually attenuates the TDL laser beam and 2f sensor signal.

4.3 Pre-Commercialization Prototype Sensor Development

Following the positive results of the first two full-scale field trials, Sandia constructed a pre-commercialization sensor prototype during 1997. Both laser-transmitter and detector-receiver modules were redesigned, resulting in a reduction of the footprint for each module by a factor of two. **(Major Milestone Achieved)** This was achieved for the transmitter module primarily by removing electronic components from the module and placing them in a secondary enclosure that were electrically connected through intermediate cabling. The installation location for the new electronics module was 4 m away from the BOF heat shield, thus lowering it's ambient operating temperature and cooling requirements. Schematic diagrams for the transmitter and receiver modules are shown in Figures 29 and 30.

A further significant improvement in both transmitter and receiver modules of the new sensor prototype was the incorporation of water-cooled enclosures using available house water. These modules are extremely robust, and have several additional features that greatly simplify their

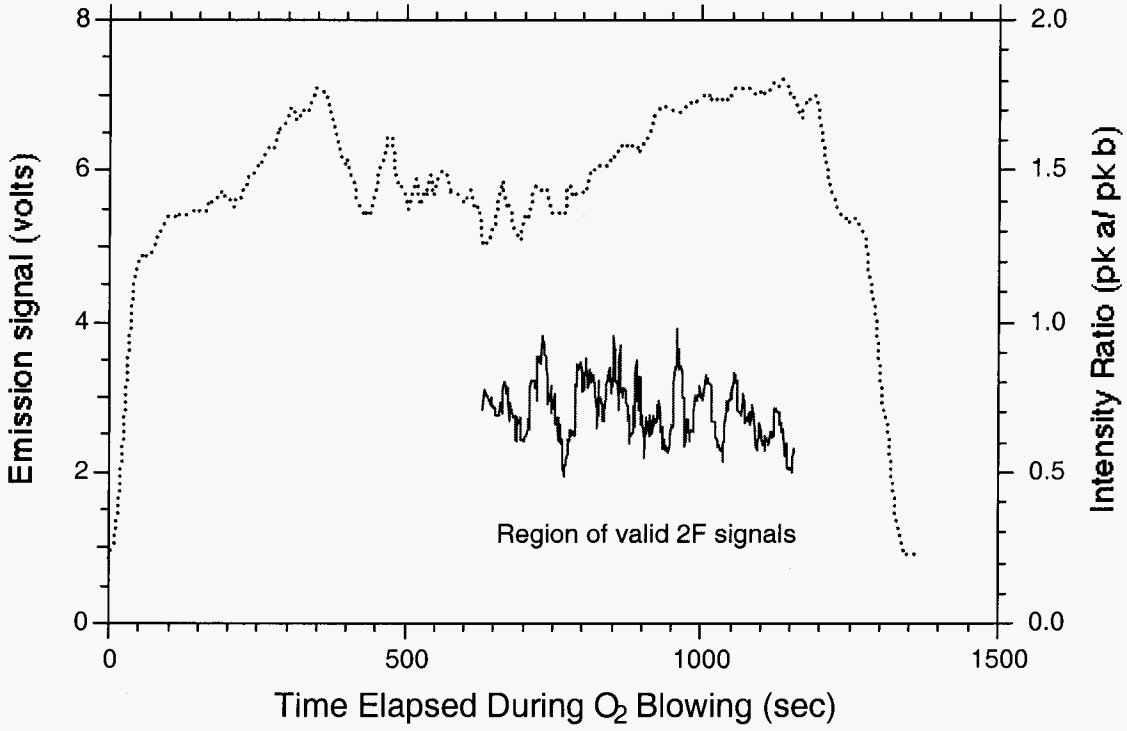

Figure 28. Comparison of emission-sensor signal (dotted curve) and 2f-sensor signal (solid curve) for oxygen blowing in Heat #330 for Sparrows Point BOF vessel #1 on 12/16/96.

installation and normal operation. Among these changes are an improved exit-window purge system, and an easily adjustable detector / collection-lens mount, both of which were designed by Insitec.

Figure 29. Layout for transmitter module in laser absorption off-gas sensor prototype

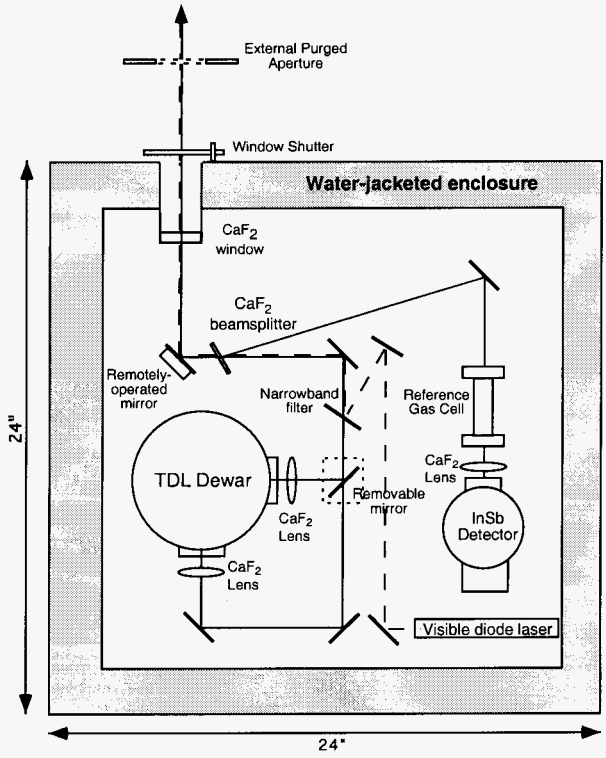

Figure 30. Layout for receiver module in laser-absorption off-gas sensor prototype.

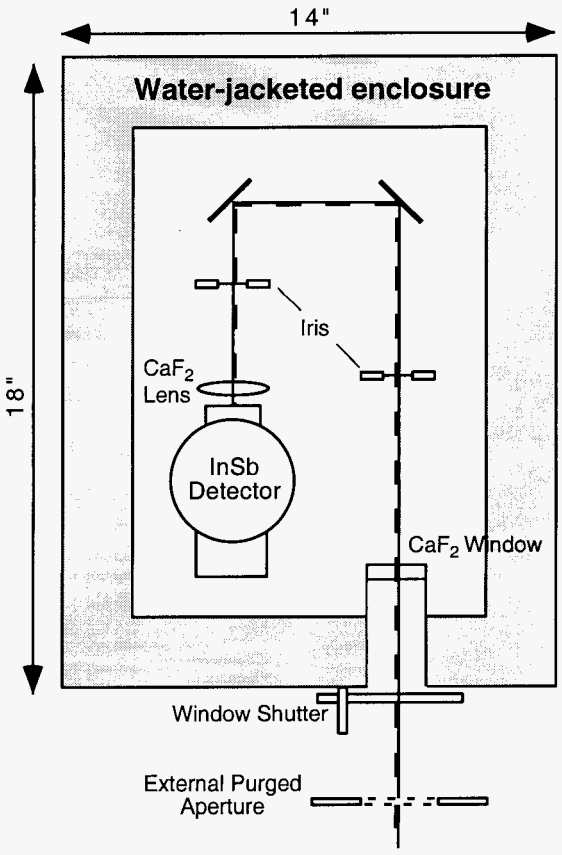

The transmitter module also takes advantage of multiple mounting positions inside the laser cryostat. Diode lasers are mounted at both available output ports, thus providing a backup laser in case of diode failure. The secondary laser output beam is prealigned at Sandia, and can be easily placed in service after installation in the plant by removing one mirror from the primary laser beam optical path.

Additional external apertures (1.5-inch diameter) were also added to the transmitter and receiver modules during long-term field trials in 1997-98, and are shown in Figures 29 and 30 for completeness. A high-velocity downward flowing air purge on each aperture provided excellent protection for the CaF_2 window in each module against impact and damage from slag and metal particles ejected from the furnace.

A preliminary test of the sensor prototype was conducted at Sparrows Point during June 1997. Over the course of four days, off-gas sensor data were acquired successfully for 21 heats. These data were of greatly superior quality compared to the results of both field trials in June and December 1996. The improvement in the results was due primarily to better collimation and alignment of the infrared laser beam. The Sandia team was able to achieve a 50% increase in detected laser power as a result. **(Major Milestone Achieved)**

The new electronics module overheated during these tests despite the new mounting location. As a result, additional active cooling measures were incorporated to provide a stable interior temperature of 80-90°F with the electronics in operation. Following the June 1997 tests at Sparrows Point, the team insulated the interior of the electronics module, and added Vortec compressed-air coolers preceded by a water-to-air heat exchanger. This system was successfully tested in an environmental heating chamber at Sandia at temperatures of 150 °F. A schematic layout of the electronics module is shown in Figure 31.

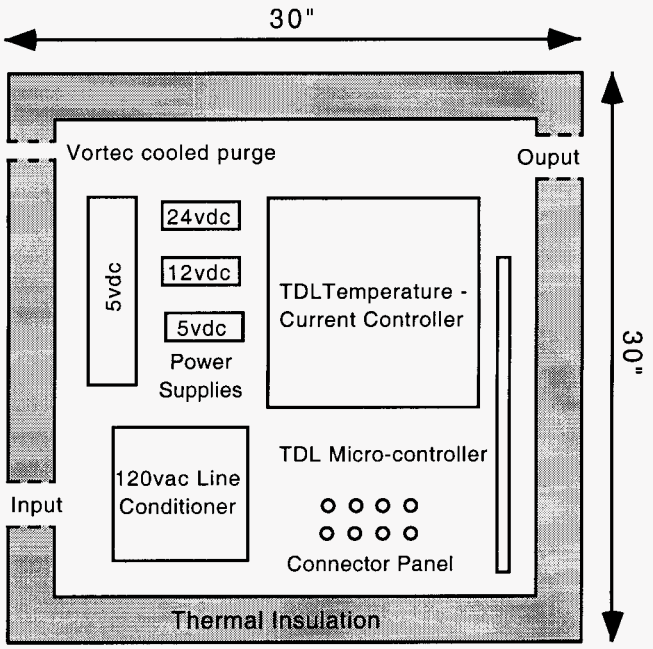

Figure 31. Layout for the electronics module associated with the sensor transmitter module in laser-absorption off-gas sensor prototype.

Finally, the sensor prototype's data acquisition system was redesigned with control and data lines extending from the data acquisition system to the receiver and, via the electronics module, to the TDL transmitter.

Long-Term Prototype Sensor Field Trials. The modified pre-commercialization prototype sensor was tested at Sparrows Point during two long-term field trials in October 1997 and April 1998. The goal of these trials was to accumulate sufficient experimental data to evaluate the potential of the optical sensor for dynamic control of turndown bath carbon concentration, bath temperature, and furnace slopping behavior. Long-term durability of the sensor system was also evaluated.

4.3.1 October 1997 Field Trial

Automated data collection using plant trigger signals was implemented during the first few days of the field trial with the assistance of a software consultant, Gary Hubbard. This greatly extended the data gathering capability since the plant was running continuously on BOF vessel #1 during this period. Sensor data were collected for some 440 heats over the course of the 24-day field trial.

Three problems were encountered during the October 1997 trial. First, a series of power outages greatly interfered with data collection during the first few days of the field trial, and was primarily responsible for the low percentage (65%) of good data sets during the initial week of the field trial.

A second problem during the test series was cracking of the optical windows in either the laser transmitter or detector module. The window material is single crystal CaF_2 (chosen for its infrared transmission properties near 5-μm wavelength). These windows are protected from particle impact by a dry-air purge, as well as by 3-inch diameter apertures in the heat shields. However, most of the heats during the test period exhibited the ejection of high velocity molten slag particles. The combination of impact and high thermal stress was sufficient to break two windows on each module during the first 16 days of the test, thus lowering the percentage of successful data sets.

The Sandia team alleviated the problem of window cracking by installing simple 1.5-inch diameter apertures approximately six inches in front of each module, as shown in Figures 29 and 30. *The use of external apertures limited particle impact on the windows to a much smaller number of particle trajectories, and no further window cracking occurred during the final six days of the field trial. This approach also had the beneficial effect of further reducing greybody emission incident on the infrared detector, thus improving the sensor's dynamic range. Additional external apertures, as well as a redesigned window assembly, were incorporated in the April 1998 field trial, discussed below.* **(Major Milestone Achieved)**

A third problem encountered in the field trials was the occasional blockage of the infrared laser beam by slag deposits on either the furnace lip ring or the bottom of the exhaust hood. This problem was somewhat more severe than normal during the long-term trials. Due to the concurrent relining of vessel #2 at Sparrows Point, the one-furnace operation during the field-trial period limited the number of times that the furnace lip ring was deskulled.

A key objective during this field trial was to extend the portion of the heat during which laser-based measurements of gas-phase concentrations and temperatures can be made. Two factors can lead to a decreased laser transmittance: attenuation by particles, and attenuation by gas-phase molecules.

Previously the team has discussed the modulated laser signal by plotting the ratio between two peaks in a spectrum (for example, Figures 26 and 28.) A different way to quantify the usable laser 2f signal is to compute a more generic "laser absorption 2f signal", which is the average of the absolute value of all data points in the corresponding 2f absorption spectrum (such as the curve shown in Figure 24.)

The lower curve in Figure 32 represents the laser absorption 2f signal strength of the transmitted laser beam for a representative heat. No laser 2f absorption signal is observed for the first half of most oxygen blows, as shown in the lower curve of Figure 32. This behavior is due principally to the very high particle loading of the off-gas during flux charging and furnace slopping events. The behavior of the optical signals presented in Figure 32 is typical for most heats, and shows the first detectable laser signal around 250,000 scfm accumulated oxygen.

There is a corresponding loss of the modulated laser signal at values of accumulated oxygen slightly above 400,000 scf (or 1150 seconds blowing time as shown above in Figures 26 and 28). The drop in the laser 2f absorption signal level near the end of the heat is attributed primarily to a rapid

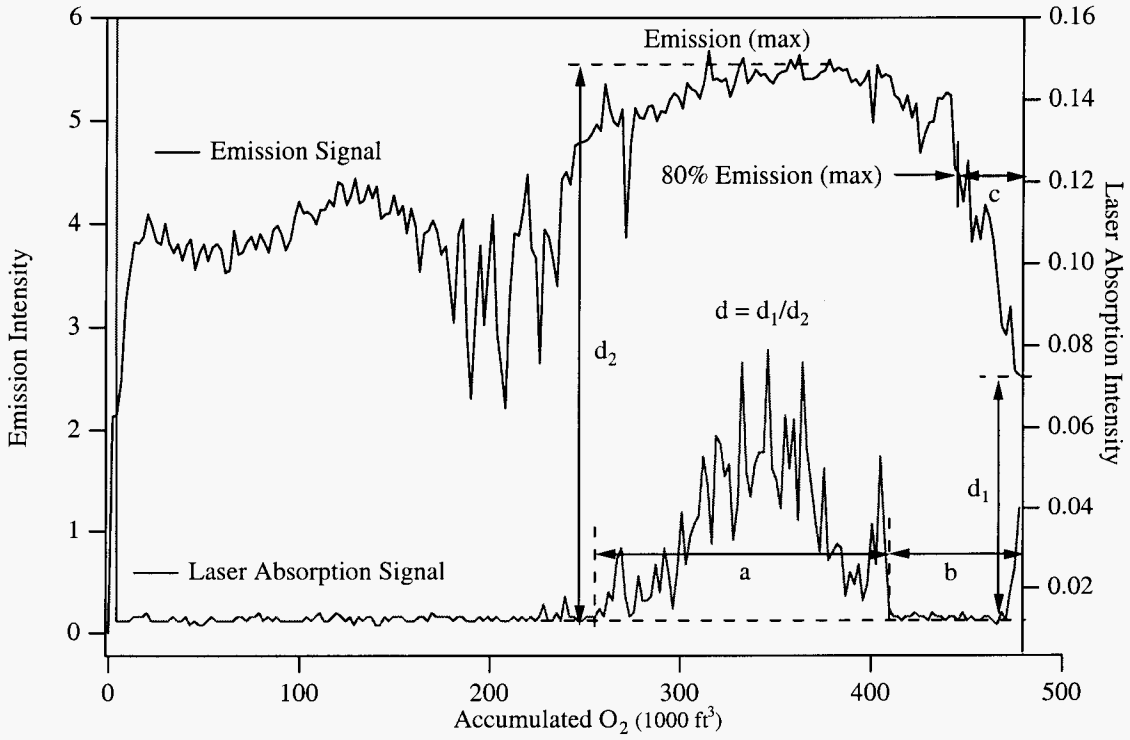

Figure 32 Off-gas sensor signals (emission, upper curve, and laser absorption signal, lower curve) for a characteristic heat. Parameters "a", "b", "c" and "d" are shown in the figure and defined below in Table 1. Laser tuning mode is located at 2090-2093 cm^{-1}.

increase in concentration of highly absorbing CO_2 during the final stage of melt decarburization.

This conclusion was substantiated by laboratory measurements for high-temperature CO_2 in laminar flow reactors at Sandia's CRF.

During this first long-term field trial, the team therefore sought to minimize the signal loss at the end of the oxygen blows by shifting the wavelength of the tunable infrared laser to the region near 4.88 μm (2050 cm^{-1}), since the optical absorption of hot CO_2 becomes progressively weaker at longer wavelengths. Indeed, analysis of the data shows that the shift to longer wavelengths successfully decreases the duration in which the laser 2f signal is lost from an average of 57,000 to 48,000 scf accumulated oxygen at the end of the blow.

The team also observed the off-gas emission signal with the sensor detector throughout the oxygen blow (shown as the upper curve in Figure 32). As discussed earlier, this signal is the combined detector response to greybody emission from both off-gas molecules and dust particles entrained in the off-gas stream. Since the operating wavelength range is in the mid-infrared region, the emission signal never completely goes to its baseline value at the end of the blow, even though the off-gas stream may become quite dark in the visible region. The large dip in the off-gas emission signal around 200,000 scf accumulated oxygen is characteristic of furnace slopping. *Furnace slopping behavior for twenty heats was videotaped from a camera on the charging floor that imaged the upper portion of the vessel and the bottom of the exhaust hood. The relation of the visible slopping events to the off-gas emission signal as a possible real-time detection and control method for furnace slopping is discussed below.* **(Major Milestone Achieved)**

Analysis of the long-term trial data shows that the behavior of the optical sensor signals is correlated with the observed turndown melt temperature and carbon concentration. **(Major Milestone Achieved).** Many of the CO absorption features in the individual laser 2f signals exhibit a substantial difference in intensity with respect to temperature. The intensity ratio of CO features in Figure 24 above is strongly dependent on the temperature of the off-gas, and is used in combination with the off-gas emission signals to predict melt turndown temperature. Off-gas sensor signals were acquired for two different laser wavelength tuning ranges, 2091 cm^{-1} (4.78 μm) and 2050 cm^{-1} (4.88 μm), in addition to signals for the off-gas emission. An analysis of the data is presented below.

4.3.1.1 Bath Turndown Temperature

The intensity of a carbon monoxide absorption feature in the 2090 cm^{-1} laser tuning range (as shown in Figure 24) exhibits a marked sensitivity to off-gas temperature. Intensities of the temperature-sensitive CO feature at 2091.54 cm^{-1} were ratioed with those of a CO temperature-insensitive feature at 2091.92 cm^{-1}. These intensity ratios were averaged over the time period during a heat for which the infrared laser signal was observed, typically 250,000 to 425,000 scf accumulated oxygen.

Table 1. Parameterization of laser absorption and off-gas emission sensor signals

Variable	Definition (units)
a	Duration of laser absorption 2f signal (accumulated O_2, scfm)
b	Duration from loss of laser absorption 2f signal until end of blow (accumulated O_2, scfm)
c	Duration from 80% maximum off-gas emission intensity to end of blow (accumulated O_2, scfm)
d	Ratio of off-gas emission intensity at the end of blow (d1) to the maximum off-gas emission intensity (d2)

A linear regression analysis was made of the optical sensor data from 93 heats. Immersion thermocouple measurements of final turndown bath temperature made by Bethlehem Steel were used as the dependent variable in the analysis. In addition to the CO intensity ratio data for each heat, optical data from both integrated laser 2f-absorption and off-gas emission signals were parameterized as shown in Figure 32. These variables ("a", "b", "c" and "d") are defined in Table 1. Although many other parameterizations of the data were examined, these four were found to be the most significant for predicted final turndown temperature.

The resultant predicted bath temperatures versus thermocouple measurements are shown in Figure 33. Although the data are quite scattered, the relation of sensor signals to turndown temperatures is shown to be statistically significant with a standard error of ± 24 °F (±13° K) in the predicted bath turndown temperature. While three parameters (b, c, and d) are statistically significant in the linear regression analysis, they are much less important to the fit than the carbon monoxide intensity ratios. A modest correlation coefficient ($R^2 = 0.28$) was obtained for this analysis. By comparison, the range of bath turndown temperatures for these 93 heats resulted in a population standard deviation of ± 27 °F.

The laser absorption data were also analyzed by a second method in an attempt to improve the regression analysis. The carbon monoxide intensity ratios used in the analysis above are obtained by time-averaging the intensities of the two absorption features for 100 laser scans (approximately 3 seconds in real time), and then forming the ratio from the averaged intensities. The second analysis of the data reverses this process, calculating intensity ratios for each scan and then forming an average ratio over 100 laser scans. This second procedure reduces the scatter shown in Figure 33 somewhat. However, the slope of the best straight-line fit to the data is flatter, and the regression analysis reveals no improvement in either the correlation factor or the standard error of the predicted bath temperature.

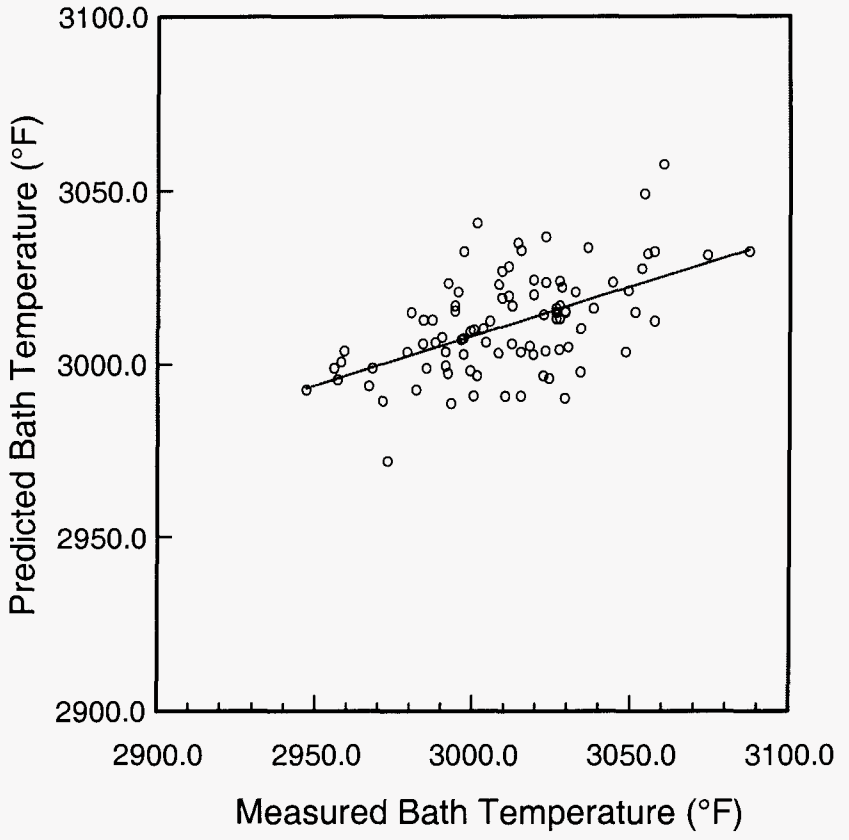

Figure 33. Results of linear regression analysis showing predicted vs. measured bath turndown temperature using laser off-gas sensor signals for the 2090-2093 cm^{-1} tuning mode during the October 1997 field trial.

The correlation of laser off-gas sensor signals with bath turndown temperature is encouraging, and offers the potential to develop a method for dynamic temperature control. **(Major Milestone Achieved).** Following this analysis, an approach to improve the accuracy and correlation of the sensor signals with bath temperature was devised, and was incorporated in a second long-term field trial conducted in April 1998 (discussed below).

Data from 125 heats using the 2050 cm^{-1} laser-tuning mode were also analyzed for prediction of bath turndown temperature. The CO absorption lines in this spectral region, however, show a much weaker dependence on off-gas temperature than those in the 2090 cm^{-1} spectral range, discussed above. A regression analysis of these data yielded no useful correlation with bath temperature, but produced a strong correlation with bath carbon concentration as discussed below.

4.3.1.2 Bath Turndown Carbon Concentration

A second linear regression analysis of the off-gas sensor data was performed using data from 125 heats in the 2050 cm^{-1} laser tuning range. Final turndown bath carbon concentrations are determined by Bethlehem Steel by off-line chemical analysis of extracted metal samples. A good correlation of the optical data is obtained with these measurements. Three of the variables described above [a, b and d] are used in the fit. The functional expression of the variables in the analysis includes the terms: a, a^2, $\sqrt{b}$, d, and d^2, as defined above.

All of the terms are statistically significant and produce a correlation factor, R^2 = 0.46, with a standard error of ± 0.0064% for predicted vs. measured bath turndown carbon concentration. **(Major Milestone Achieved)** Figure 34 shows the results of the regression analysis. The correlation of laser off-gas sensor signals with bath carbon concentration is also very encouraging, and were received with great enthusiasm by Bethlehem Steel personnel.

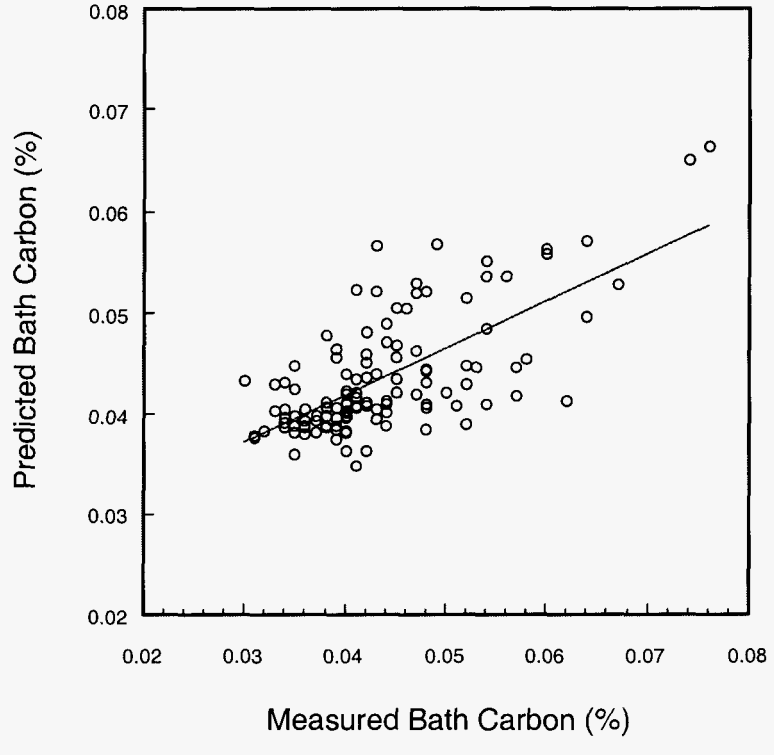

Figure 34. Results of linear regression analysis showing predicted vs. measured bath turndown carbon concentration using laser off-gas sensor signals at 2050 cm^{-1} for the October 1997 field trial.

Similar results are produced in an analysis of the 93 heats obtained at the 2090 cm^{-1} laser tuning mode, but are not presented here due to the smaller size of the data set. Additional tests comprising a larger data set were planned in order to refine the accuracy of the optical sensor for final turndown carbon prediction, and these results are discussed below.

4.3.1.3 Furnace Slopping

Data from the first long-term field trial were analyzed in an attempt to correlate sensor signals with furnace slopping behavior. Time-stamped videotapes were made of 20 heats with the camera field-of-view encompassing the furnace tap-hole to the bottom of the exhaust hood. The tapes provide a clear visual record of furnace slopping, typically occurring between 150,000 and 300,000 scf accumulated oxygen.

The Sandia team compared the emission intensity recorded by the off-gas sensor with the videotape record, and observed a good correlation of sustained drops in the sensor signal intensity with visible ejection of liquid slag from the furnace mouth. On the basis of these preliminary results, an extensive series of heats was videotaped during the following April 1998 field trials, and two follow-on field trials (November 1998 and February 1999). An automated computer analysis was made of both the videotape and optical sensor data, and these results are presented below.

4.3.2 April 1998 Field Trial

The encouraging results of October 1997 led Sandia team to modify the sensor hardware in order to develop a stronger correlation of our optical data with final turndown bath temperature. Since the most statistically significant variable in the regression analysis of the October data was the CO intensity ratio factor, one possible avenue for improvement was the measurement of other spectral regions with CO absorption lines that exhibit an even stronger dependence on off-gas temperature.

Calculations for high-temperature CO absorption were performed, and experimental FTIR absorption measurements of potential water vapor interference were made in a Sandia low-pressure flame facility. A candidate spectral region was identified as shown in Figure 35 for temperatures of 1800° and 2100° K (2780° and 3320 °F). Intensity ratios for the absorption line pair at 1966.76 and 1966.89 cm^{-1} are calculated as a function of off-gas temperature. The strong dependence of intensity of the latter absorption line on temperature is clearly illustrated in the figure.

Intensity ratios for these two 2f absorption lines are computed and are plotted as a function of off-gas temperature in Figure 36 (lower curve, filled squares). These values are compared with the intensity ratio variable used in the analysis above (upper curve, filled circles) based on 2f absorption lines in the 2091 cm^{-1} spectral range. *A significant improvement in sensitivity (i.e., steeper slope) of the CO intensity ratio is clearly seen for the "Mode 1966" curve shone in Figure 36. Appropriate lasers were acquired, installed and characterized in the prototype sensor. A useful laser tuning range was identified that allows one to observe both absorption lines, and an appropriate set of narrow-bandpass optical filters was fabricated to facilitate the detection of the new TDL wavelength.* **(Major Milestone Achieved).**

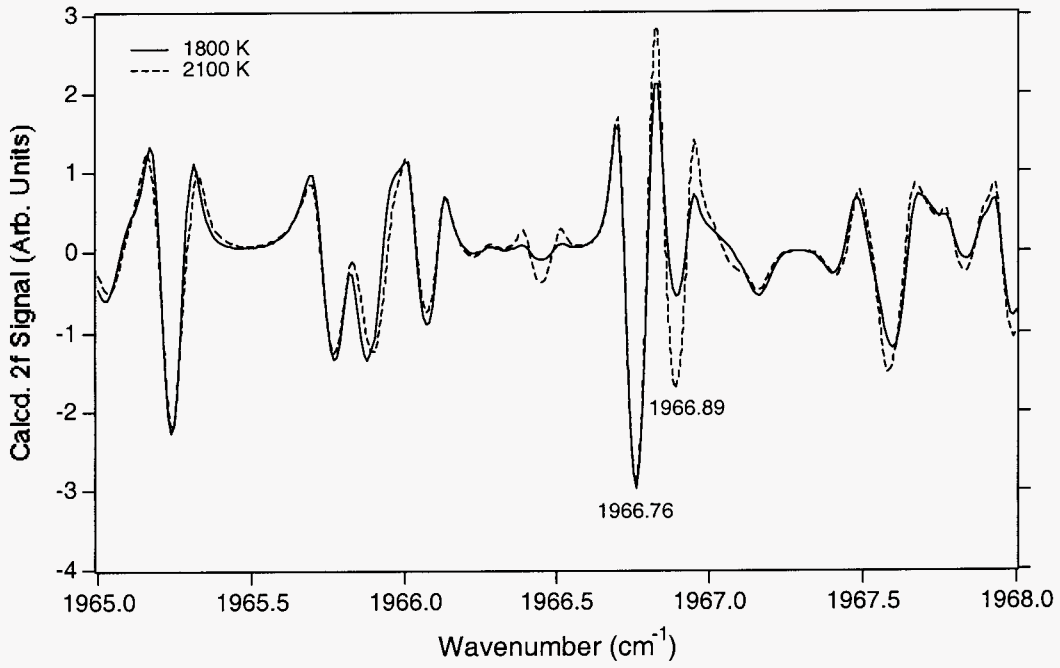

Figure 35. Calculated laser absorption 2f spectra for CO for two off-gas temperatures (solid curve, 1800° K; dashed curve 2100° K). Absorbing path length is 3.65 m, concentration is 80%, and pressure is 1 atmosphere.

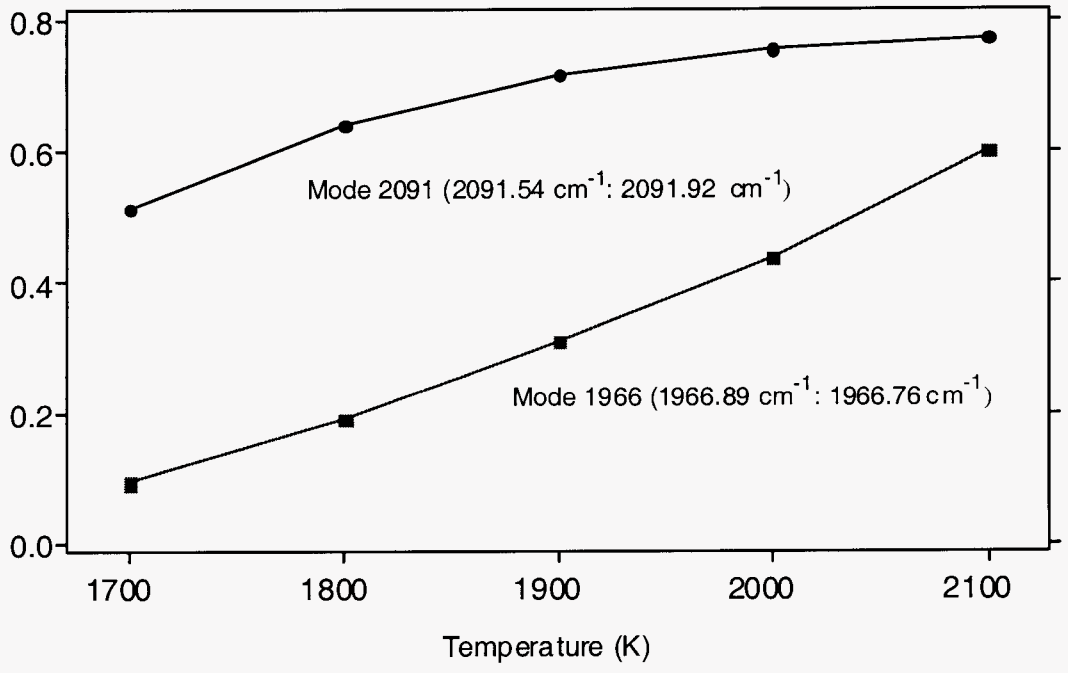

Figure 36. Comparison of CO intensity ratio variables versus off-gas temperature for two spectral regions (upper curve, 2091 cm^{-1}; lower curve 1966 cm^{-1}).

The modified optical sensor equipment was tested at Sandia and deployed at Sparrows Point for a final field trial during April 1998. In addition, the previous success of external apertures in protecting the optical windows on the sensor modules was incorporated into the modified prototype. A down-flow purge was added to each aperture to further decrease the number of high-velocity particles impinging on the module windows.

4.3.2.1 Bath Turndown Temperature

Optical sensor data, final turndown temperatures, and bath carbon concentrations were obtained for a total of 219 heats during the April 1998 field trial. The resultant predicted bath temperatures (using TDL mode 1966) versus thermocouple measurements are shown in Figure 37. The standard deviation of turndown bath temperatures for the 219 heats is ± 37 °F (± 21° K), and represents a much larger spread in turndown temperatures than was observed in the earlier October 1997 set of field trial results. As before, the optical data from both laser absorption and off-gas emission signals were analyzed using a multiple linear regression. Using melt turndown temperatures measured by thermocouple as the input data, the predicted turndown temperatures from the optical measurements show a standard deviation of ± 31 °F (± 17° K) with a correlation coefficient of $R^2 = 0.30$. These results are based on a 7-parameter fit using the variables defined in Table 2. All factors are statistically significant in the analysis and were uncorrelated with one another.

In accordance with standard industry practice, the Sandia team also compared the same set of predicted turndown temperatures with the "aim" temperature calculated by the Bethlehem Steel static charge model and obtained a standard deviation of ± 25 °F (± 14° K). The correlation for this regression analysis is much poorer, however ($R^2 = 0.15$). The smaller standard deviation is probably a reflection of the more limited range of aim temperatures (± 27 °F) compared to the range of thermocouple temperature measurements (± 37 °F).

The BOF process at the Bethlehem Steel Sparrows Point plant typically exhibits a long-term bath turndown temperature variation of ± 30 °F based on thermocouple measurements. Based on the results of our October 1997 and April 1998 field trials, the laser-based optical sensor method will provide a dynamic control on the order of ± 25 °F under these conditions. This precision is considerably inferior to the instantaneous precision of the optical off-gas temperature measurements. An example of the experimentally measured temperature for a typical BOF heat is shown in Figure 38.

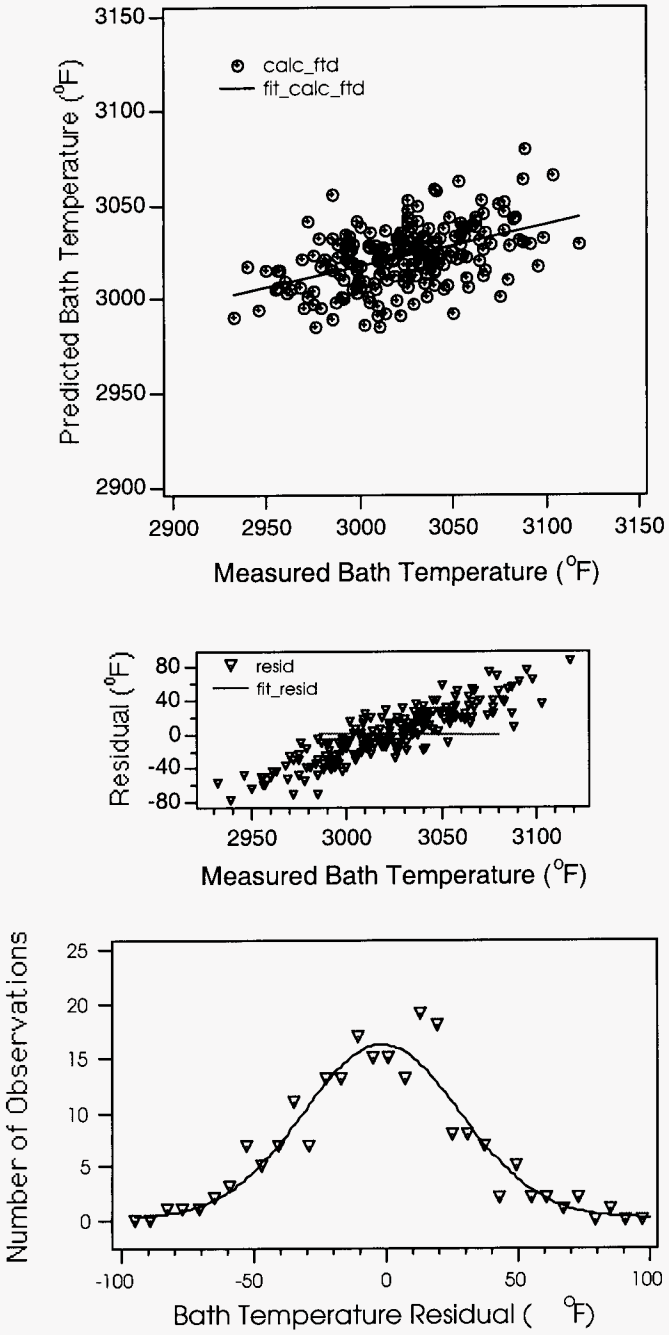

Figure 37. Top: Predicted versus measured final turndown bath temperatures for the April 1998 field trial, mode 1966. Middle: residuals. Bottom: PDF of the residuals.

Table 2. Sensor variables used in turndown temperature regression analysis

Variable	Definition
R1	CO line intensity ratio (1966.89 / 1966.76 cm^{-1}) at acc. O_2 = 240,000 scfm
R2	CO line intensity ratio (1966.89 / 1966.76 cm^{-1}) at acc. O_2 = 420,000 scfm
R3	Average CO line intensity ratio (1966.45 / 1966.76 cm^{-1})
2f-Max	Maximum value of integrated absolute value of laser 2f signal
0f-Slope	Linear slope of off-gas emission signal between acc. O_2 values of 240,000 and 400,000 scfm.
d^2	Square of variable "d" (defined in Table 1, above).
O_2 tscf	Real-time total accumulated oxygen, scfm.

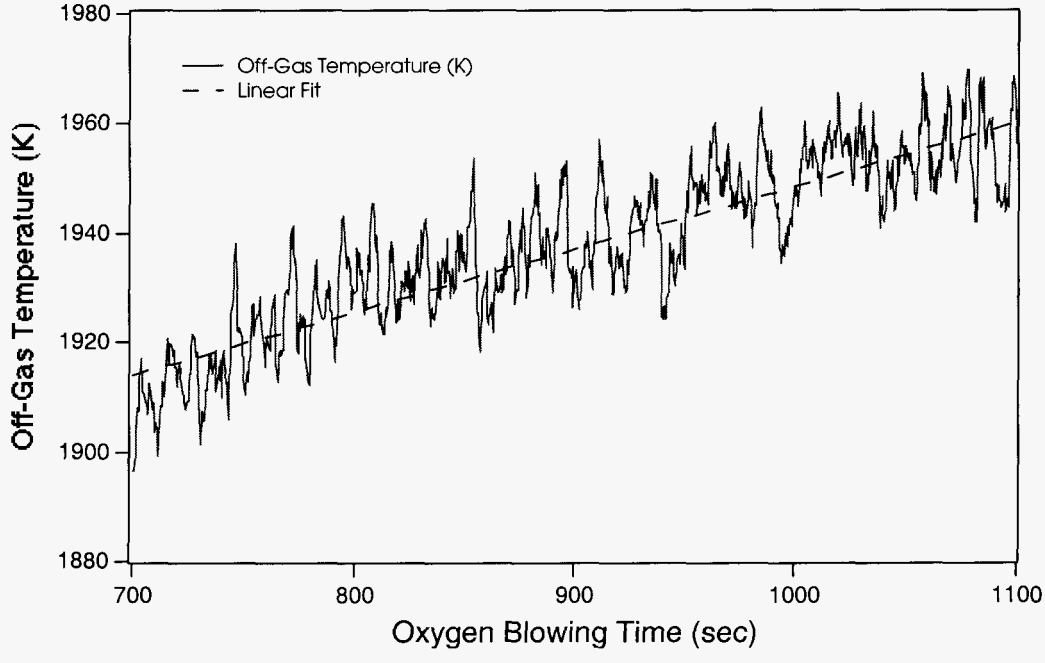

Figure 38. Measured off-gas temperature from laser-absorption sensor data (solid curve) compared with linear best-fit (dashed line).

The standard deviation of the optically measured off-gas temperature about the best straight-line fit (as shown in Fig. 38) ranges from ± 10° to 20 °F for the 219 heats measured during the field trial. This range of variation does not actually represent the precision of the optical measurement since there is no reason to expect the off-gas temperature to precisely follow a linear increase during the oxygen blow. The precision of the optical sensor is expressed in this fashion since it is a straightforward and objective method, and the actual time-dependent nature of the off-gas temperature cannot be determined by an independent method for comparison. Furthermore, much of the variation in the optically measured temperature is of a "longer-term" nature, involving transients of several seconds duration over which a smaller high-frequency variation is superimposed. It is quite likely that the longer-term variations are, in fact, real changes in off-gas temperature associated with process related events.

The accuracy of the optically determined off-gas temperature also cannot be determined since no independent measurements were made. Furthermore, the optically determined temperatures are derived from line-of-sight measurements that sample non-uniformities across the off-gas stream. Since the absorption-line intensity ratio is not linear with gas temperature (see Figure 36 above), a composite average temperature as measured by the optical sensor will include an error associated the time-dependent spatially non-uniform nature of the furnace off-gas.

Much of the off-gas temperature non-uniformity is expected to be associated with "edge effects" at the boundary of the flow with ambient air entrained into the exhaust hood. Additional combustion of the carbon monoxide in the off-gas takes place in this region, along with mixing and dilution with cold ambient air. As discussed earlier in the report, the effect of this non-uniform thermal region on the optical measurements were minimized by establishing the sensor's line-of-sight as close as possible to a normal angle of incidence to the off-gas flow.

Despite these uncertainties in both the measured off-gas temperature's precision and accuracy, the regression analysis shows that the two intensity ratio variables, R1 and R2, are by far the most statistically significant factors. A customary value of 2.0 was required of T-test values for statistical significance of variables in a regression analysis. Values of 5.01 and 6.55 were obtained for R1 and R2, respectively, compared to values ranging between 2.65 and 3.34 for the other five variables in the regression. It is believed that a stronger correlation of the bath turndown temperature with off-gas temperature is not obtained due to other processes during oxygen blowing that affect the off-gas, but which are more weakly coupled with the metal bath temperature. An example might be heat-to-heat variations in the chemical and physical properties of the slag phase that subtly affect the heat transfer process from the furnace reaction zone to the evolving off-gas.

During a project review following the April 1998 field trials, a consensus was reached among Sandia, Bethlehem Steel and Insitec personnel. It was concluded that the demonstrated level of control improvement in turndown temperature is not sufficient to merit commercialization of the optical sensor system as a stand-alone device. Further improvement to the ± 20 °F level is necessary for dynamic process control, and this perhaps can be achieved by the integration of the current laser-based off-gas sensor with other sensor methods and a dynamic process control computer model. A first approach is to use optimal estimation theory; a simple example is as follows.

One can use the data of the static-charge model (SCM) endpoint temperature prediction along with a value derived from the off-gas sensor (TDL), combined by an optimal estimator, to improve

endpoint temperature estimation. If the TDL value is fully statistically independent of the SCM value, then the optimum estimate should have a mid-20s °F standard deviation, better than the low-30s °F standard deviation of either used alone. Demonstrating a portion of this 7°F gain has been done, by combining the two noisy but statistically independent values by weighting them inversely with their standard deviations:

$$T_{opt} = \frac{\sigma_{TDL}^2}{\sigma_{SCM}^2 + \sigma_{TDL}^2} T_{SCM} + \frac{\sigma_{SCM}^2}{\sigma_{SCM}^2 + \sigma_{TDL}^2} T_{TDL}$$

with a standard deviation of $\sqrt{1/\left(1/\sigma_{SCM}^2 + 1/\sigma_{TDL}^2\right)}$. Thus, this simple rule implies that the value T_{opt} is statistically better than either T_{SCM} or T_{TDL}; that is, adding an independent sensor measurement, even if it is noisier than an existing one, must improve the estimated value of the observed variable.

T_{opt} is calculated using the April 1998 data set of SCM aim temperatures and TDL temperatures, with σ_{SCM} = 35.7°F and σ_{TDL} = 31.2°F. The standard deviation of the resultant T_{opt} relative to measured temperature, is 30.7°F, while the model shown above predicts a standard deviation of 23.4°F. While there is a small improvement in the standard deviation, it is not as much as predicted. This is likely because the calculated T_{TDL} depends on the total amount of O_2 blown in that heat, which was initially based on the results of the SCM calculation. In other words, this is not the best example of optimal estimation because the SCM and TDL temperatures are not completely independent. Further development and demonstration of such a control system, including the identification appropriate and fully independent variables, should take place in a follow-on project.

Further, it was agreed that a more immediately fruitful application of the laser-based optical sensor is in the realm of post-combustion control. This is particularly important for electric furnace operations, which typically exhibit large fluctuations in the production of CO and CO_2. Dynamic optimization of CO post-combustion can substantially improve the energy efficiency of the electric furnace process while also proactively controlling CO emissions from an environmental standpoint. The capability of detecting H_2O in the furnace off-gas (see above, pp. 6-7) also provides a measure of the completeness of hydrogen combustion, which is an important control variable for some EAF processes. As a result of our work in the Advanced Process Control program, a new AISI Technology Roadmap project has been approved (TRP 9851) and is now underway to develop this technology for the electric furnace process.

4.3.2.2 Bath Turndown Carbon Concentration

One of the most striking facts to emerge from a statistical analysis of the optical sensor data from October 1997 for turndown carbon concentration was the strong dependence of the correlation on sensor variable "d." This variable is the ratio of the final to maximum off-gas emission intensity (see Figure 32), and as such is not dependent on the tunable diode laser portion of the sensor system. This result offers the opportunity to develop a *single-ended* infrared optical sensor for dynamic control of bath carbon concentration.

In this format, such an off-gas emission sensor resembles the carbon "light-meter" sensor developed and patented by Bethlehem Steel [Sharon, 1997]. That device uses an inexpensive broadband visible detector system to measure off-gas light emission during oxygen blowing, and yields bath carbon control between concentrations of 0.030 and 0.060%. While testing the Sandia sensor system and analyzing the resultant data, however, it was noticed that the response range of the infrared-based equipment to carbon concentration was both lower and higher than that achieved by the carbon light-meter system.

The Sandia team therefore supplemented the experimental results of the April 1998 field trial with two additional field trials (November 1998 and February 1999) that were conducted solely for the purpose of acquiring off-gas infrared emission data at the sensor design wavelength of 4.78 μm. Furthermore, during the latter two field-trial periods, Bethlehem Steel deliberately halted oxygen blowing prematurely on a number of heats and provided carbon analyses for the melt at those points. This yielded valid sensor data for 49 heats with carbon concentration values greater than 0.060%.

The aggregate results of these three field trials are discussed together in this section. The team acquired data for a total of 539 heats with valid carbon concentration values ranging from 0.023 to 0.177%. The results show a very strong dependence of the measured carbon concentration on sensor variable "d" as illustrated in Figure 39.

A multiple linear regression analysis has been performed on the aggregate data from the three field trials. A single variable ("d") was used in third through sixth-order polynomials to fit the carbon concentration data. The best fit was obtained with a fifth-order polynomial. All factors were statistically significant, and a standard error of ± 0.007% carbon was obtained with a very good correlation coefficient of $R^2 = 0.81$. **(Major Milestone Achieved)** These results compare well with the Bethlehem Steel light-meter performance, which yields carbon control with a standard error of ± 0.005% carbon for heats with final carbon content of 0.03 to 0.06% carbon. The larger error in the present results arises primarily from the 49 heats with carbon concentrations greater than 0.060%. This is probably due to the sparseness of the data in the high carbon concentration region, and to the fact that the parameter "d" is responding with decreasing sensitivity for carbon concentrations greater than about 0.12%. *Nevertheless, the infrared-based sensor represents a significant improvement over current technology since the range of carbon control has been extended to significantly higher (and lower) values.* **(Major Milestone Achieved)**

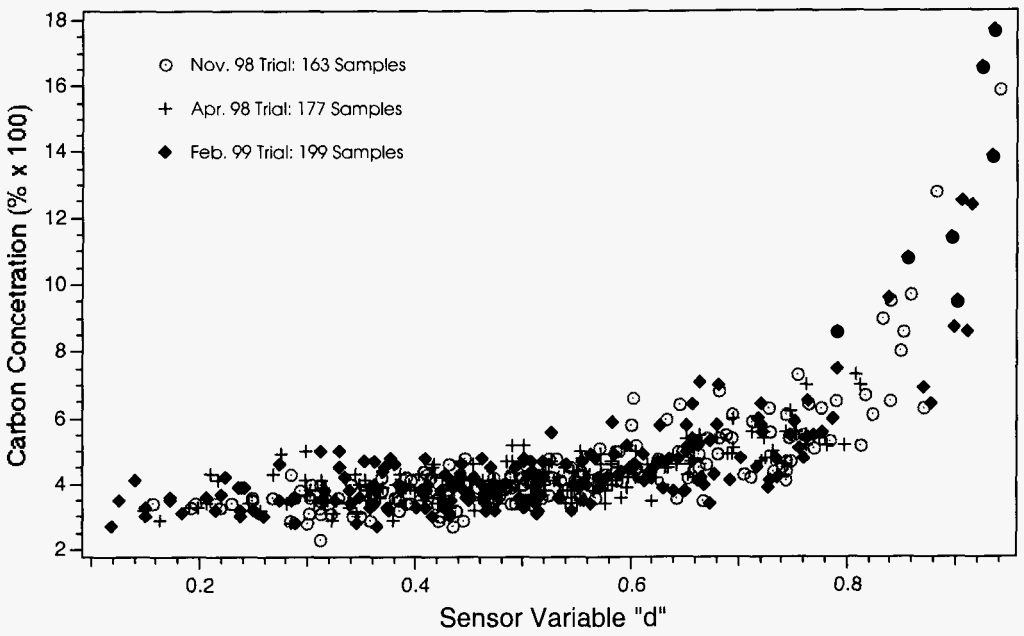

Figure 39. Dependence of final turndown bath carbon concentration on off-gas infrared emission sensor variable "d" (defined above, Fig. 32). Data are shown for the April 1998 field trial, and two supplementary field trials in November 1998 and February 1999.

A plot of all 539 measured and predicted bath carbon concentrations from the fifth-order polynomial fit is shown in Figure 40, along with a plot of the residuals and the probability density function plot of the residuals. Although a very good fit of the experimental data is achieved, the precision significantly decreases above carbon concentrations of 0.06%, as is clearly seen in the plot of the residuals. Some additional improvement in the control range at higher carbon values may be achieved by a more sophisticated, perhaps multi-functional, analysis of the data and the incorporation of additional emission detectors at one or more wavelengths into the sensor.

The anticipated improvement in data analysis by multi-functional techniques, as well as the inclusion of other sensor variables, is a result of the difference in sensor signal response to changes in carbon concentration for values above 0.060% as shown in Figure 39. It is also expected that the current sensor configuration, based on an operating wavelength of 4.78 μm, is sensitive to a combination of saturated gas-phase emission lines of carbon monoxide and greybody emission from entrained dust particles. Incorporating a second detector operating at a different wavelength sensitive to either CO_2 and particulate emission, or perhaps only particulate emission, may provide an additional sensor response with different functional dependence at high levels of bath carbon concentration. These differences may also be further enhanced by selecting a longer wavelength that is less susceptible to light-scattering by the highly particle-laden off-gas.

This in turn permits probing deeper into the off-gas stream by the optical sensor with a more independent second output signal as a result.

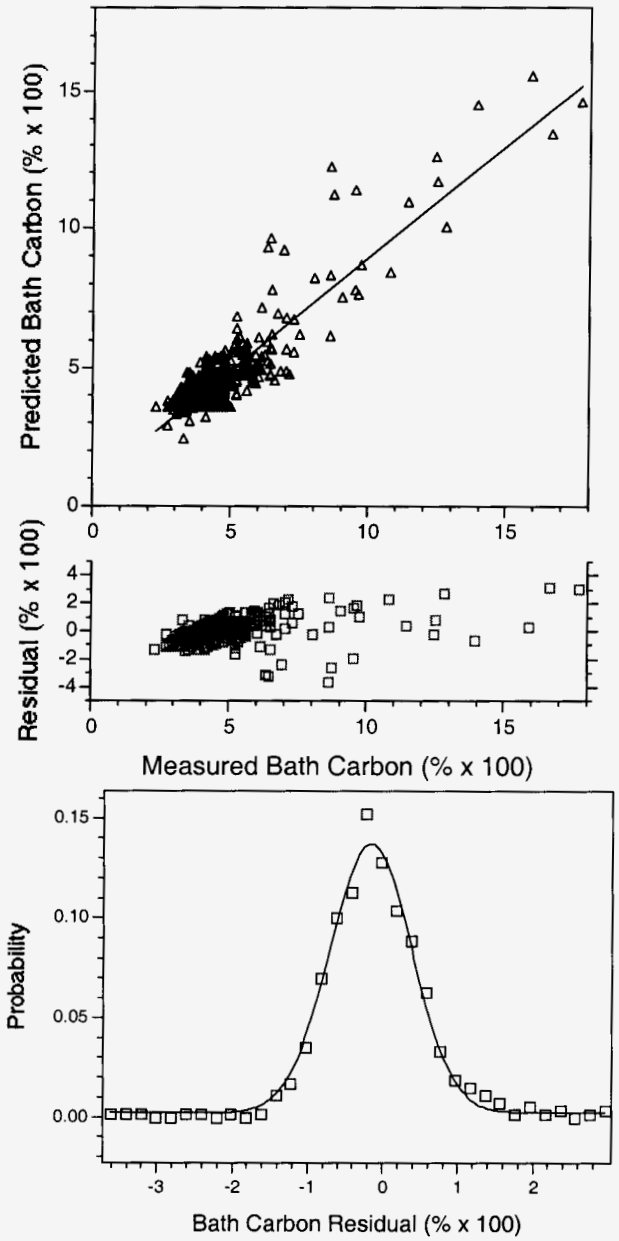

Figure 40. Predicted versus measured bath turndown carbon concentration (top plot), residuals (middle plot), and probability distribution function for the residuals of the measured versus predicted turn-down bath carbon for three field trial data sets using a fifth-order polynomial fit of the experimental data.

It is concluded by the Bethlehem, Sandia and Insitec team that the development and optimization of such an enhanced carbon-control sensor should be pursued in order to improve BOF operations.

4.3.2.3 Furnace Slopping

Ejection of liquid slag from the furnace during slopping events was recorded by videotape during the November 1998 and February 1999 supplementary field trials. Approximately 100 heats were taped, and the slopping behavior was characterized by average light levels within a specified field-of-view. These signals were compared with the sensor off-gas emission signals, and the results are shown for the initial phase of the oxygen blow for one heat in Figure 41.

It is apparent that a good correlation exists between observable slopping behavior (dashed lines) and large transients in the sensor signal (solid curve). The team is able to discriminate between the effect of "noise" events in the sensor signal as contrasted with the ejection of large amounts of slag from the furnace by a combination of the event duration and the time of its occurrence during the oxygen blow. **(Major Milestone Achieved)**

The team also observes that a gradual decrease in the emission sensor signal precedes most of the furnace slopping events. For the heat pictured in Figure 41, this change begins near 100 seconds blowing time, and is the basis for a simple algorithm to produce an alarm signal to predict the onset of furnace slopping. Using this simple procedure, the team successfully predicted slopping onset for 90% of the heats measured. **(Major Milestone Achieved)**

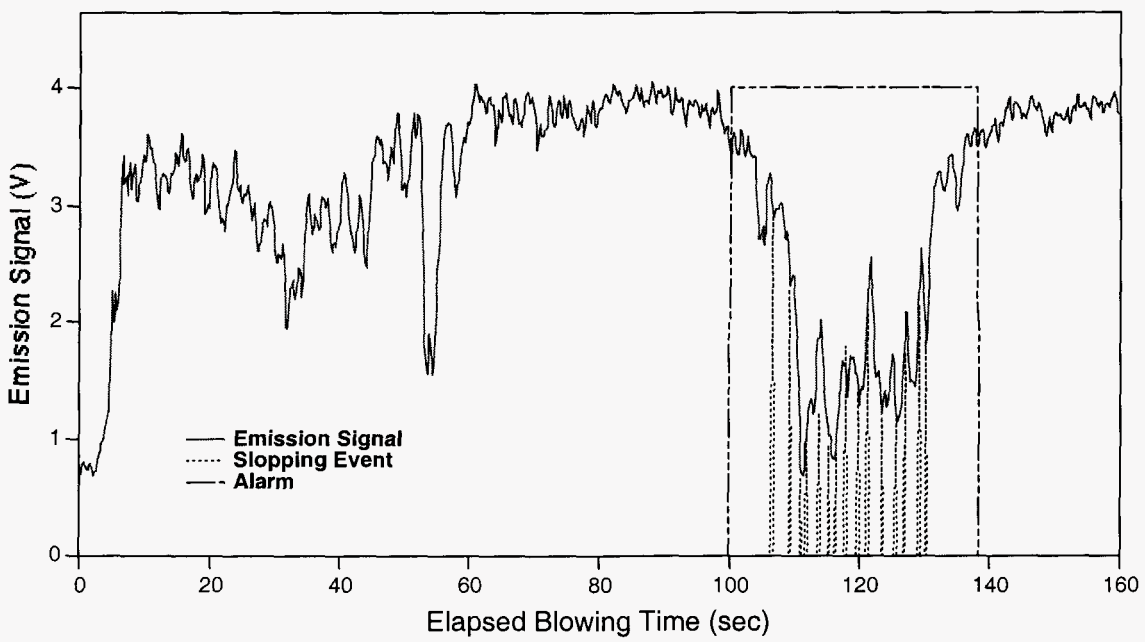

Figure 41. Comparison of off-gas infrared emission sensor signal (solid curve) with furnace slopping events (dashed lines). A "slopping alarm" prediction signal (multiple-dash line) is also shown.

As explained above, the measured decrease in emission sensor signal during slopping is probably due to the ejection of relatively cool liquid masses into the sensor's field-of-view, thus momentarily blocking the higher intensity greybody emission from the off-gas. Considerable amounts of slag ejection into the exhaust hood precedes furnace slopping, and this behavior is likely to be responsible for the drop in sensor signal around 100 seconds blowing time in Figure 41.

Due to the large capacity of the BOF vessels at both Sparrows Point and Burns Harbor plants, Bethlehem Steel does not have a strong need for a furnace slopping sensor and control mechanism. Such a device would be very useful, however, for shops possessing smaller vessels. Under those conditions, furnace slopping becomes an important economic consideration from both the standpoint of product loss and increased maintenance. A real-time control device that can either prevent or substantially reduce slopping behavior is extremely attractive, particularly since the same sensor signal provides dynamic control of turndown bath carbon concentration. Future work, following the conclusion of this project, should be devoted to the development of an optimized bath-carbon / furnace-slopping control sensor.

5. Intellectual Property

On the basis of the successful full-scale field trials in 1996 using pre-prototype sensor equipment, a Department of Energy Technical Advance (SD-8125) was filed in July 1997. The disclosure covered four applications of interest to the AISI and its member companies:

1. CO post-combustion control
2. Measurement of desired endpoint carbon concentration
3. Control of liquid slag ejection ("furnace slopping")
4. Detection of water vapor in furnace off-gases

This Technical Advance was updated and formed the basis for a patent disclosure filed in April 1998 (U.S. Patent Appln. No. 08/970,826; Fitzpatrick, Cella Harper, and Scinto Ref. No. 1559.400500), "Method and Apparatus for Off-Gas Composition Sensing." In addition to the four applications listed above in the Technical Advance, the application of the method for dynamic bath turndown-temperature control was also claimed. The fields-of-use in the patent application were also expanded to specifically include electric arc furnace and bottom-blown oxygen steelmaking processes. U.S. Patent 5,984,998 was issued November 16, 1999.

6. Conclusions and Recommendations

The development of an optical sensor for basic oxygen furnace (BOF) off-gas composition and temperature in this Advanced Process Control project has seen a laboratory spectroscopic method evolve into a pre-commercialization prototype sensor system. The sensor simultaneously detects an infrared tunable diode laser (TDL) beam transmitted through the process off-gas directly above the furnace mouth, and the infrared greybody emission from the particulate-laden off-gas stream. The sensor prototype was successfully tested in four long-term field trials at Bethlehem Steel's Sparrows Point plant in Baltimore, MD.

The original intended application of the laser-based off-gas sensor was dynamic control of turndown bath carbon concentration for BOF operations. During the course of the five-year development project, the range of potential applications was expanded to include dynamic control of: (1) bath turndown temperature; (2) furnace slopping behavior; and (3) carbon monoxide post-combustion. The possibility of detecting significant changes in the water vapor content of the off-gas as a function of hydrogen concentration may be of significance for some electric furnace processes.

Following pilot-scale developmental work in 1993-1994 and a brief full-scale feasibility trial at Bethlehem Steel's Bethlehem BOF plant in early 1995, full-scale testing with a laser-absorption based optical sensor was conducted through February 1999. During this period, the feasibility of off-gas composition and temperature measurements in real time was demonstrated. A hardened pre-commercial prototype instrument was constructed and performed reliably during two one-month field trials. The optical data were analyzed and revealed correlations with four important process variables: (1) bath turndown temperature; (2) carbon monoxide post-combustion control; (3) bath carbon concentration; and (4) furnace slopping behavior.

The correlation of bath turndown temperature relies most strongly on the optical sensor measurement of the off-gas temperature. Results from a detailed regression analysis of over 200 heats shows a potential dynamic control of bath temperature for a stand-alone laser-based optical sensor of ± 25 °F with a modest correlation coefficient of $R^2 = 0.30$. This estimate is based on a long-term average range of bath turndown temperature at Sparrows Point of ± 30 °F. The consensus of Sandia, Bethlehem Steel, and Insitec personnel was that a control level of ± 20 °F or better would be necessary for such an independent method to be commercially successful. **This goal may be attainable by combining the laser-based sensor with other independent sensor systems, or with additional static and real-time input from the plant computer control system, and should be pursued in a separately funded development program.**

During late 1996, post-combustion oxygen lance technology was installed at Sparrows Point and was marked by a distinct increase in both off-gas CO_2 concentration and temperature as revealed in the laser-based sensor data. While these data were useful in an assessment of BOF hood design by Bethlehem Steel, the steady-state nature of the post-combustion process at Sparrows Point does not benefit greatly from a real-time control system. Much more fruitful would be the implementation of the laser-based sensor for real-time post-combustion control in the electric arc furnace steelmaking process. The rapidly changing off-gas in that process is very amenable to a dynamic control system for optimizing energy efficiency and reducing CO emissions. **As a result of this work in the Advanced Process Control program, an AISI Technology Roadmap Project (TRP 9851) to develop this technology for the electric furnace process has been approved and is now underway.**

In addition to the laser-based absorption spectroscopy data collected by the sensor, a concurrent signal generated by greybody emission from the particle-laden off-gas was collected and analyzed. A detailed regression analysis shows an excellent correlation ($R^2 = 0.81$) of a single variable with bath turndown carbon concentration. This sensor configuration is single-ended and resembles the recently developed and patented Bethlehem Steel "carbon light meter." Operation in the mid-infrared region, as dictated by the Sandia tunable diode laser, yields valid dynamic control data over a much wider range of bath carbon concentrations. Extended field trials in 1998 and early 1999

show a response range from below 0.03% to at least 0.15% carbon concentration with a precision of ± 0.007%. **Follow-on work has been approved by the AISI Technology Roadmap Program to develop and optimize the off-gas emission sensor method for improved dynamic control of bath turndown carbon concentration.**

Finally, significant changes in the real-time off-gas emission sensor signal during furnace slopping events are also observed. During the final two sets of field trials a series of time-stamped videotapes were made of 100 heats, and computer-aided analyses of furnace slopping were compared with simultaneous off-gas emission signals. A strong correlation is observed with prolonged drops in the emission signal and furnace slopping. A simple computer algorithm was written that successfully predicts furnace slopping for 90% of the heats observed. Over 80% are predicted with at least a 30-second warning prior to the initial slopping events. Although Bethlehem Steel does not experience a severe problem with furnace slopping, perhaps as many as 50% of the BOF shops in North America suffer product loss and increased maintenance costs as a result of slopping due to smaller capacity furnaces. **A project to develop dynamic furnace slopping control based on an optimized off-gas emission sensor in conjunction with dynamic bath carbon control has also been approved by the AISI Technology Roadmap Program.**

7. References

Bomse, David S., Stanton, Alan C., and Silver, Joel A. (1992), "Frequency modulation and wavelength modulation spectroscopies: comparison of experimental methods using a lead-salt diode laser," *Appl. Opt.* **31**, 718-731 (1992).

Farrenq, R., Guelachvili, G., Sauval, A.J., Grevesse, N., and Farmer, C.B., "Improved Dunham Coefficients for CO from Infared Solar Lines of High Rotational Excitation," J. Molec. Spectr. **149**, 375-390 (1991).

Ottesen, D.K., Hurt, R.H., and Hardesty, D.R., "Real-Time optical Diagnostics for the Basic Oxygen Steelmaking Process," Presented at Western States Section/The Combustion institute 1992 Fall Meeting, Berkeley, CA, October 14, 1992; SAND93-8409.

Sharon, 1997: "Method and Apparatus to Determine and Control the Carbon Content of Steel in a BOF Vessel," U.S. Patent 5,603,746, Feb. 18, 1997.

Pierluissi, J.H., Vanderwood, P.C., and Gomez, R.B., "Fast Calculational Algorithm for the Voigt Profile," J. Quant. Spectrosc. Radiat. Transfer **18**, 555-558 (1977).

Sharon, A., "Light Sensors for BOF Carbon Control in Low Carbon Heat," Proc. 81st Steelmaking conference of the ISS **1998**, 337.

Stelts, Phillip, 1994, Private Communication, Bethlehem Steel Corporation.